THE DEVELOPMENT OF A DOPPLER GLOBAL VELOCIMETER FOR WHOLE-FIELD VELOCITY MEASUREMENT AND ITS IMAGE PROCESSING SCHEMES USING SINGLE CAMERA

A Thesis

by

YONG ZHENG

Submitted to the Office of Graduate and Professional Studies of
Texas A&M University
in partial fulfillment of the requirements for the degree of

MASTER OF SCIENCE

Chair of Committee,	Gerald L. Morrison
Committee Members,	Robert E. Randall
	David Staack
Head of Department,	Andreas A. Polycarpou

May 2015

Major Subject: Mechanical Engineering

ABSTRACT

In this study, the development of a Doppler Global Velocimetry (DGV) system using single high speed camera including both hardware and data reduction software is described. DGV is an emerging technique for whole field velocity measurement based upon the Doppler frequency shift of the light scattered by the seeded particles in the flow field. Determination of the Doppler shift is achieved by applying a frequency-to-intensity image conversion in the form of an Absorption Line Filter (ALF) cell containing iodine vapor inside the cell. The Doppler frequency shift of the light scattered by the moving seed particles is then employed to calculate the velocity of the moving particles. Using light sheet generated by applying a set of optics and the laser source and imaging optics, the DGV measures the global velocity of a two-dimensional section of the seeded jet flow.

Based upon the DGV system first developed by C. Gaharan [1] in 1996, this study describes a simplified optical system and corresponding data reduction code developments in Matlab. A new laser light source, single lens imaging optical system and a single high speed camera (Phantom V711, Vision Research Inc.) are the main modifications on the hardware. For the previous DGV system developed by C. Gaharan [1], two separate cameras were required for simultaneously recording ALF and REF images of the flow field, while the simplified imaging optical system in this study is able to record both the ALF and REF images on the same screen, which makes applying a single camera adequate to capture the data images required for data reduction and speed

calculation without having to sync the capturing operation between separate cameras. An integrated LabView code and a Matlab data reduction code were developed to perform the functions of spatial calibration, intensity calibration, ALF cell calibration, speed calibration and velocity calculation.

The system is tested by measuring the surface speed across a 99.06 mm diameter white disc rotating at varied speed from 6000 rpm to 18000 rpm under selected transmission ratios of the ALF cell, as well as a 12.7mm diameter free-expansion turbulent jet operating at a primary Mach number of 0.15.

In the DGV system, telecentric lens is applied between the test plane area and the imaging optical system to eliminate the image distortions on the edge area of the lens. In this study, 0.16X Techspec Silver Series Telecentric Lens and 0.06X Gold Series Telecentric Lens are respectively applied, the 0.06X telecentric allows over 6.25 times the light of 0.16X telecentric lens to be collected and recorded by the high speed Phantom camera, corresponding difference resulting from this two telecentric lens is quantified.

DEDICATION

This work is dedicated to my wife Qingxia Wang and our daughter Victoria Zheng.

ACKNOWLEDGEMENTS

I would like to express my sincere appreciation and gratitude to my advisor and committee chair, Dr. Gerald L. Morrison, for all of his guidance, patience and support throughout my master's degree at Texas A&M University. Without his help and his limitless knowledge, this work would never have been possible.

I would like to thank my committee members, Dr. Robert E. Randall and Dr. David Staack, for their kindness of being my committee members and their guidance throughout the course of this research.

I would also like to thank my friends Mustafa Karabacak, Peng Liu, Sujan Reddy Gudigopuram, Dr. Scott Chien, Dr. Sahand Pirouzpanah for their help and support on my work.

Finally, I would like to express my thanks to my wife Qingxia Wang, for her love, support and encouragement.

NOMENCLATURE

ALF	Absorption Line Filter
C	Linear Variogram scale parameter
c	Speed of light, m/s
CCD	Charged Coupled Device
CMOS	Complementary Metal Oxide Semiconductor
D	Seed particle diameter, μm
DGV	Doppler Global Velocimeter
fc	Unit of illumination, 0.1 lux or 0.1 Lumen/m^2
FWHW	Full width half magnitude of spectral line
h	Anisotropically rescaled grid node
h_{ij}	Distance between the grid node and the data point
I	Transmitted light intensity
I_{camera}	Intensity at each pixel on camera
$I_{doppler}$	Doppler shift intensity
I_0	Incident Intensity
I/O	Input/ Output device
k	Boltzman's constant
L	Calibrated Lumen level
LDA	Laser Doppler Anemometry
LDV	Laser Doppler Velocimetry

lux	Unit of illumination, Lumen/m^2
LV	Laser Velocimetry
$\hat{l}$	Laser beam direction unit vector
M	Mach number
m	Gradient of the absorption line
ND	Neutral Density filter
OD	Optical density
$\hat{o}$	Observer or receiving optics direction unit vector
P	Atmospheric pressure, kPa
P_t	Stagnation pressure, kPa
PIV	Particle Image velocimetry
R	Ideal gas constant, J/kg·K
REF	Reference image
RGB	Red, Green, and Blue
T	Temperature, K
T_f	Transfer function
T_r	Transmission of laser light
TSI	Thermal System Inc.
V	Velocity calculated at jet exit plane, m/s
R	Ideal gas constant, J/kg·K
Z	Interpolated grid node
Z_i	Neighboring data point

β	Weighting power
δ	Smoothing parameter
θ	Scattering angle, deg
λ	Laser wavelength, nm
Γ	Laser wavelength, nm
ξ	Thermal line width, Hz
ν_d	Frequency offset from resonance, Hz
ν_o	Laser light frequency, Hz
Δx	Misalignment in the measurement direction, mm
$\Delta\nu$	Doppler shift of light frequency, Hz
ϕ	Laser propagation angle, deg
Υ	Dewarped physical vertical distance, mm
χ	Dewarped physical axial distance, mm
ω_i	Uncertainty in variable(s) i

TABLE OF CONTENTS

Page

LIST OF FIGURES

Page

LIST OF TABLES

Page

1. INTRODUCTION

Since the development of the first laser anemometry system, many nonintrusive laser based methods for fluid flow field velocity measurement have been developed, including LDV (Laser Doppler Velocimetry), PIV (Particle Image Velocimetry) and DGV (Doppler Global Velocimetry).

LDV uses two beams of collimated, monochromatic, and coherent laser light in the flow of the fluid being measured. The two beams are usually obtained by splitting a single beam into two, thus ensuring coherence between the two beams. The two beams are both focused to intersect at their waists (the focal point of a laser beam), where they interfere and generate a set of straight fringes. As particles entrained in the fluid pass through the fringes, they reflect light that is then collected by a receiving optics and focused on a photo detector. The reflected light fluctuates in intensity, the frequency of which is equivalent to the Doppler shift between the incident and scattered light, and is thus proportional to the component of particle velocity which lies in the plane of two laser beams. By combining three devices (e.g.; He-Ne, Argon ion, and laser diode) with different wavelengths, all three flow velocity components can be simultaneously measured. However, LDV system is based on point by point measurement, so it will be extremely time consuming to obtain the velocity distribution of a whole flow field.

PIV is the now the most widely applied technique for flow field velocity measurement. In PIV, a pulsed laser light is applied together with a series of optics to generate a laser light sheet to illuminate a flow field into which very small particles are

introduced, and a camera is used to record images. At known times, the camera takes pictures and measures the distance that the targeted individual particle has just travelled. PIV can measure simultaneously over the area that the camera sees. The system depends on the imaging of the travelling individual seeded particles and requires a mathematic algorithm to track particles and measure velocity. PIV is less accurate than LDV in a complicated flow field, since the resulting velocity vectors obtained from PIV are based on cross-correlating the intensity distributions over small areas of the flow, the resulting velocity field is a spatially averaged representation of the actual velocity field. This obviously has consequences for the accuracy of spatial derivatives of the velocity field, vorticity, and spatial correlation functions that are often derived from PIV velocity fields. Also, since PIV is based on velocity measurement of individual particles, the accuracy of velocity measurement applying PIV for high-density seeded flow will be better than that for low-density seeded flow, which further indicates that PIV is not adequate for whole field velocity measurement.

DGV (Doppler Global Velocimetry) was first introduced by Komine in a US Patent in 1990. In particular, since DGV relies on light scattered by clouds of particles (high concentration) carried by the flow, rather than the imaging of each individual particle, it has the ability to generate velocity vector field information more quickly than LDV, and over a plane of larger area than that for PIV. Each pixel within the sensor array could yield a potential velocity vector, therefore, a mega pixels imaging camera would potentially output a million velocity vectors at video rate. In DGV, the velocity information is obtained by means of an optical & spectroscopic

frequency converter (a pre-selected linear spectral line optical transfer function), known as an absorption line filter (ALF), that transforms the Doppler shifted frequency of light scattered by the particles in the flow to real intensity variations in the imaging plane. Once this transformation is completed, the converted Doppler signal intensity map can then be processed by light intensity detectors (CCD camera or CMOS camera) and computers to obtain a velocity map of the flow of interest. To eliminate the problem of both scattering signal and illumination intensity variations spatially in the measurement window, the Doppler signal intensity map is normalized by a reference intensity map from the same view of the flow. The measurement area within the flow field is defined by the position and physical dimension of a fan of laser light and the measured velocity component is dependent on the direction of laser sheet propagation and the camera viewing angle. Currently, however, DGV is considered to be more suitable for the measurement of high speed flows (estimated to be above 30 m/s) because of the limit on velocity resolution which is approximately equal to 1 m/s, the absolute error of a very good DGV system. It is one of the very few Mie-scattering whole-field velocimetry techniques that could be truly regarded as instantaneous with the use of a short duration (~10 ns) pulsed laser.

2. PRINCIPLE OF OPERATION

Yeh and Cummins [21] developed an LDV system, since that the arrangement for the LDV has been used also in DGV. A Schematic diagram of the DGV system and how to determine a measured velocity component vector is shown in Figure 1. The main principle for DGV is to measure the Doppler shift frequency of a laser light, the laser propagation angle and the camera's observing angle, and relate these to the velocity components of a fluid flow. In 1990, an absorption line filter (ALF) was developed and patented by Komine, the absorption line filter contains molecules which absorb light near a certain laser frequency. In the DGV for this study, one ALF is installed on the side of the laser source, and a very tiny portion of the laser light generated is directed by a splitter to go through this ALF, another ALF is installed on the camera side between the light receiving lens and the imaging sensor, both ALF are for calibrating the transmission ratio curve against the Doppler frequency shift. A diode pumped solid state continuous wave laser with frequency 5.6×10^{14} Hz (532 nm) is used. The properties of molecular iodine in the ALF cell can produce an absorption filter line as presented in Figure 2.

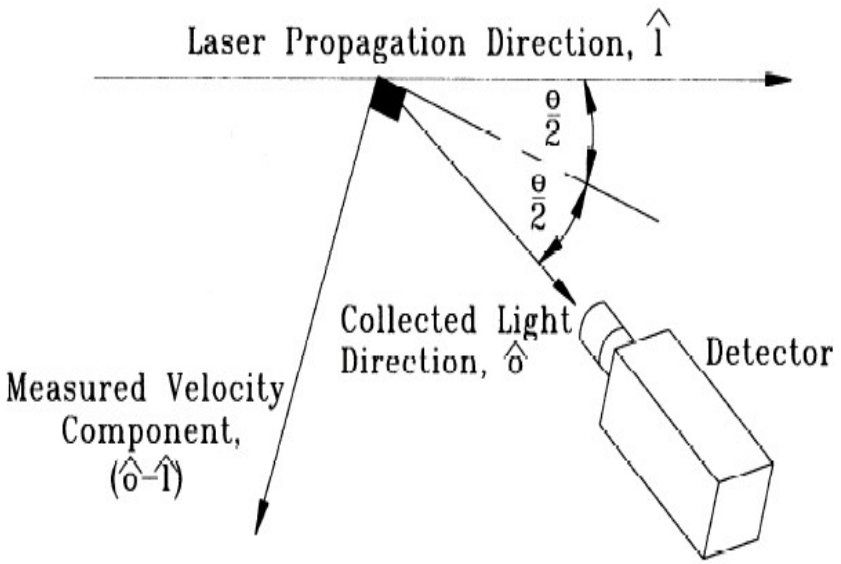

Figure 1 Determination of Measured Velocity Component Direction

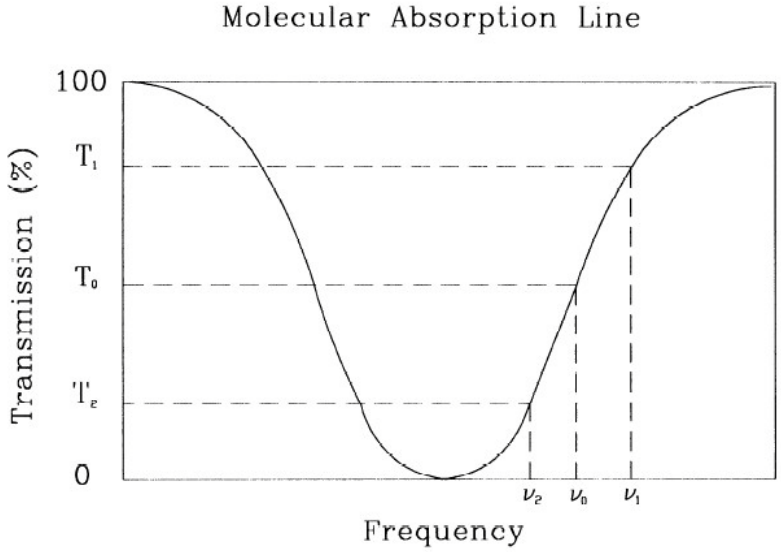

Figure 2 Transmission Curve vs. Frequency Shift Of Scattered Light

The laser light source must be stable in frequency, monochromatic, and also have a bandwidth which is much narrower than that of the absorption line filter. At the

beginning of each test, a transmission ratio curve calibration on both the camera side and the laser side are performed, and the laser frequency υ_0 is tuned to a midpoint of the one side of a u shape, within a certain range of the frequency, the transmission ratio changes approximately linearly as the frequency changes. The ALF filter absorption is about 50% in this frequency, so if the particle is moving with the fluid flow, the transmission ratio will change depending on the direction of the flow velocity. For the transmission ratio curve calibration on the laser side, a very small portion of the laser light generated is extracted and redirected by a splitter to go through the ALF, the power of this portion of laser light will be measured by a power meter before it enters the ALF. Right after this portion of laser light goes through the ALF, its power is measured again by another power meter, hence the power of filtered laser light and the power of unfiltered laser light are known. By dividing the filtered power reading over the unfiltered power reading, the transmission ratio vs. frequency curve is obtained for the laser side. Since the actual filtering characteristics of the ALF filter is highly dependent on the thermal state of the filtering medium inside, the temperature of the ALF cell needs to be stable and controlled by a temperature controller. This system allows us to be able to observe a frequency drift of the laser, and the transmission ratio curve of the ALF cell. Doppler shifted frequency which is higher than υ_0 indicates positive velocities via an increase in transmission ratio, and a Doppler shifted frequency which is lower than υ_0 indicates negative velocity via a decrease in transmission ratio. The relative relation between the transmission ratio and the laser light frequency can be reversed by tuning the laser to a lower frequency side of the absorption profile. This change in the transmission is

proportional to the Doppler frequency shift of the scattered light that is produced by the particle's motion along the measurement vector shown in Figure 1. The governing equation is given by:

$$\Delta\upsilon = \upsilon_0(\hat{o} - \hat{I}) \cdot \frac{\vec{V}}{c} \qquad (1)$$

where Δv is the Doppler frequency shift, $\hat{o}$ and $\hat{l}$ are the unit vectors in the scattering and laser light propagation directions, respectively. $\vec{V}$ is the velocity vector of the moving particle or object, $v_0$is the laser light frequency, and c is the speed of light. DGV system can measure one velocity component for given optical geometry. For three-dimensional velocity measurements, three different sets of observation direction ($\hat{o}$) or three different laser beams oriented in three different directions ($\hat{l}$) are required.

Since the ALF cell is able to be a relatively large diameter optical device, it is not restricted to filtering the light scattered by an individual particle in the flow detected by a single point detector as it is in LDV. Instead, the laser light can be expanded into a light sheet, and a cloud of particles in the flow can be detected by a camera, this makes the DGV system able to be a global velocity measurement device. Images of the flow field illuminated by the light sheet are captured by the camera, and these images contain an intensity level at each pixel of the camera's sensor, whose relationship is a function of the flow velocity via the equation (1) and the relation:

$$I_{camera}(x, y, z) = I_{Doppler}(x, y, z, \Delta v) \cdot T_f(\Delta v) \qquad (2)$$

where $I_{Doppler}$ is the intensity due to the Doppler shift, T_f is the transfer function of the ALF cell, and I_{camera} is the obtained intensity at each pixel. Figure 3 shows this arrangement and the vector nature of the DGV system.

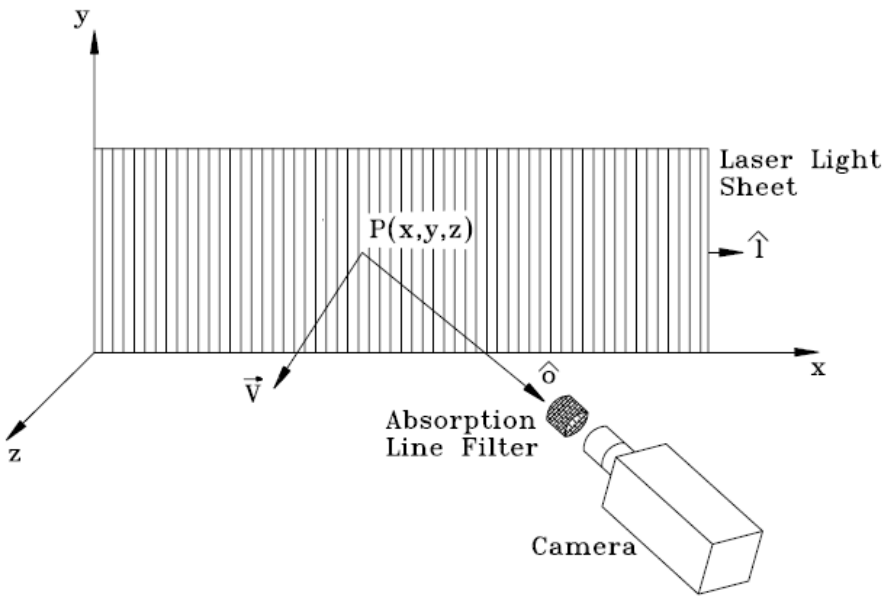

Figure 3 Global Doppler Shift in Laser Light Sheet

For traditional DGV system, the most common form of the Doppler image analyzer applies CCD (Charge Coupled Device) video cameras. During the process of image and data acquisition, the seed density, seed size, and laser light sheet illumination are not necessarily uniform, which may result in intensity variations not associated with optical attenuations in the iodine vapor induced by velocity. To compensate for these effects, a reference image is required to be separated from the camera optical system by placing a transfer lens and beam splitter ahead of the ALF and then recorded

independently by a second reference camera. This reference image along with the Doppler shifted image need to be genlocked to guarantee the reference image and the filtered image are taken at the same time and stored into computer memory by read and write access via two frame grabber boards. Also, since two cameras are applied for images, it is necessary to perform alignment and spatial calibration to make sure these two cameras are observing exactly the same area in space, which will inevitably bring in errors to some extent and influence the final velocity measurement. Figure 4 shows the optical arrangement of lenses and cameras for traditional DGV necessary to accomplish this process. By means of this reference image (REF), the image transmitted through the ALF can be normalized to yield an intensity map which corresponds exclusively to the velocity caused variations in the illuminated flow field.

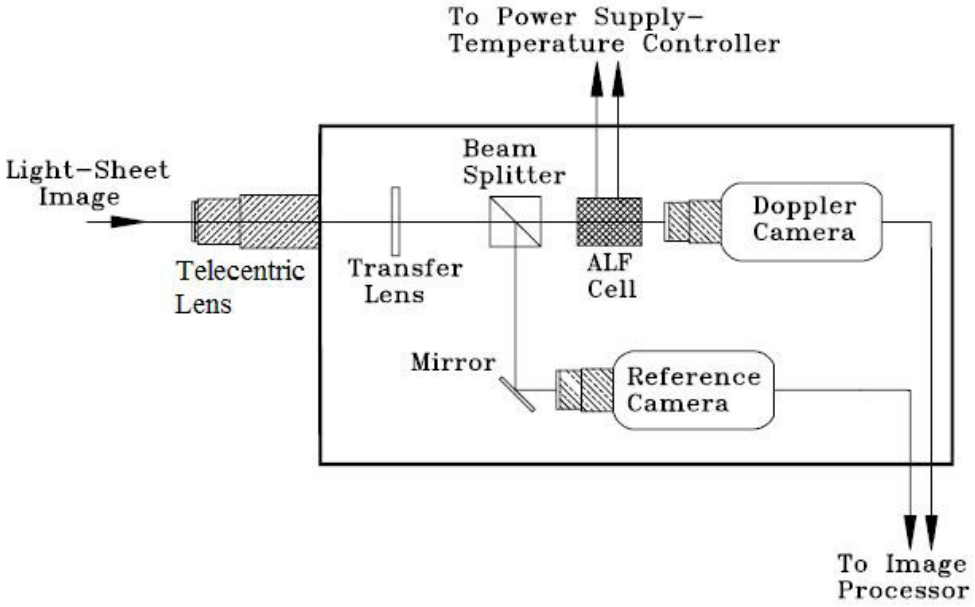

Figure 4 Optical Schematic of Traditional Doppler Image Analyzer

For the simplified DGV system applied in this study, arrangement of the optics are adjusted so as to be able to use single camera to capture both filtered image and unfiltered image, as shown in Figure 5. A transfer lens and beam splitter is placed right ahead of the ALF cell in the portion of 50:50 to split original incoming light into two beams. One beam is directed into the ALF and then filtered. The other just goes through the air and is unfiltered. At the end of the ALF, the filtered light beam and the unfiltered light beam are collected together by another reversely installed splitter and form two images simultaneously on the sensor of the camera. Using this simplified DGV system, the potential uncertainties and errors brought by genlocking the two separate cameras are eliminated, and also the potential difference in the actually observed spatial area by the two cameras is eliminated.

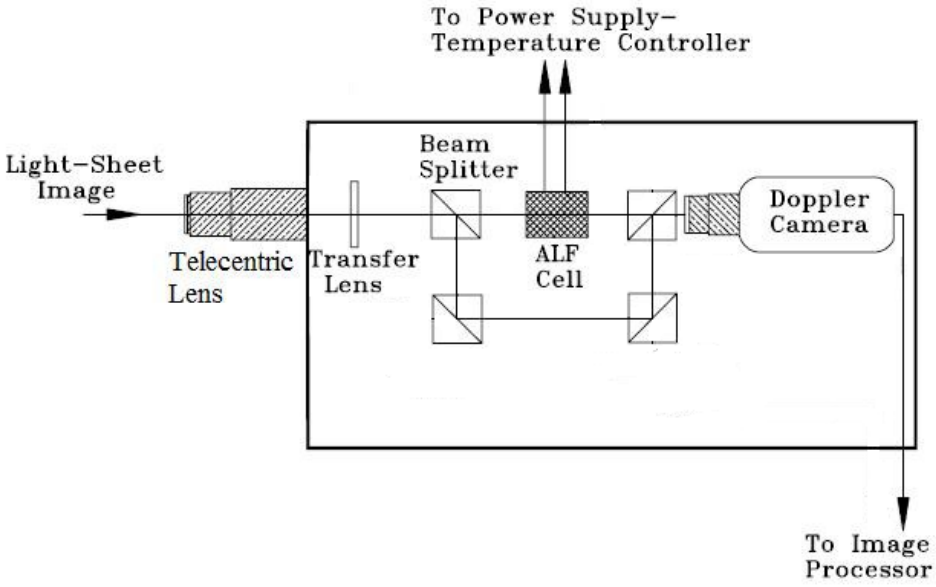

Figure 5 Optical Schematic of Single-Camera Doppler Image Analyzer

3. LITERATURE REVIEW

Doppler Global Velocimetry was first developed and patented by H. Komine for real-time Doppler frequency-based fluid flow velocity measurement. The system consists of an absorption line filter (ALF), two cameras and a laser light source. The absorption line filter was positioned external to the fluid flow and in front of one camera to determine the Doppler shift of the laser light scattered by particles in the flow field, and then the velocity components of the flow field was determined. The ALF and the laser light were both tuned to achieve 50% transmission at the mean velocity range being considered, and a frequency-intensity converter is obtained, two cameras were applied to capture images to quantify intensity differences thus the Doppler frequency shift. As shown by Komine, applying Argon-ion laser with iodine vapor inside the ALF cell, velocity components of the flow field up to ±150 m/s can be obtained with a 2 m/s resolution [3].

A one component DGV system with signal processing electronics was developed by Meyers and Komine. A 5.25 inch floppy disc rotating up to 18500 rpm and a subsonic jet velocity seeded with a fogger were used to measure the velocity. Comparing the results obtained with previous five holes probe and fringe-type laser velocimeter, it is indicated that the DGV system has potential to measure velocity of fluid flow [4].

Meyers measured a 75 degree delta wing with a DGV system, and the results were compared with previous measurement which was taken by a fringe-type laser velocimeter and five-hole probe. Meyers indicated that influence of a particle size,

particle density, and laser light sheet intensity errors were minimized by using unfiltered images. [5].

Meyers developed an optical technique to eliminate a signal processing step and measure three dimensional velocity of a 75 degree delta wing flow. Meyers clarified that exact overlay for signal and reference images were not achieved by simple physical alignment of cameras and this was caused by factors including mismatched depths of field, imperfect beam splitter, mirrors, ALF and non-uniformity pixel distribution. A new image processing technique was developed to overcome this problem. Dot paper was used to align both cameras and, centroid position of each grid point was moved from its imaged position to its ideal position [6].

Meyers changed the flow condition from incompressible (Mach<0.3) to Mach 2.8 and also the measurement distance was changed from 1 to 15m, and an additional laser frequency monitoring system was applied to detect any unexpected laser drift during each measurement. Then velocity of a 75 degree delta wing was measured again and compared with previous results [7].

In Ford and Tatam's research, CCD cameras were applied for the first time in DGV system based on Komine patent. The geometry of the optical arrangement was adjusted to observe the geometry's effects on the errors of the system. Further, due to the camera noise brought by the uncooled camera, the velocity resolution was restrained [8].

To reduce the complexity of experiment, Smith applied pulsed Nd:YAG laser operating at 30 HZ , optically thin ALF filter and single CCD camera. Most important part of this experiment was that single camera replaced two cameras to measure one

component velocity, achieved by using splitters to split and recollect signal and reference images side by side on the same camera. By using this single camera, it is guaranteed that the filtered and reference images are both taken at the exactly the same angle, which eliminates Mie scattering lobes which might affect the transmission ratio. Smith realized that most of the errors came from laser speckle usually accompanied with a pulsed laser, while using the lowest applicable f-number is a simple way to minimize those speckle error. Another error source is laser frequency locking, so during measurement frequency of the laser should be monitored to avoid any laser frequency drift [9].

In order to minimize errors brought by laser speckles, it was recommended that a frequency doubled Nd:YAG laser and a He-Ne laser beam be applied. Except for applying lowest possible f-number, M. Smith also suggested using large particles to seed the fluid flow to help further minimize laser speckle error [10].

McKenzie used a Nd:YAG pulsed laser and a single high quality scientific grade CCD camera in his experiment. It was shown that single high quality camera is better than using two average quality cameras since it improved the performance of photometric device based on the fact that it has lower noise and higher sensitivity. Other cameras have a greater noise portion when compared with CCD camera [11]. McKenzie also measured the speed of a rotating wheel to determine the low speed accuracy of the DGV system by using a frequency doubled, injection seeded Nd:YAG laser. 15.2 cm iodine filter was used, which is longer than any other filters which were previously used in DGV system. Longer filter reduces thermal gradient effect of filtering medium inside, but it decreases the field of view. A polarized beam splitter was used to minimize

polarization effect and possible smallest f-number was applied to minimize laser speckle error as suggested by Smith. Results showed that velocity lower than 2 m/s could be measured [12].

Morrison, Gaharan and DeOtte developed one component DGV system at Texas A&M University, following the principle applied by Komine and Meyers. However, the cameras applied in this system had gain settings problem in that the gains settings were changing independently hence it was necessary for the cameras to operate under fixed gain. Without operating under fixed gain settings, invalid light frequency to light intensity calibration for measure velocity field may be obtained. Also, the intensity of light that came through the optical system and reaches the camera sensor were not uniform in intensity among pixels, so a green lens that allows just green light to pass through was applied. Other problems brought by Lenses and polarization effect were also described. For intensity calibration, the intensity level of light that formed the reference and signal images needs to be as closely the same as possible, to achieve this, neutral density (ND) filters were applied on both cameras. In conclusion, inaccuracies may result from the system apparatus performance, and necessary settings for cameras, lenses, beam splitter and iodine filter cell to minimize inaccuracies was recommended [13].

In Roehl's research, a three dimensional DGV system was used to measure the velocity of a fuel spray nozzle as well as the wake region of a car. Roehl revealed the importance of laser stabilization for velocity measurement, and it was quantified that a 2.7 MHz drift in laser light equals 1 m/s uncertainty when the light sheet and measured component angle is less 90 degree, and a laser frequency stabilizing and a monitoring

system were used, and the measurement errors caused by laser drift was reduced to less than 0.5 m/s. Three-dimensional velocity measurement could be achieved by either using one light sheet together with three synchronized cameras in different positions to measure three dimension or using one camera together with three light sheets with different orientations. A non-polarized beam splitter with minimized polarization effect and 12 bit CCD cameras were used. Improved image processing technique required about 30 seconds for post processing of the images, and it was proved by Roehl that DGV has a good potential to serve as a practical and efficient device for flow field velocity measurement [14].

Muller et al used a three dimensional DGV system to measure flow in pipes. Three light sheets with different orientations and one camera system were used. Three dimensional velocity data obtained were compared with those obtained by LDA, and results indicated relatively high deviations in DGV results, however, the potential of DGV for measuring three dimensional velocity of flow field was proved, and the time required by DGV is relatively shorter than that required by LDA [15].

Nobes, Ford and Tatam used fiber bundles for three-dimension velocity measurement which only required application of two cameras and a single absorption line filter. Three light sheet directions were needed to measure the three dimensional velocity field and fiber imaging bundles were set accordingly. A fourth fiber bundle was applied to monitor laser frequency drift and perform correction for any laser frequency drift during each measurement. Speed calibration was performed using a 200 mm white painted rotating disc perpendicular to laser propagating direction, then velocity

measurement on a 70 mm diameter jet flow uniformly seeded with exit velocity of 30 m/s was measured [16].

Arnette et al applied two pulsed Nd:YAG lasers in a two color DGV technique and to measure the velocity of a free-jet. The red light laser was generated by a Nd:YAG pumped dye laser at 618 nm in wavelength, and green light laser was generated by a Nd:YAG frequency doubled laser at 532 nm. These two beams overlapped and together created a light sheet, and scattered light was passed through an iodine cell and recorded on CCD cameras. The green laser was tuned and used for frequency shift while the red laser light intensity was independent. Application of only one camera meant simple, faster data acquisition and no more spatial calibration was required. The problem of the system lies in the particle size, which had influence on Rayleigh limit and the ratio between the filtered and reference images formed by the scattering of red and green laser [18].

Willert combined PIV and DGV systems to measure the velocity of a single sector combustor rig under pressures varying from 2 to 10 bars. Three components of the velocity and how to create volumetric map of velocity were explained. Three different laser sheets were used and stereoscopic measurement was done to create velocity volume. Aluminum particles were used to have the flow seeded in combustor. Results indicated uncertainty of about 1.5 m/s, which was due to the noise in frequency shift, and also PIV had an uncertainty of about 0.3 m/s on average for 100 images [19].

The main purpose of the paper by Chain et al is to determine influencing factors of absorption line filters and how to get the absorption line filters optimized during the very construction stage. Given that the absorption filter is highly dependent on the frequency of

the laser light and the fluid flow velocity. Absorption profile from 0 to 100% is not achieved and the absorption line filter profile is not steep enough for detecting very low velocity changes, therefore, DGV generally has better performance in measuring high speed flows than low speed flows. To optimize absorption line filter, purity of iodine, Chan suggested focus on several factors, including purity of iodine during filling and degassing of filter cell, absorption cell materials, the way the cell is constructed, control of stable cell performance, relationship between dimensions and operating conditions of filter, temperature control [20].

Miles et al used sharp cut off molecular absorption line filter to measure velocity in Rayleigh scattering images of gas flows. Background scattering from reflecting surfaces such as walls, windows and plastics was difficult to eliminate, the scattering of which is one main problem when boundary flow field is to be measured. Sharp cut-off filter might be used to avoid background scattering. The scattered was too low since there was no seed particle, thus high power laser source was needed to generate strong enough laser light for the observing unit to collect enough light signal [21].

Naylor and Kuhlman setup a two dimensional velocity measurement DGV system with CCD cameras as observing camera, which reduced the noise but increased the cost. Iodine vapor cell was used as a frequency discriminator to detect any laser frequency drift while measuring the velocity of the flow field. Rotating wheel velocity was measured to determine the accuracy of DGV system. Application of high f-number lenses introduced speckle noise and also decreased the amount of incoming light. The RMS value was found to be ±1.1 m/s for Y direction, and ±0.9 m/s for X direction. 8 bit

imaging system and inaccuracies of ALF cell calibration was considered to be a general source of errors [22].

4. OBJECTIVES

The objectives of this study are: 1. Proving the ability of the simplified DGV system developed and modified by Dr. Morrison based upon the first DGV system of Texas A&M University developed by C. Gaharan to measure the global velocity of a free-expansion subsonic flow field; 2. Increasing the accuracy of the velocity measurement of the DGV system by simplifying the two-camera data acquisition model using two Dalsa Pantera TF 1M30 cameras into single camera data acquisition model using single Phantom V711 CMOS high speed camera, which totally eliminates the potential errors introduced by imperfect synch of the two cameras and spatial alignment between two cameras; 3. Simplifying and fastening the data reduction and data processing by developing systematic Matlab codes.

5. EXPERIMENTAL APPARATUS

This chapter presents an overview of the DGV experimental system with which the global velocity measurements are performed. This system was developed and modified based on C. Gaharan's PhD dissertation [1], the first DGV system developer at Texas A&M University, with the concept and logistical operational aspects of DGV following the general format of Komine's (1990), the inventor and patent holder of DGV system. The actual DGV system used for this study is presented in Figure 5.

The DGV system is composed of 8 subsystems including laser light source, power meters, temperature controllers, Doppler image analyzer unit, image acquisition and processing computer, calibration device, and free-expansion subsonic jet.

5.1. Laser Light Source

The laser light source used in C. Gaharan's study was a continuous-wave Lexel model 95 argon-ion laser opearting in the TEM_{00} single frequency mode with a maximum output of 1.0 W at 514.5 nm. In this study, a continuous-wave Oxxius 532-S diode pumped solid state laser, as shown in Figure 6, with an output power of 0.3 W at 532 nm is applied, its laser stability is 8 pm within 8 hours of operation.

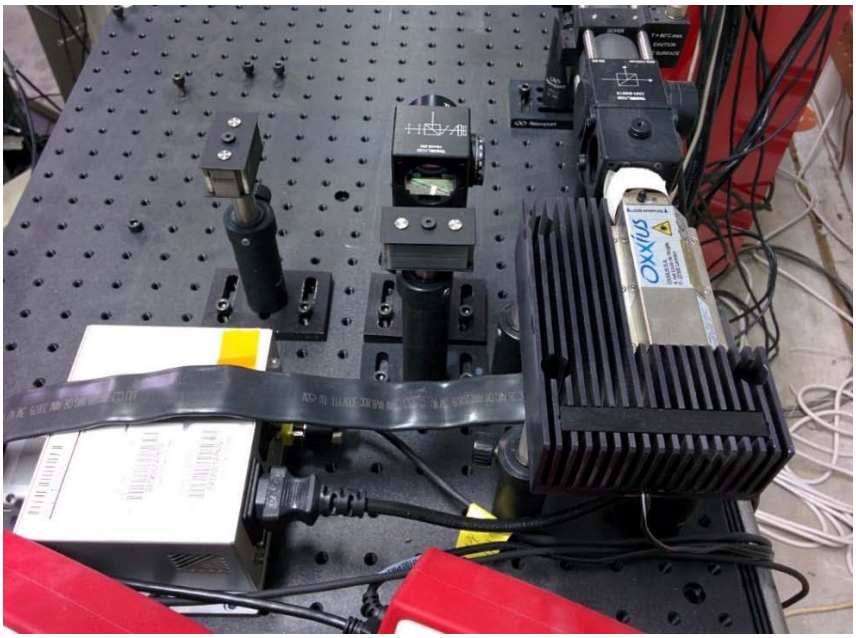

Figure 6 Laser Light Source Oxxius 532 S-300-COL-PP

As presented in Figure 6 there is an absorption line filter (ALF) in front of the laser light source. Through the calibration of the ALF cell, the transmission ratio vs. frequency shift relationship is known, then the frequency of the laser is able to be preset to a specific value for a required transmission ratio of the ALF cell, this is achieved by using a beam splitter to extract a small amount (about 1%) of the laser light which is then directed through the ALF cell, the remaining part of the laser light is redirected by the beam splitter to go through a series of first surface mirrors to generate the laser light sheet which is used for velocity measurement. For the small portion of the laser light that goes through the ALF cell, there are two Thorlabs PM100A Power Meters connected to two power sensors, one of which is attached right before the ALF cell, while the other is attached right after the ALF cell. Through these two power meters, the laser light power values for the small portion of the laser light before and after it goes through the ALF

cell can be measured and recorded. Therefore, after the calibration of the ALF cell, the laser light frequency shift and the actual laser light frequency can be calculated by knowing the actual transmission ratio according to the calibration result of transmission ratio vs. frequency shift.

The wavelength of the laser light is adjustable by changing a parameter named WL through the LabView code. Once the laser becomes stable after the start-up procedure, the values of WL can be set to change automatically ranging -2000~2000, which is equivalent to the wavelength change ranging -5 pm~5 pm. In the current study, the range WL value is set to be -500~500, namely -1.25 pm~1.25 pm, which well covers the velocity range of the rotating disc.

5.2. Thorlabs PM100A Power Meters

The Thorlabs PM100A Optical Power Meter as shown in Figure 7, is designed to measure the optical power of laser light or other monochromatic or near monochromatic light sources and the energy of pulsed light sources, it is featured with a fast USB device interface which is connected to the Image Acquisition/Processing Computer via the LabView code to record the real-time power values of the laser light before and after it goes through the ALF cell. The unit combines a precise 4 digit power readout with a mechanical, mirror supported analog needle meter to perform laser tuning tasks or watching trends.

Figure 7 Thorlabs PM 100A Power Meter

5.3. Thorlabs TC 200 Temperature Controller

The TC200 Temperature Controller, as presented in Figure 8, is a bench top controller intended for use with resistive heating elements rated up to 18 Watts. This general purpose instrument can drive various types of heaters, including foil and resistive coil types. It accepts feedback from either positive or negative temperature coefficient thermistors, and has programmable P, I, and D gains, and will display the temperature in °C, °F, or K. In addition, it can be programmed for up to five sequential temperature settings along with associated ramp and hold times for each level. A user-programmable maximum temperature limit provides protection to the device being heated, and a user-programmable power limit protects the heating element from being over driven. In this study, the upper limit of the temperature to which the ALF cell is heated is set at 50 °C.

Figure 8 Thorlabs TC 200 Temperature Controller

5.4. Doppler Image Analyzer Unit

The Doppler Image Analyzer Unit in this study is composed of an Edmund Optics 0.16X Techspec Silver Series Telecentric Lens/ 0.064X Techspec Gold Series Focusable Telecentric Lens, a Thorlabs FLH 532-4 band pass filter, transfer lens, beam splitter, ALF cell and a Phantom V711 CMOS high speed camera. The Doppler Image Analyzer Unit is housed by an enclosure (constructed with black hardboards and aluminum rails) to block the light and noise coming from the environment.

Figure 9 Edmund Optics 0.16X Techspec Silver Series Telecentric Lens

Figure 10 Edmund Optics 0.064X Techspec Gold Series Focusable Telecentric Lens

The Edmund Optics 0.16X Techspec Silver Series Telecentric Lens/ 0.064X Techspec Gold Series Focusable Telecentric Lens (as presented in Figure 9 and Figure

10, respectively) collects the light signal scattered by the rotating disc during the velocity calibration and the light signal scattered by the seeded particles in the flow field generated by the free-expansion subsonic jet. Compared with conventional transfer lens, telecentric lens is able to make objects appear to be the same size independent of their location in space and remove the perspective or parallax error that makes closer objects appear to be larger than objects farther from the lens. Further, in conventional transfer lens, the outer edge of the image is distorted and the light intensity decreases due to the curvature of the lens, while telecentric lens reduces the edge effects and make the light intensity collected by the telecentric lens more even, which together significantly increases the image quality. The Edmund Optics 0.16X Techspec Silver Series Telecentric Lens applied in this study has a primary magnification of 0.16X, the working distance is 175 mm ±3 mm, depth of field is ±19.7mm at f10, maximum sensor format is 1/2", with telecentricity <0.1°and distortion <3%. The Edmund Optics 0.064X Techspec Gold Series Telecentric Lens has a magnification of 0.064X, the working distance is 170mm~220mm, depth of field is ±129mm at f10, maximum sensor format is 1/1.8", with telecentricity < 0.2° and distortion < 0.5%.

The Thorlabs FLH 532-4 band pass filter is an enhanced isolation of diode laser lines, it provides a transmission>90% at center wavelength of 532 nm, the bandwidth (FWHM) is 4 nm, which is narrow enough to block most of other light signals from entering the Doppler Image Analyzer Unit while well covers the varying range of the expected varying range of the wavelength brought by changing the WL values from -500~500. The Thorlabs FLH 532-4 band pass filter also offers an excellent (>5 OD)

suppression in the blocking regions of 200nm~512nm and 552nm~1200nm. The filter's clear aperture is Ø21.1 mm.

Transfer lens applied is a THORLABS LB1671-A biconvex transfer lens that has a 100 mm focal length and it is paired to maintain a constant image size after the main receiving lens.

Two Thorlabs CM1-BS013 non-polarized 50:50 beam splitter are used for the splitting and collecting images. Right after the telecentric lens and the transfer lens, the light scattered by the rotating disc or the jet flow field is first evenly split (50:50) by one beam splitter into 2 portions, one of which goes through the ALF cell (same as the ALF cell applied for transmission ratio calibration on the laser side) to the observer lens while the remaining 50% of the light is directed to the observer lens. Before the two portions of the light reach the observer lens, they are collected by the other beam splitter assembled in an opposite direction and form the filtered image and unfiltered image on the same screen.

The ALF cell is a CQ19100-I Quartz Reference Cell with iodine sealed inside with a dimension of 100 mm in length and 19 mm in diameter. Also, the windows of the cell are designed with 2 degree wedge to eliminate etalon effects. The ALF cell is mounted with Thorlabs GCH18-100 heater rings to heat the ALF cell to temperature designated by a Thorlabs TC200 temperature controller. The ALF cell and heater rings can be seen in Figure 11.

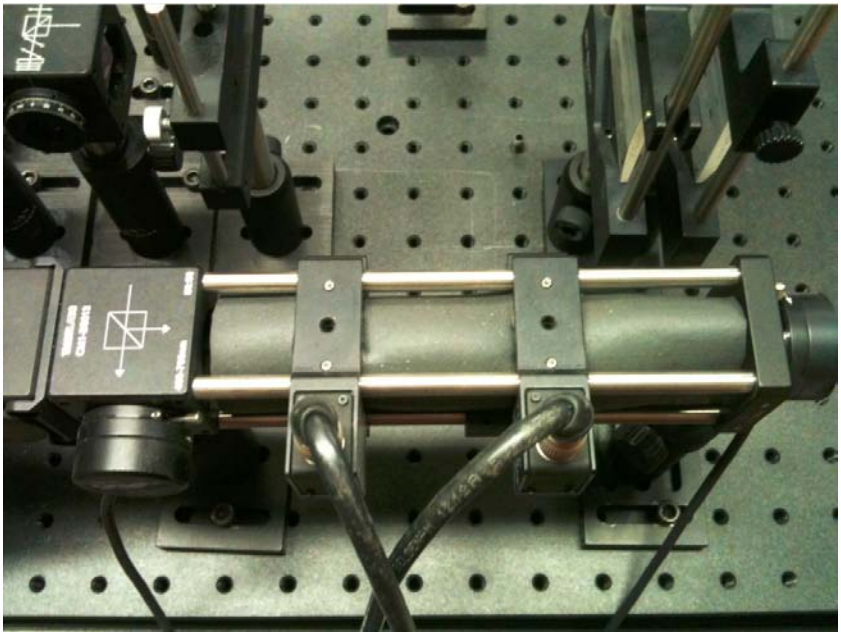

Figure 11 CQ19100-I Quartz Reference Cell, Power Meter Sensors and Heater Rings

The camera applied in this study to capture the pictures of all the images during the processes for calibration and velocity measurement is a 12-bit Phantom V711 CMOS (Complementary Metal-Oxide-Semiconductor Transistor) high speed camera, as shown in Figure 12. The CMOS sensor has 1280×800 pixels, single pixel size is 20μm, and the physical size of the sensor is 25.6 mm×16 mm. This high speed camera allows keep moving targets in the frame longer and see more of the event you are recording. At full resolution, the maximum speed is 7530 f/s. Compared with Gaharan's DGV system, the 12-bit CMOS sensor significantly increases the accuracy of the DGV system over the 8-bit cameras in Gaharan's DGV system, accordingly, the gray scale resolution of the camera increased from 256 to 4096 increments, the camera spatial resolution was also increased from 240×512 pixels to 1280×800 pixels. This all together greatly increases

the image quality for the current study. Cannon EFS 55-250mm and an extra TIFFEN 55mm +2 magnifying lens are assembled on the Phantom high speed camera.

Figure 12 Phantom V711 CMOS High Speed Camera

5.5. Image Acquisition/Processing Computer

Phantom Camera Control Application PCC 2.5 and LabView code are used in combination for data acquisition. Two LabView codes were written to control the DGV system and the laser source. The filtered and unfiltered images were simultaneously recorded and saved by using the PCC 2.5 in 12-bit Cine Raw video format and then converted into 12-bit TIFF format for analysis. PM100D.vi LabView code was written to calibrate the ALF cell automatically. The LabView software front panel is shown in Figure 13. This PM100D LabView code serves for three purposes. First, the wavelength

of the laser changed from WL +500 to WL -500 automatically, with a step being 25 in WL. Second, the control module for the two TC200 THORLABS temperature controllers is integrated in PM 100D. Finally, the power of the filtered and unfiltered laser light is monitored and saved under each WL value for calculating the corresponding transmission ratio for each WL value.

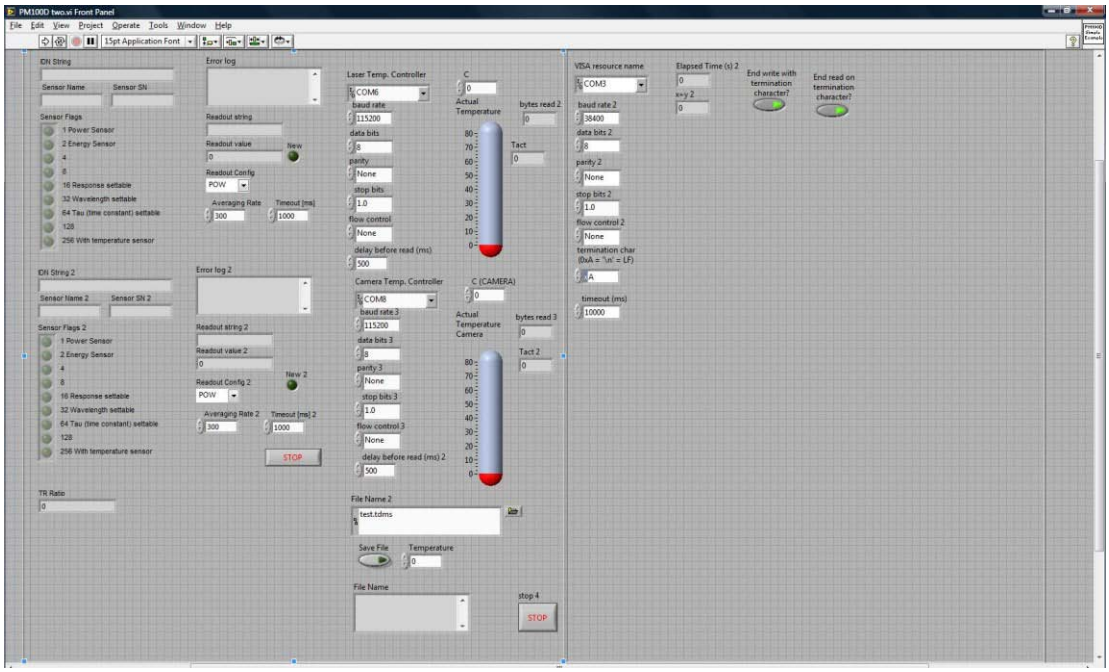

Figure 13 Front panel of the PM 100D LabView Code for ALF cell calibration

A Matlab program for spatial calibration is developed, obtaining the matching relationship between the unfiltered and filtered image for the same spatial location. A Matlab program for intensity calibration is also developed, through which 1280 x 800 pixels were calibrated for the filtered and unfiltered images, obtaining intensity

calibration equations for each pixel. Then with images acquired by the Phantom V711 camera, the transmission ratio of the rotating disc and the jet flow can be obtained by dividing the lumens of filtered image by the lumens of unfiltered image. The frequency shift can be calculated from the transmission ratio referring back to the curve of transmission ratio vs frequency shift obtained from the ALF cell calibration. Based upon the original transmission ratio curve, a curve fit is performed via a Matlab code developed. A 6-order polynomial equation is obtained, so the frequency shift of each pixel was calculated by using these equations. The transmission ratio of each pixel was known value, so the frequency shift of each pixel can be calculated.

5.6. Free-Expansion Subsonic Jet

The primary measurement device used in this research is a 12.7 mm diameter free-expansion subsonic jet. An overall schematic of this facility is shown in Figure 15. The laser sheet was aligned to propagate directly along the jet axis, illuminating a two-dimensional “slice” of the jet, while the analyzer unit was oriented at an angle of 90° from the laser sheet. This orientation produced a measured velocity component normal to the jet axis at 45°.

Figure 14 DGV Analysis Unit and Free-Expansion Subsonic Jet

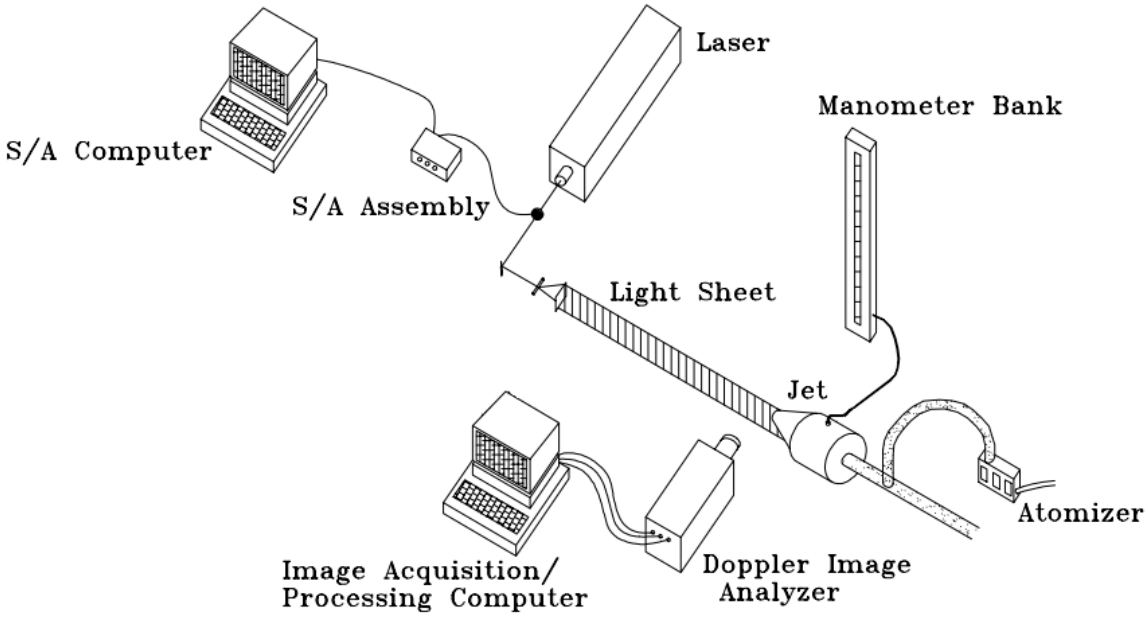

Figure 15 Simplified DGV for Measuring the Velocity Field of a Subsonic Jet

The fluid of the jet is air and supplied at room temperature. To obtain the desired Mach number, the jet plenum stagnation pressure was adjusted by use of a gate valve positioned right upstream of the jet plenum and a monitoring manometer.

Basically all laser-based flow measurement techniques require some form of 'seeded' flow which contains enough extremely tiny 'seeds' or particles that will faithfully follow the flow so as to reflect laser light back to the receiving optics of the velocimetry technique. It is actually the velocity of the seed/particles that these measurement techniques actually measure, not the velocity of the flow itself. For this reason the selection of seed should be as neutrally buoyant as possible with size and density constraints set to ensure that the particles will faithfully follow the smallest turbulent scales of interest. Therefore, the chosen seed/particles must simultaneously provide adequate signal strength for the receiving optics and detector, as well as follow the smallest turbulent scales that must be measured.

In this study, optical energy the scattered laser light collected by the Phantom camera is the parameter to be measured. This approach did not require realization of a single particle as needed by other laser velocimetry methods such as PIV, thereby allowing velocity measurements for extremely small particles to be possible. These particles consisted of a commercial fogging liquid containing primarily triethylene glycol and water, the mixture of which are generated from a Mariam TSI Model 9306 aspirating six-jet atomizer. The atomizer is pressurized with air and equipped with a rotameter to control the air flow rate, three valves are utilized to control the rate of seed production. The seeds/particles are then injected into the jet plenum via another gate

valve and finally exit the nozzle together with the air flow to provide the desired seeded flow. Nail (1991) and Panak (1990), utilizing a Mariam TSI Model 3310 Aerodynamic Particle Sizer, previously determined the diameter distribution of the atomized fog fluid to be 0.76 µm and 0.69 µm respectively with an uncertainty of ± 0.5 µm.

6. IMAGE PROCESSING TECHNIQUE

6.1. Spatial Calibration

Given that all the information and data critical to the data processing and final flow speed calculation in DGV system originally come from the comparison results between the unfiltered image (REF) and the filtered image (ALF). Further the very basis supporting correct and dependable comparison is to make sure that the pixel regions in two images to be compared are both corresponding to the same spatial area, and that tiny errors in spatial calibration will result in significant errors in transmission ratio contour and final flow velocity calculation, correct spatial calibration is of essential importance for the DGV system. Also, in previous studies of Meyers and Usry on DGV, it has been concluded that it is essential for the signal and reference images to be accurately aligned with one another before calculating the intensity ratio. Requirement for more dependable and accurate alignment between REF and ALF images suggests that physically manual operation for alignment applied in early DGV systems are inadequate and a comprehensive image processing strategy for DGV is more efficient and more dependable.

Resulting from imperfections in the optical system such as astigmatism and imperfect alignment among optical components, as well as a number of other possible differences between the REF image and the ALF image, the REF image and ALF image will not look exactly the same, even if they are recorded by the same single camera at the same time. For example, one image maybe slightly rotated with a certain angle relative to the other. Slightly different magnification between the two images may also be

experienced, or distortion at some specific areas within either or both the two images due to the performance of the lenses in the system. Based upon the above mentioned, the accuracy with which the images must be aligned in order to yield accurate quantitative velocity measurements requires a systematic and sophisticated image processing approach, to achieve this, the following procedures are applied.

6.1.1. Centroid Calculation

For centroid calculation, a square dot array with known size and spacing is plotted and printed onto a sheet of white paper and placed in a physical plane which is coincident with the axis of the subsonic free-expansion jet flow, in front of the Doppler Image Analyzer Unit. Images of the dot array in the physical plane are captured by the Phantom high speed camera under the resolution of 1280×800. Since the pixel counts 0~1279 horizontally and 0~799 vertically, before taking images of the dot array, the relative positions of the REF and ALF images are adjusted to make sure that the center for the REF image is located at the pixel (320, 320), while the center for the ALF image is located at the pixel (960, 320). After the 12-bit TIFF image is obtained from the CINE RAW format video recorded, the REF and ALF images are respectively extracted from the 1280×800 image to form two separate 640×640 images. By this stage, the relative position of the signal area in REF image is exactly the same as the signal area in ALF image. In both separate images, the centers of the two signal areas lie exactly at the pixel point (320, 320). The pixel locations of centroids in both images are then calculated and extracted automatically into two separate M×2 arrays.

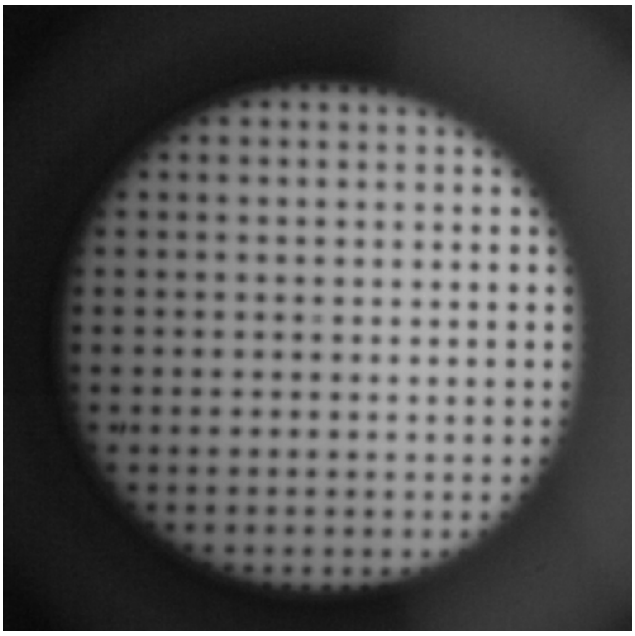

Figure 16 Original Dot Array (REF)

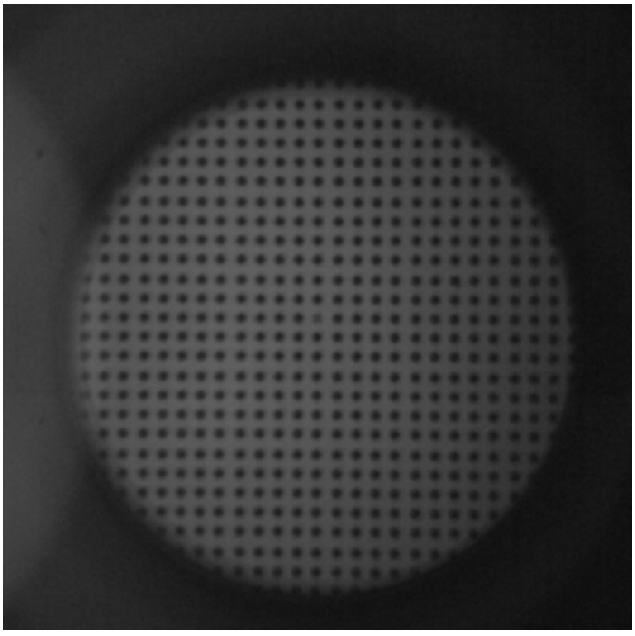

Figure 17 Original Dot Array (ALF)

Figure 16 and Figure 17 present the original dot array images of REF and ALF captured by the camera. In order to obtain more accurate and dependable spatial calibration results, calculation and adjustment on the intensity information for both REF and ALF images is performed to further distinct the dots from the whole REF and ALF images, respectively. For REF image of dot array, the average of grayscale level for the 640×640 pixels are calculated and set as a threshold, then the grayscale level of each pixel in REF image is compared with this threshold. For each pixel, if its grayscale is lower than the threshold, the grayscale of the pixel is set to 0, if its grayscale is equal or higher than the threshold, it will be kept unchanged. After comparison of all pixels, the updated grayscale values are stored into another 640×640 matrix, which is used to display as the processed image of dot array, called as processed dot array. Then the centroid coordinates in the form of (i, j) are calculated using Matlab and stored into a new M×2 matrix. Similar process is followed for ALF image of dot array to obtain the pixel coordinates of each dot and stored into another M×2 matrix.

To evaluate the accuracy of the calculated pixel coordinates for each dot, coincidence comparison between original dot array and new dot array based on calculated centroid coordinates is performed, for REF image and ALF image, respectively. Processed dot arrays for REF and ALF images are presented in Figure 18 and Figure 19.

Figure 20 shows the Centroid Comparison between Original-Calculated Dot Array (REF). Figure 21 presents the Centroid Comparison between Processed and Calculated Dot Array (REF).

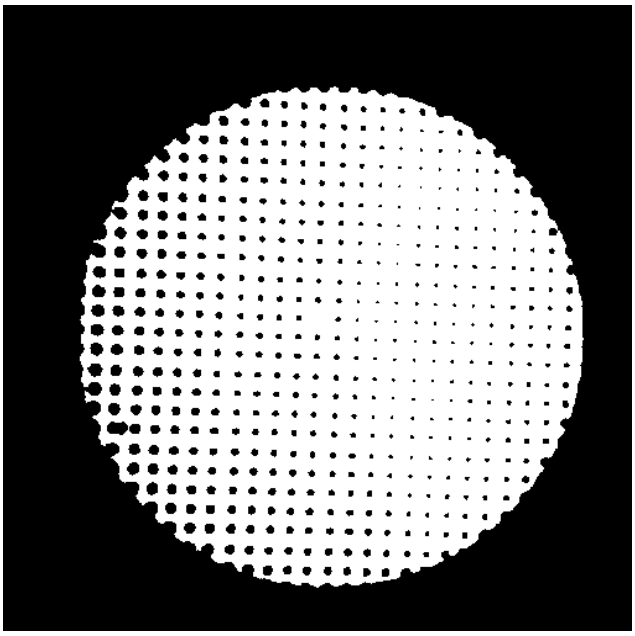

Figure 18 Processed Dot Array (REF)

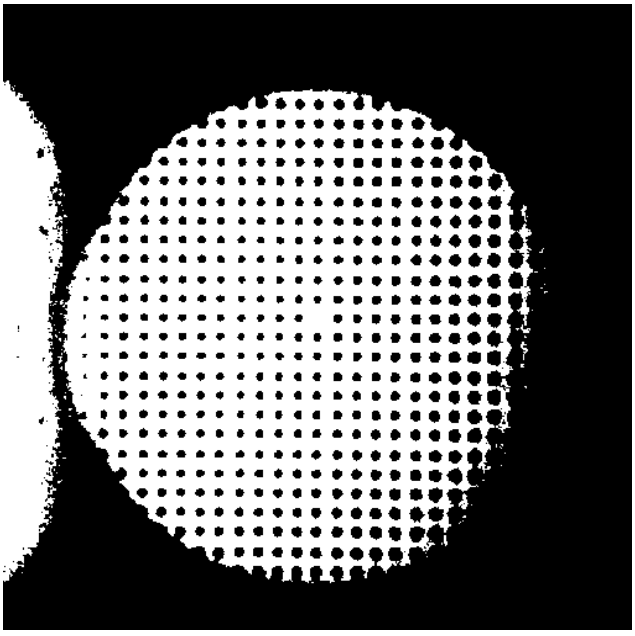

Figure 19 Processed Dot Array (ALF)

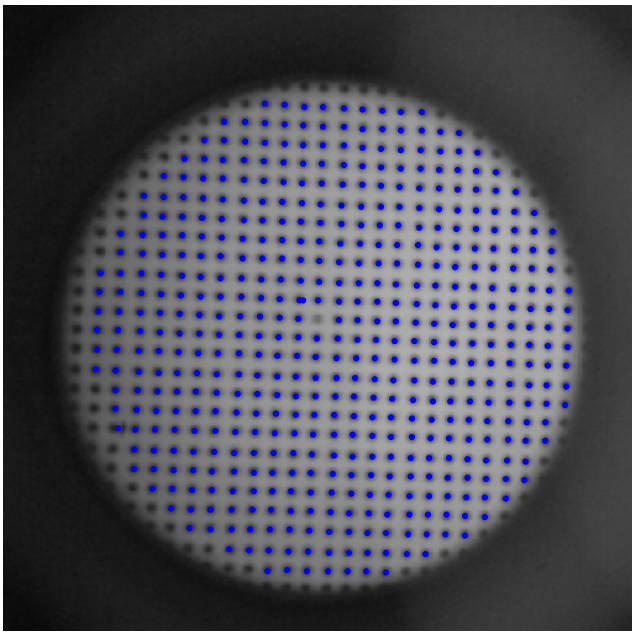

Figure 20 Centroid Comparison between Original and Calculated Dot Array (REF)

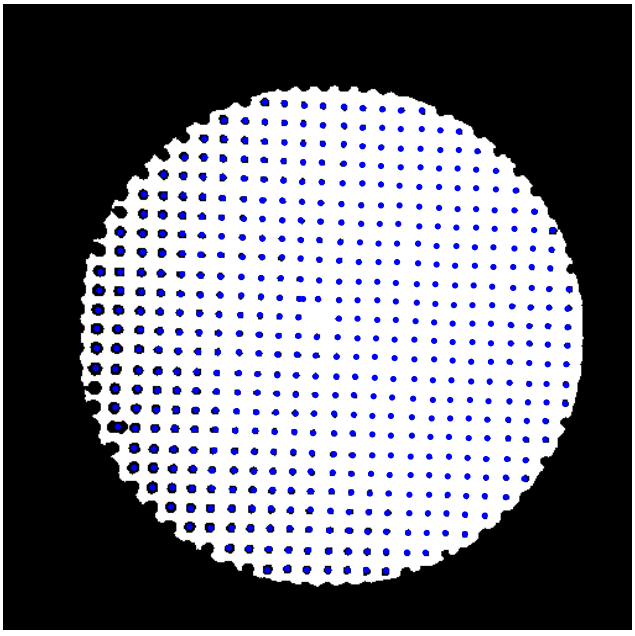

Figure 21 Centroid Comparison between Processed and Calculated Dot Array (REF)

Figure 22 presents the Centroid Comparison between Original and Calculated Dot Array (ALF). Figure 23 shows the Centroid Comparison between Processed and Calculated Dot Array (ALF). All the above mentioned for spatial calibration including extracting information to form separate REF and ALF images, data processing for better distinction between dots and the whole REF or ALF image, calculating and extracting centroid pixel locations and coincidence comparison between image centroid and calculated centroid are all performed by a Matlab code 'centroid_estimation' developed for this study.

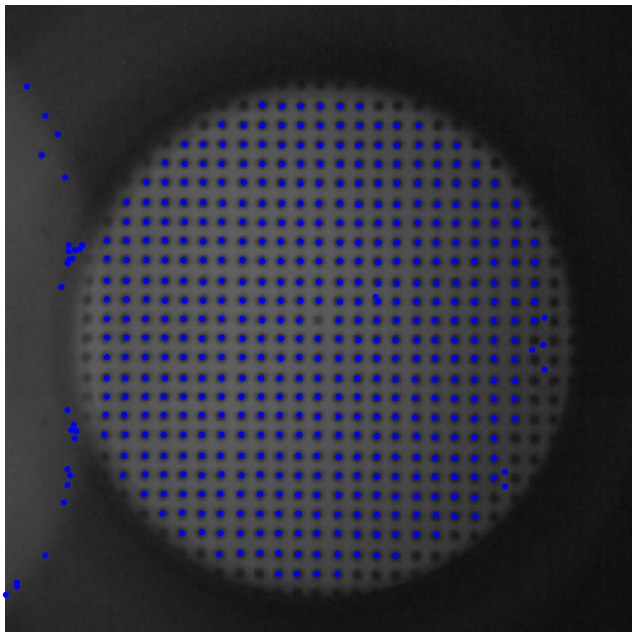

Figure 22 Centroid Comparison between Original and Calculated Dot Array (ALF)

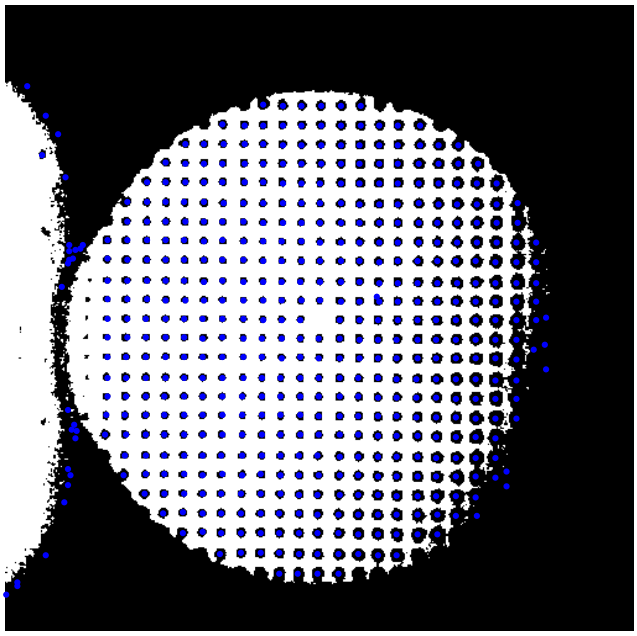

Figure 23 Centroid Comparison between Processed and Calculated Dot Array (ALF)

6.1.2. Linear Transform and Pixel Matching

After the centroid calculation and coincidence comparison, linear transform from the pixel coordinates (i, j) in both REF image and ALF image to physical spatial coordinates (x, y) is performed to calibrate the pixel location in both REF region and ALF region on the screen of the camera to a known physical plane, the dot array printed on paper. Upon obtaining the corresponding (x, y) corresponding for each set of (i, j) for REF and ALF image, (i, j) in REF is matched with the (i, j) in ALF which is corresponding to the same spatial location. Through accomplishing this, it is ensured that the pixels with data information to be processed and analyzed in both REF image and ALF images are corresponding to the same spatial locations and the ratio information is obtained via

comparing the pixels in REF with the right pixels in ALF image. In this way, it is guaranteed that the ratio and any other comparison taken over the two images for subsequent analysis and calculation are dependable and useful. Based upon the centroid calculation results obtained from the code 'centroid_estimation.m ', space coordinates (x, y) calculation and matching for (i, j) ~ (x, y) in both REF and ALF image are also performed executed through developed code named 'pixel_to_spatial_calculation_and_matching.m'. Linear transform from pixel to spatial coordinates is performed by a developed code 'pixel_to_space_transform.m'.

Figure 24 and Figure 25 show the linear transform result from (i, j) to x in space, Figure 26 and Figure 27 present the linear transform result from (i, j) to y in space.

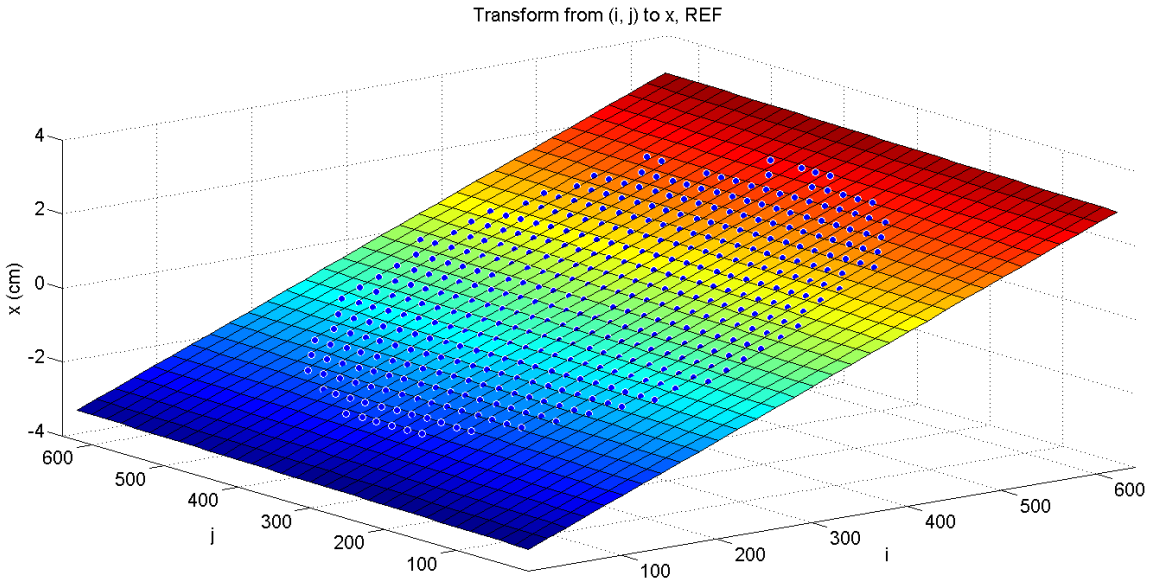

Figure 24 Transform from (i, j) to x in REF Image

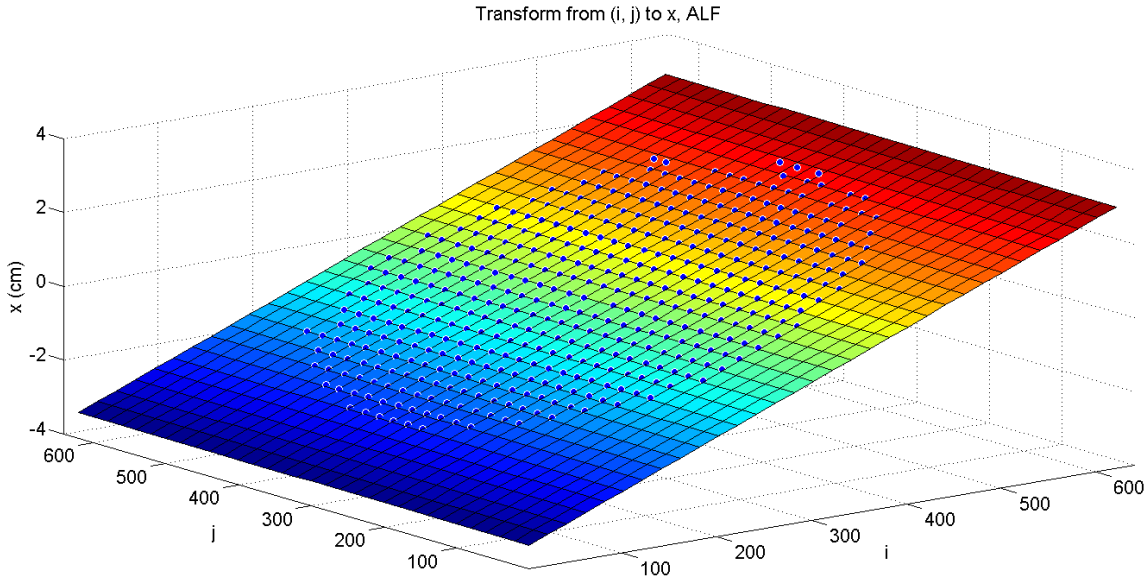

Figure 25 Transform from (i, j) to x in ALF Image

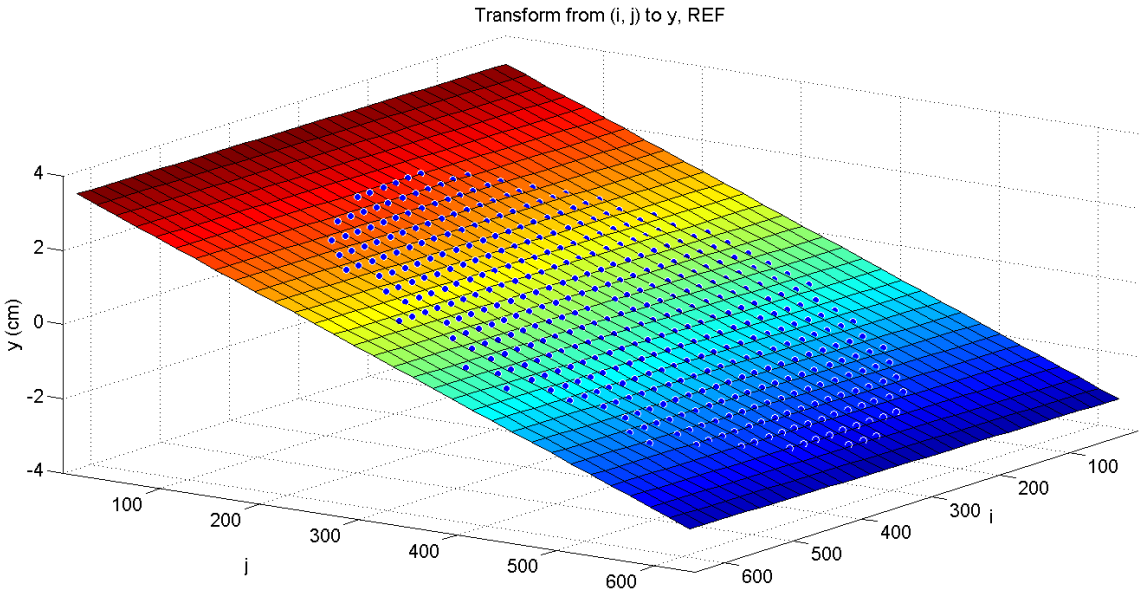

Figure 26 Transform from (i, j) to y in REF Image

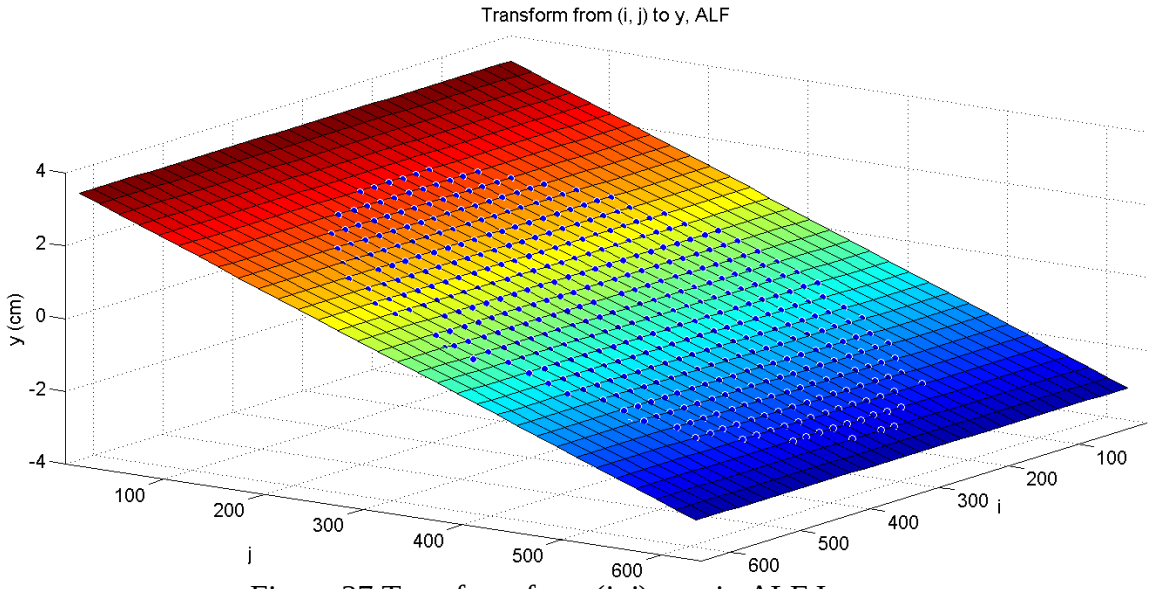

Figure 27 Transform from (i, j) to y in ALF Image

Reverse linear transform from spatial to pixel coordinates is also performed by a developed code named 'space_to_pixel_transform.m'. Figure 28 and Figure 29 indicate the linear transform from (x, y) to i in pixel. Figure 30 and Figure 31 present the linear transform result from (x, y) to j in pixel in REF image and ALF image, respectively.

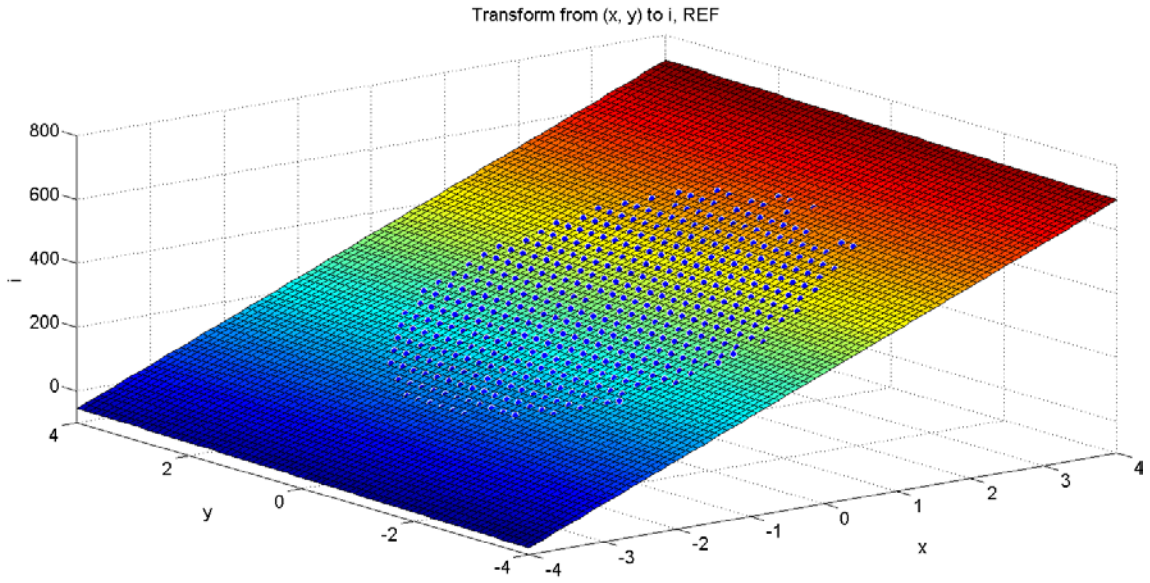

Figure 28 Transform from (x, y) to i in REF Image

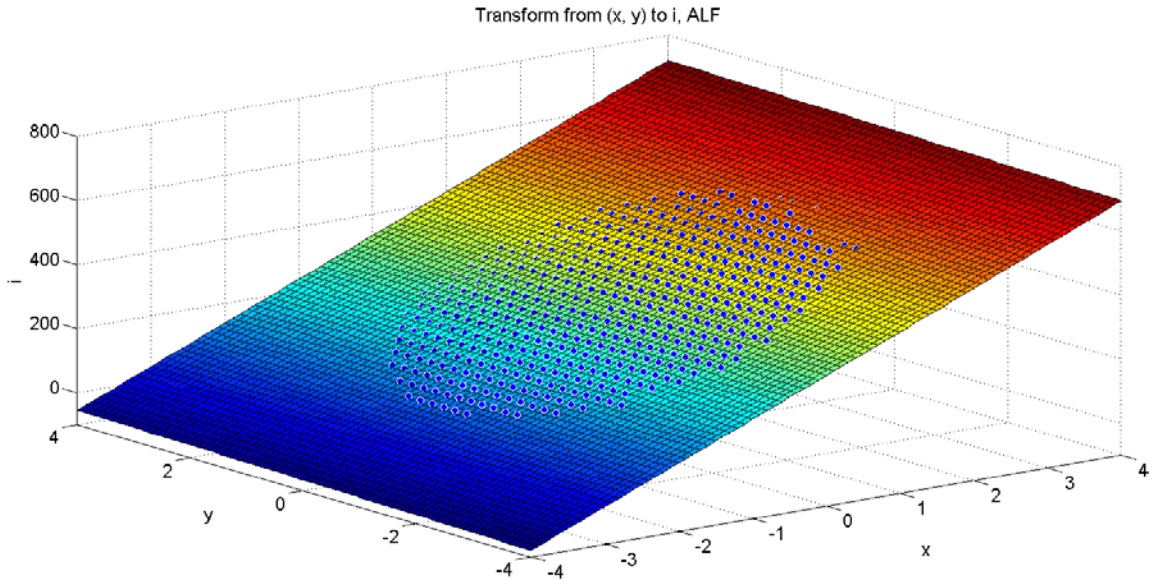

Figure 29 Transform from (x, y) to i in ALF Image

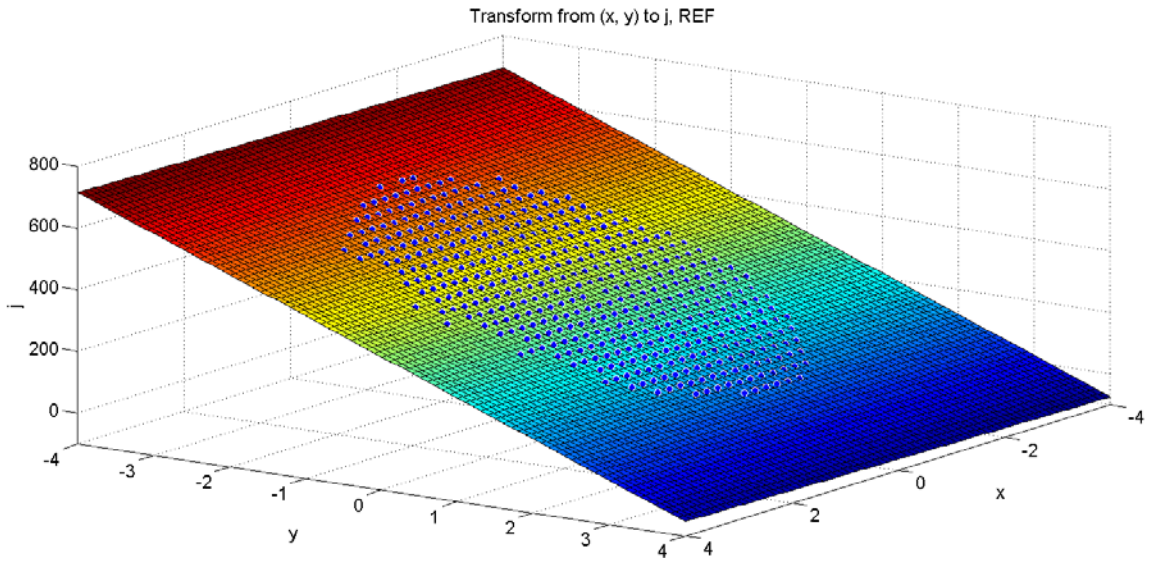

Figure 30 Transform from (x, y) to j in REF Image

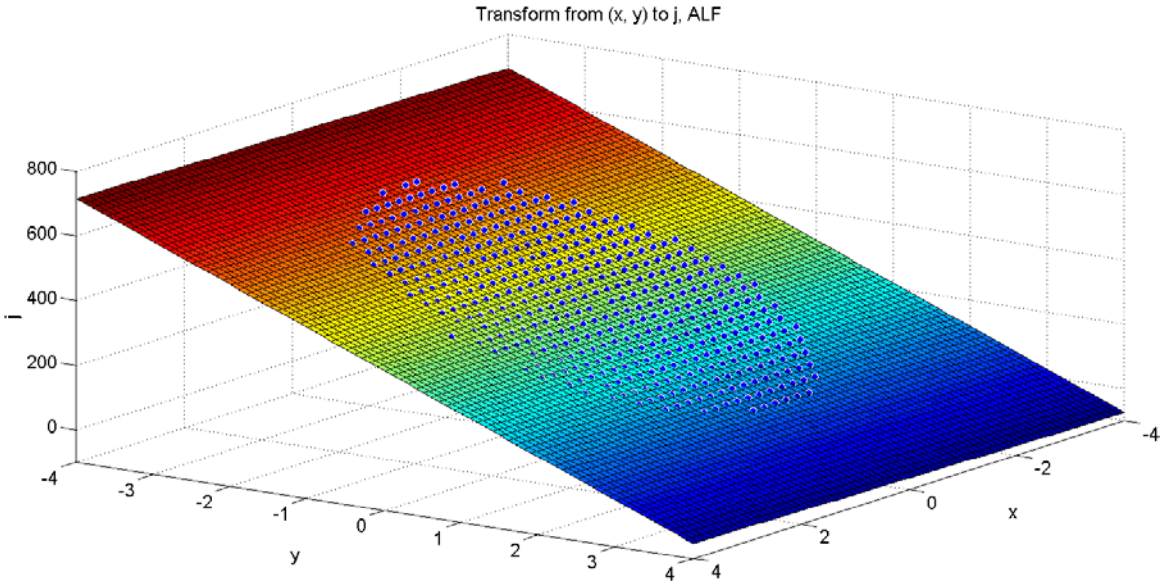

Figure 31 Transform from (x, y) to j in ALF Image

Table 1 Linear Transform for REF Image

Direction	*Equation form*	*a*	*b*	*c*
(i, j) to x	$x=a+b\times i+c\times j$	-3.409727455	0.010315336	3.396310849E-4
(i, j) to y	$y=a+b\times i+c\times j$	3.237905346	2.900435494E-4	-0.010383722
(x, y) to i	$i=a+b\times x+c\times y$	319.990741470	96.827576428	3.173536101
(x, y) to j	$j=a+b\times x+c\times y$	320.774078285	2.694636220	-96.147784403

Table 2 Linear Transform for ALF Image

Direction	*Equation form*	*a*	*b*	*c*
(i, j) to x	$x=a+b\times i+c\times j$	-3.365183529	0.010398183	6.735106395E-5
(i, j) to y	$y=a+b\times i+c\times j$	3.311636422	5.855822634E-5	-0.010349180
(x, y) to i	$i=a+b\times x+c\times y$	319.540741460	96.447576249	3.137536131
(x, y) to j	$j=a+b\times x+c\times y$	320.734288148	2.634331220	-94.421784403

Through the development and application of the above mentioned Matlab code for spatial calibration, effective and accurate spatial calibration is achieved.

6.2. Intensity Calibration

Unlike the CCD (Charge Coupled Device) cameras applied in previous studies of C. Gaharan featured of having linear response to light, the Phantom V711 High Speed Camera applies CMOS (Complementary Metal-Oxide-Semiconductor) sensor, which, due to having a transistor for each pixel, exhibits a logarithmic response to light.

Using virtual 'lumens' which stands for the luminous flux and the amount of visible light, calibration from intensity level of each pixel to 'lumens' is performed and then this

lumen level is compared to a known light source. By doing this, the system can be effectively calibrated. An image of a piece of white paper illuminated by an incandescent light table is captured by the Phantom V711 in CINE RAW format video and then further converted into 12-bit TIFF format. Neutral Density filters with optical density ranging from 0.3 to 0.9 are installed on top of a green filter (so that only a sensitivity to green light was recorded) in combinations of 0.3, 0.6, 0.9, 0.3+0.9, 0.6+0.9 and 0.3+0.6+0.9 to cover the intensity range of the Phantom V711 High Speed CMOS camera. This ranged from almost saturated to no change, on the dark end, it also allows more accurate interpolating of data intensities. The 'lumens' (transitivity of ND filters) is given by:

$$OD = log_{10}(1/T) \text{ or } T = 10^{-OD} \qquad (4)$$

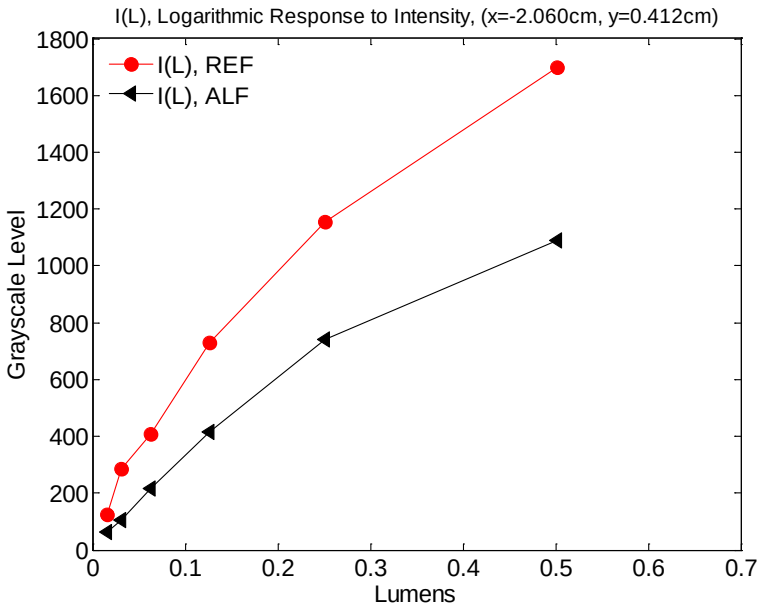

Figure 32 I(L), Logarithmic Response to Intensity

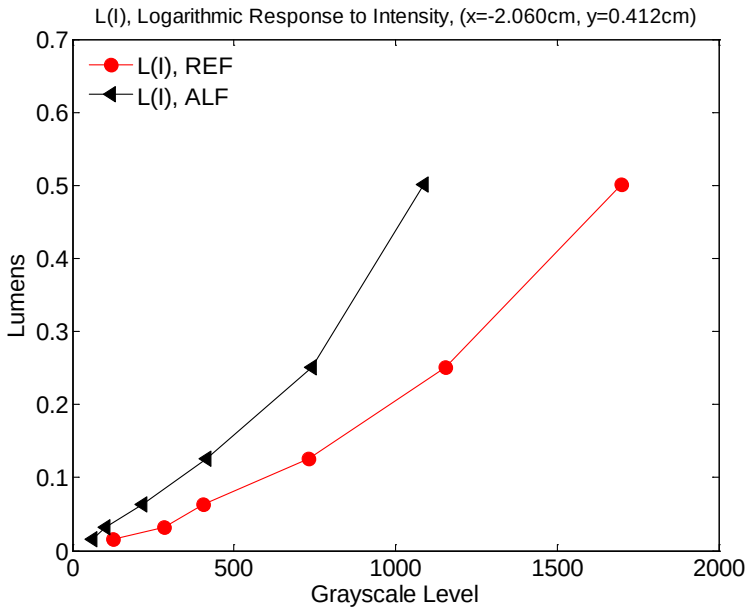

Figure 33 L(I), Logarithmic Response to Intensity

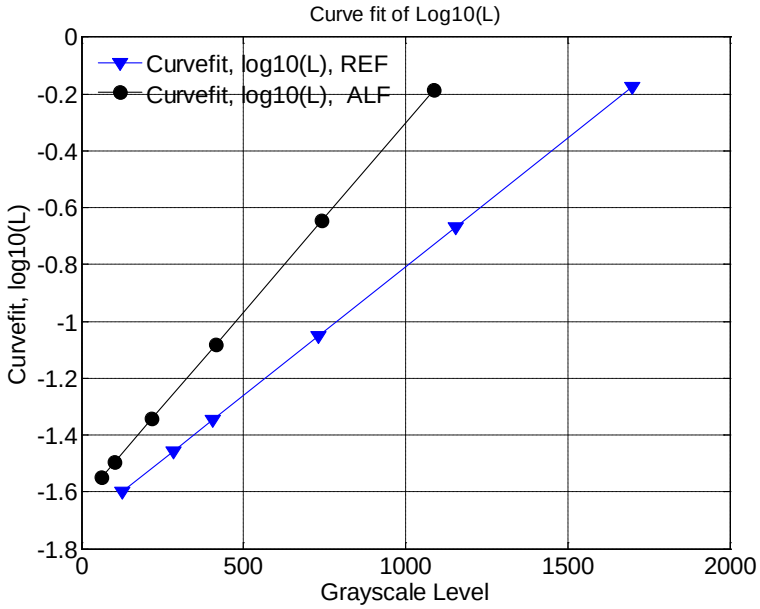

Figure 34 Exponential Curve of L(I) (x=-2.060cm, y=0.412cm)

Placing the incandescent light table right in front of the DGV analysis unit in the plane where the jet axis lies, with Neutral Density Filters of 0.3, 0.6, 0.9, 0.3+0.9, 0.6+0.9 and 0.3+0.6+0.9 being installed in front of the telecentric lens of the Doppler Image Analysis Unit, a set of six pairs of tiff images are captured and forwarded to the program Intensity_Calibration.m in MatLab, seen in Appendix A. Due to the fact that the grayscale-to-light intensity response characteristics of CMOS camera is logarithmic, the intensity calibration is performed in the form of $\log10(L)= a\times I+b$, where L refers to the virtual 'lumens' of the light, I refers to the grayscale level of each pixel, 'a' and 'b' are coefficients to be calculated, since in this way, the scope of the curve fit for intensity calibration is fixed eliminating the possibility of oscillating relationship between the independent variable (grayscale) and dependent variable (lumens). The intensity calibration result is shown in Figure 32, Figure 33 and Figure 34.

7. RESULTS AND DISCUSSION

This chapter presents the results obtained by the DGV technique along with analysis and sources of error. Before the analysis of the final results, a stepwise image processing procedure, which shows the elimination of errors for increase the accuracy of the DGV system, is covered.

Measurements are performed across the rotating disc and for four flow cases across the axisymmetric free-expansion subsonic jet.

7.1. Laser Stability

Laser stability is a factor of critical importance in this study of the DGV system. Since the fundamental mechanism for the flow field velocity measurement and calculation is based upon the Doppler frequency shift, if any laser frequency shift occurs in the experiment, it will result in significant error in the velocity calculation. Therefore, the laser frequency must be stable during the image recording and data acquisition process. The laser system requires a 5-minute warm-up period after the power supply is turned on, at this time, the indicator is constant orange. Then the laser is switched on and then the boot sequence starts, now the indicator is blinking in green. After the 20-minute boot sequence, the indicator turns from blinking green into constant green, which indicates that the laser system is stable and ready for use. Whenever the indicator starts blinking again in green during processes of ALF cell calibration and measurement, unstable laser light and laser frequency drift are suggested. During the ALF cell

calibration, since the WL value is set through the PM 100D LabView code to decrease by 25 automatically in every 20 seconds, the indicator will be observed blinking in green whenever the WL is changing, the blinking will last for about 12 seconds and then become continuously green again, which means that the laser light is stabilized again for the test of next new WL value.

7.2. Calibration of the Iodine Cell

The absorption line filter must be calibrated prior to each test to obtain the relationship between the transmission ratio and the laser frequency shift. Since as the operation time accumulates, unexpected frequency drift of the laser source may be experienced. In this study, the laser light source applied is an Oxxius 532-S diode pumped solid state laser with its wavelength and stable frequency being 532nm and $5.6x10^{14}$ Hz (namely, $5.6x10^{5}$ GHz), respectively.

The wavelength of the laser light source is adjustable through a LabView code by changing the value of a parameter named WL, therefore the frequency of the laser light source is adjustable. The available range of WL value is -2000 to 2000, which represents a change in wavelength from -5 pm (pm means picometer, $1pm=1x10^{-3}$ $nm=1x10^{-12}$ m) to 5 pm. In this study, the range of WL value actually applied is -500 to 500, representing a change in wavelength from -1.25pm to 1.25pm, resulting in a corresponding wavelength range of the laser light source being from 531.99875nm to 532.00125nm. According to the equation (3), the corresponding frequency shift represented by this wavelength range is 2.648119 GHz.

$$f = \frac{c}{\lambda} \qquad (3)$$

where f is the frequency of the laser light, λ is the wavelength of the laser light, c is the light speed, c=299792458 m/s.

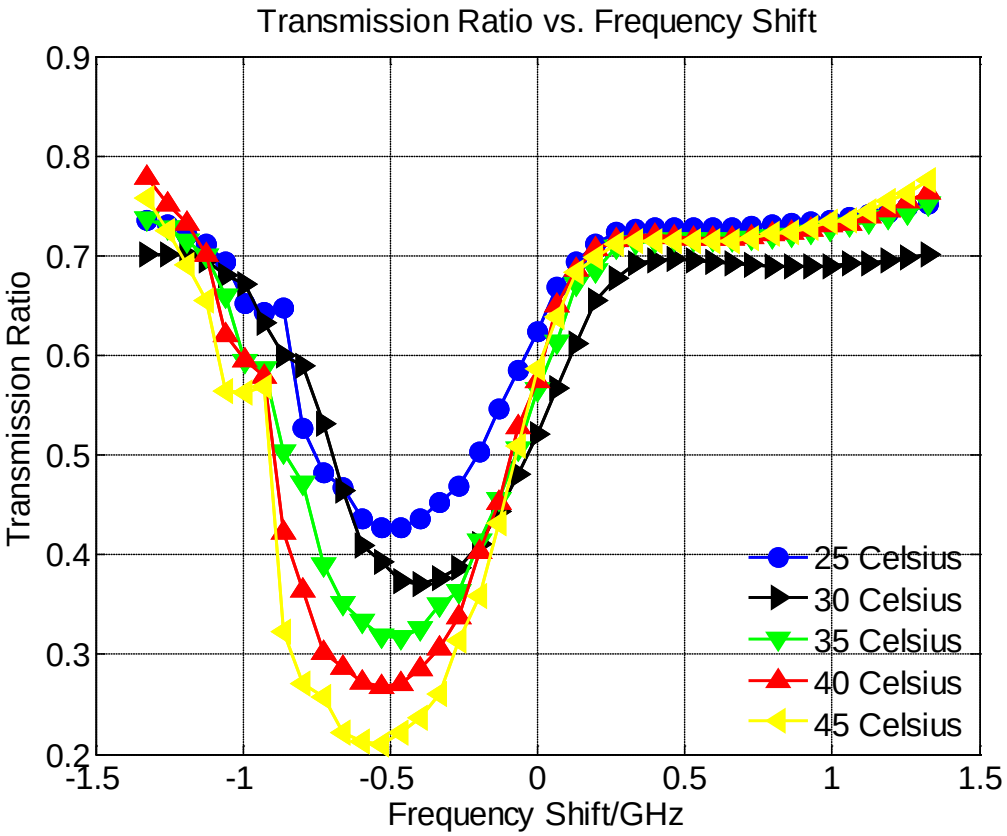

Figure 35 Temperature Dependence of Iodine inside ALF Cell

The filtering ability of the Absorption Line Filter (ALF) cell comes from the filtering medium inside the ALF cell, which is iodine vapor. Since the filtering ability of the iodine vapor is dependent on its thermal state, the relationship between transmission ratio and frequency shift of the ALF cell needs to be calibrated under different

temperatures. Calibration is also required before each measurement of the velocity of the free-expansion subsonic jet flow field. The temperature of the ALF cell is controlled through LabView which can directly set the desired temperature to which the ALF cell needs to be heated. To accomplish this controlled heating on the ALF cell, two Thorlabs GCH25 heater rings are attached to the ALF cell which is assembled with a CQ 19100-I quartz glass tube with iodine vapor sealed inside. In this study, the temperature of the ALF cell is set from 25℃ to 45℃, the original transmission curve obtained under each specific temperature within this range is shown in Figure 35.

Curve fit is performed through Matlab function 'polyfit' in this study to obtain an equation reflecting the relationship between the transmission ratio and the frequency shift for the above mentioned absorption line profile. Information on 'polyfit' function in Matlab code can be found in Appendix A. Matlab Program for Data Reduction and Processing. Taking transmission ratio curve for ALF cell under 45℃ for example, the obtained curve fit equation is a 12-order polynomial: $\mathrm{Tr} = -0.0760 \times \Delta\nu^{12} - 0.4454 \times \Delta\nu^{11} + 0.3954 \times \Delta\nu^{10} + 2.1171 \times \Delta\nu^{9} - 0.4732 \times \Delta\nu^{8} - 3.7736 \times \Delta\nu^{7} - 0.6636 \times \Delta\nu^{6} + 3.4307 \times \Delta\nu^{5} + 1.6991 \times \Delta\nu^{4} - 2.1185 \times \Delta\nu^{3} - 0.8371 \times \Delta\nu^{2} + 0.8833 \times \Delta\nu + 0.5702$, with R^2=0.9858 indicating that the variation relationship between the laser frequency shift and the ALF cell's transmission ratio is well described by the curve fit equation, where Tr refers to the transmission ratio of the ALF cell, $\Delta\nu$ represents the laser frequency shift. The comparison between the original transmission curve and the curve fit transmission curve under 45℃, 40℃, 35℃, 30℃, and 25℃ are presented in Figure 36, Figure 37, Figure 38, Figure 39, and Figure 40.

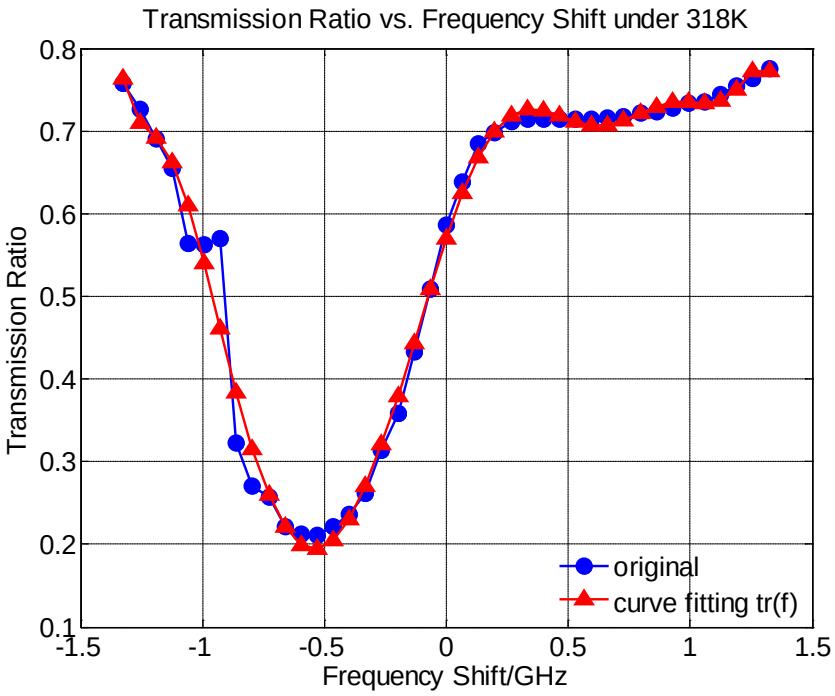

Figure 36 Transmission Ratio vs. Frequency Shift under 318K, R^2=0.9916

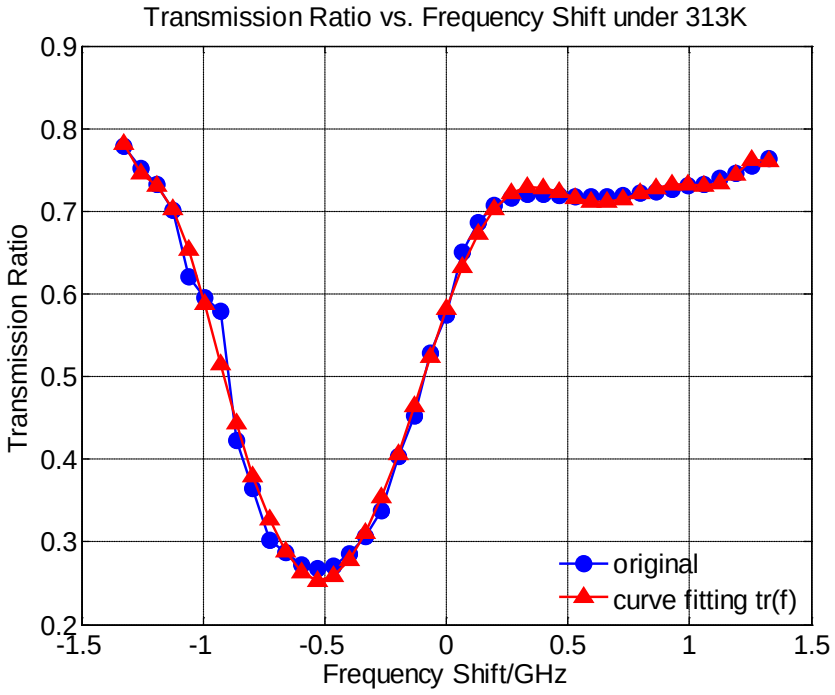

Figure 37 Transmission Ratio vs. Frequency Shift under 313K, R^2=0.9951

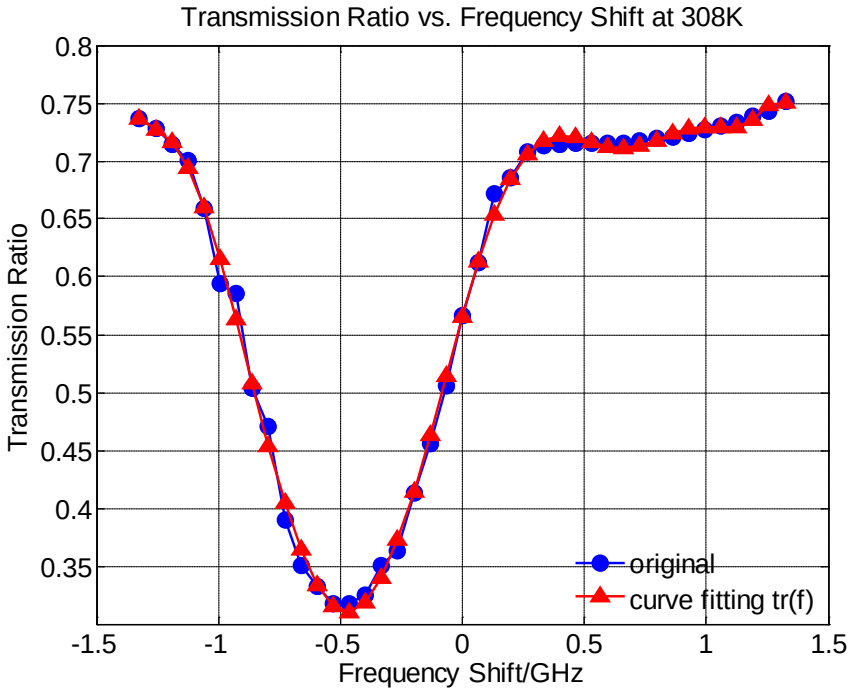

Figure 38 Transmission Ratio vs. Frequency Shift under 308K, R^2=0.9972

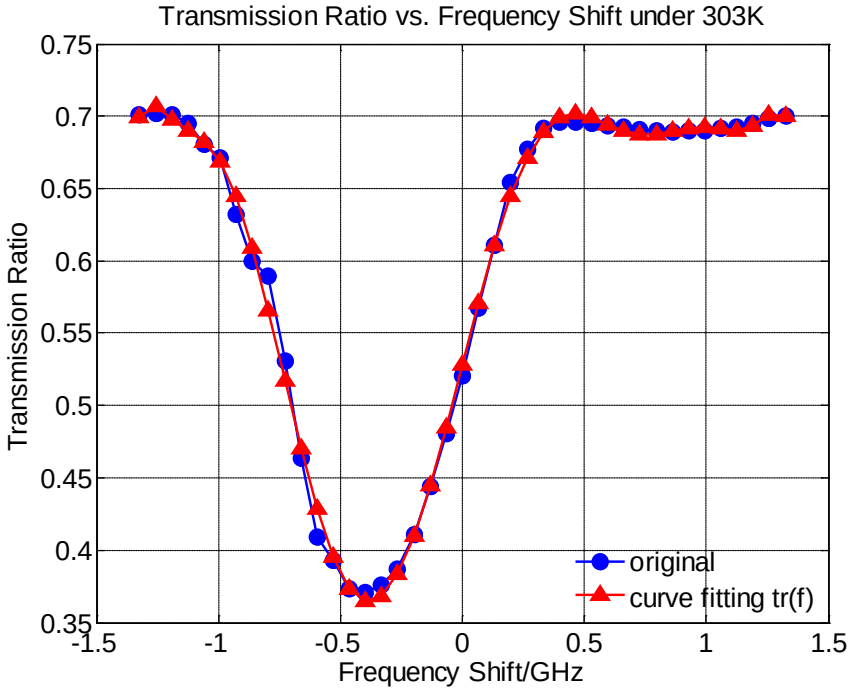

Figure 39 Transmission Ratio vs. Frequency Shift under 303K, R^2=0.9967

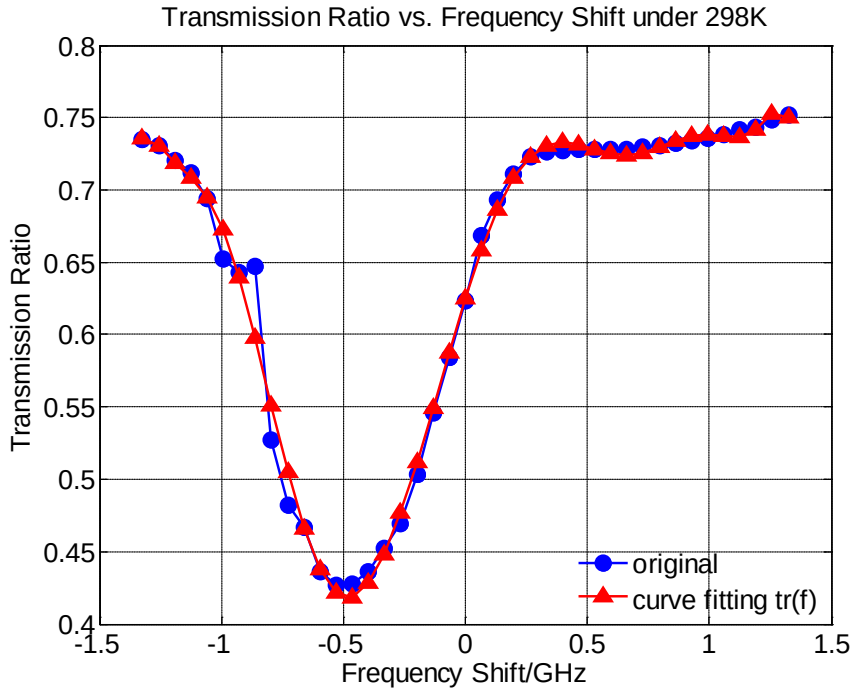

Figure 40 Transmission Ratio vs. Frequency Shift under 298K, R^2=0.9910

As indicated in Figure 36 to Figure 40, as well as in Figure 35, the ALF cell exhibits better transmission-frequency shift relationship as the temperature to which the ALF cell is heated increases. Based upon the transmission curve obtained under each specific temperature, a section of the absorption line profile with the frequency shift ranging from -0.5 GHz to 0.5 GHz is selected for subsequent velocity measurements.

7.3. Image Processing Methods and Analysis

At the very beginning, the ALF cell in the DGV analysis unit and the ALF cell on the laser side are both heated to a same specific temperature through setting the two temperature controllers to a same temperature. After the thermal status of both ALF cells gradually stabilizes at that selected temperature, the ALF cell filtering characteristics is

calibrated and then the laser source frequency is set through inputting a specific WL value via LabView code. As the laser source becomes stable in its newly set frequency and ready for use, the shutter is removed and the laser light goes through a series of optic lens and forms a light sheet, the plane of which is coincident with the plane where the subsonic jet flow axis lies.

Once the seeded flow is turned on, laser light scattered by the particles travelling with the air flow is collected by the Phantom V711 high speed camera of the DGV analysis unit, CINE RAW format video is recorded and then converted into 12-bit TIFF images. For each 12-bit TIFF image, a 640 × 640 pixel area is extracted from REF image and ALF image, respectively.

Due to application of a series of convex and concave optic lens within the DGV analysis unit, the image orientation captured by Phantom is actually rotated by 180° compared with the physical situation. Therefore, the original grayscale matrix of each image is first restored back to its physical orientation by flipping pixel information upside down in rows ('Irefs(i,j,k)=Iref(640-i+1,j,k)') and then flipping pixel information left to right in columns ('Iref(i,j,k)=Irefs(i,640-j+1,k)'), and then the restored matrix is saved for further processing. By this step, the image ready for further processing is consistent with the physical situation in orientation. Figures regarding light table and subsonic jet flow shown below are all consistent with their corresponding physical situations in orientation. Figure 41 and Figure 42 present the restored grayscale contour of REF and ALF images for incandescent light table applying Neutral Density Filter ND003.

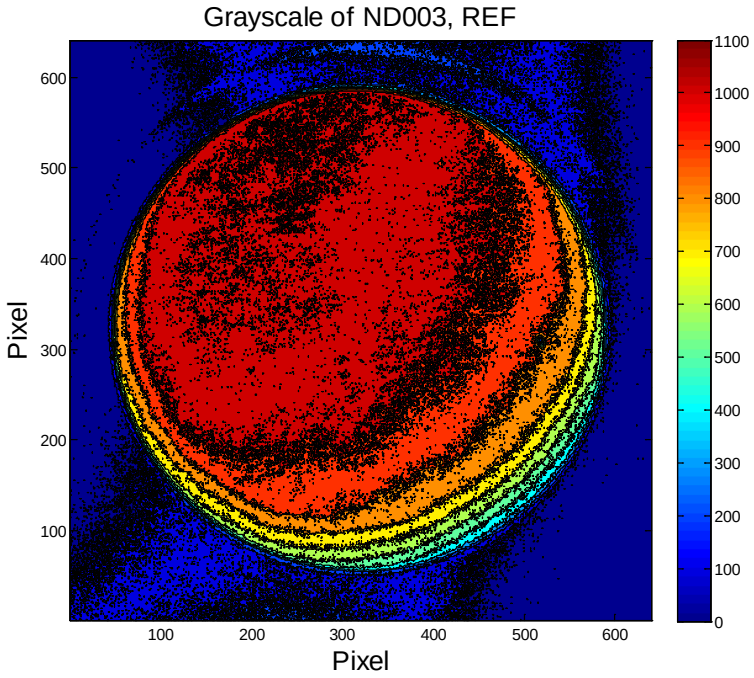

Figure 41 Grayscale of Incandescent Light Table Applying ND003, REF

Once the original grayscale matrix is restored back to its physical situation in orientation, results obtained from spatial and intensity calibration are applied to convert grayscale of each pixel into lumens. Lumens information of the ALF image is compared with the REF image to obtain the transmission ratio distribution. Since we already know the ALF cell calibration transmission ratio curve, we know the relationship between transmission ratio and frequency shift. Therefore, corresponding frequency shift for a given transmission ratio is to be calculated. This obtained frequency shift is then applied into the equation (1) for the velocity at that single point. Following the same process, the velocity profile for the subsonic jet flow captured by the Phantom camera is achieved.

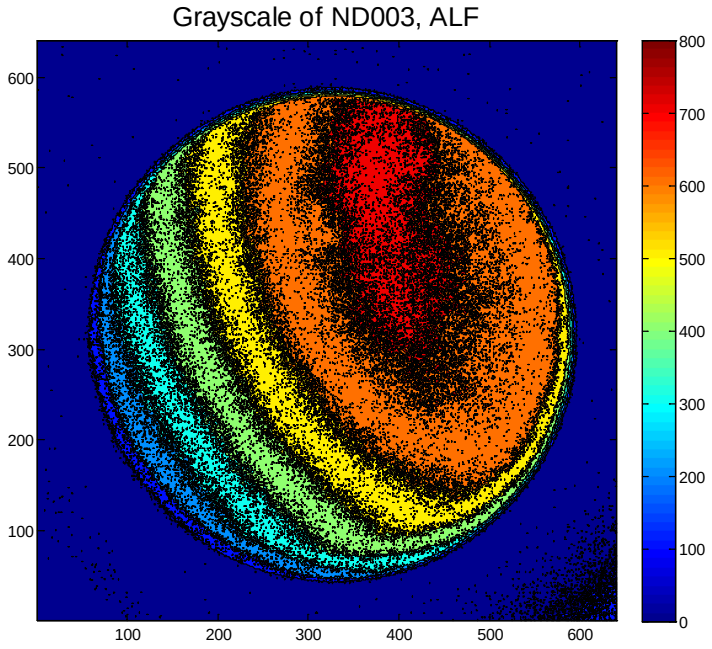

Figure 42 Grayscale of Incandescent Light Table Applying ND003, ALF

7.4. Free-Expansion Subsonic Jet Velocity Measurement

The free-expansion subsonic jet applied in this study has an outlet of 12.5mm in diameter. The air flow is supplied by an air compressor and seeded by a TSI Six-Jet Atomizer Model 9306. The jet is also connected to a Meriam 30PG10-TM-61-A manometer indicating the actual speed of the jet flow.

7.4.1. Subsonic Jet Flow Measurement under 45℃, 110mph

With both ALF cell heated to and stabilized at 45℃ and laser source set to be WL=75, the grayscale contours of the jet flow for REF and ALF are shown in Figure 43 and Figure 44.

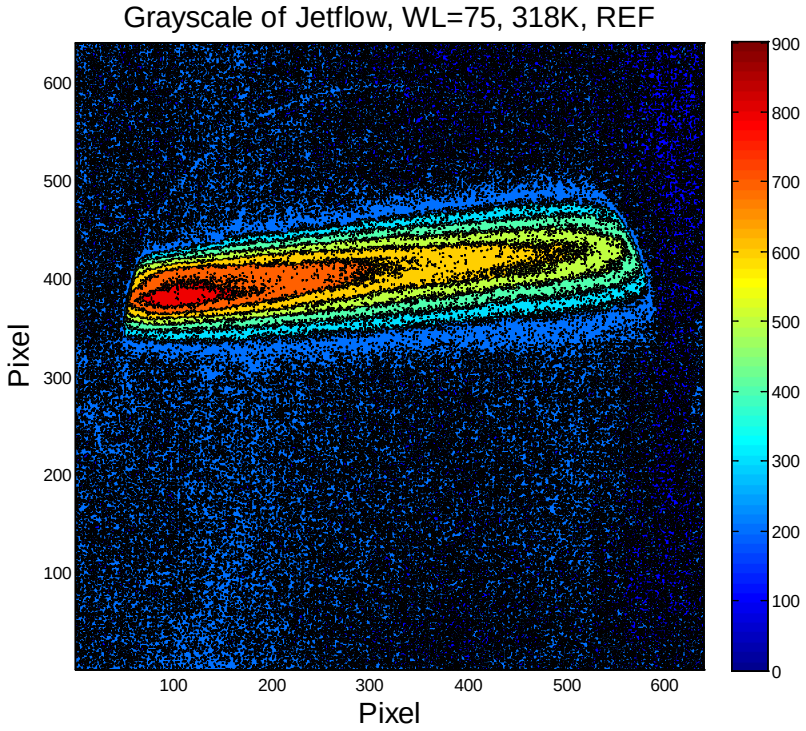

Figure 43 Grayscale of Subsonic Jet Flow, WL=75, 45℃, REF

According to intensity calibration results for each pixel obtained in Section 6.2, the grayscale information is transferred into 'lumens', the virtual parameter indicating the power of the scattered light collected by Phantom camera.

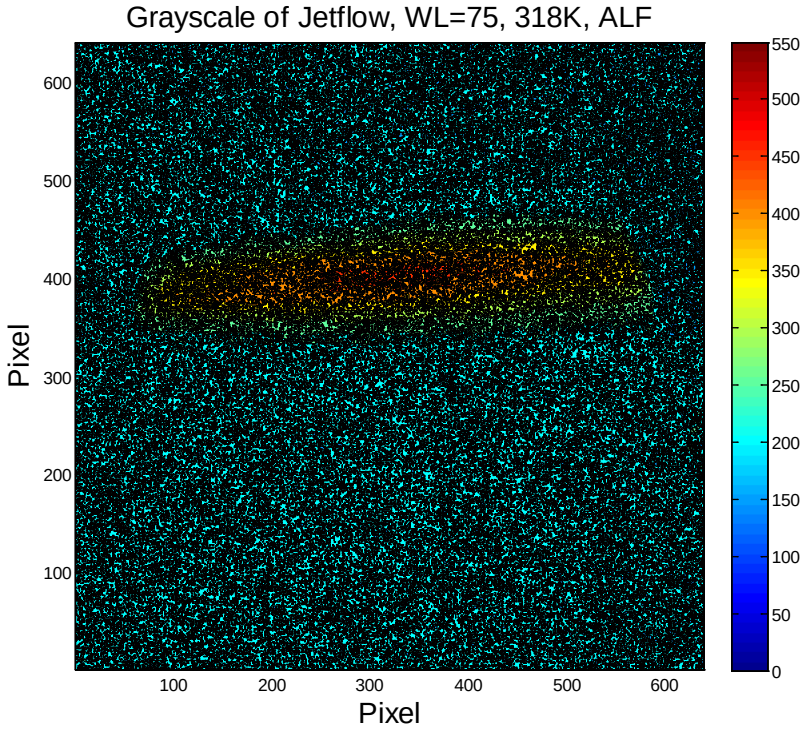

Figure 44 Grayscale of Subsonic Jet Flow, WL=75, 45℃, ALF

At this stage, the raw lumens contour still contains significant noise in the signal, including noise from singular point in intensity calibration results, as well noise coming from the test environment. Therefore, a threshold is applied to the raw lumens to obtain more accurate lumens distribution for the jet flow. Figure 45 and Figure 46 present the lumens distribution in REF and ALF images for jet flow before thresholding.

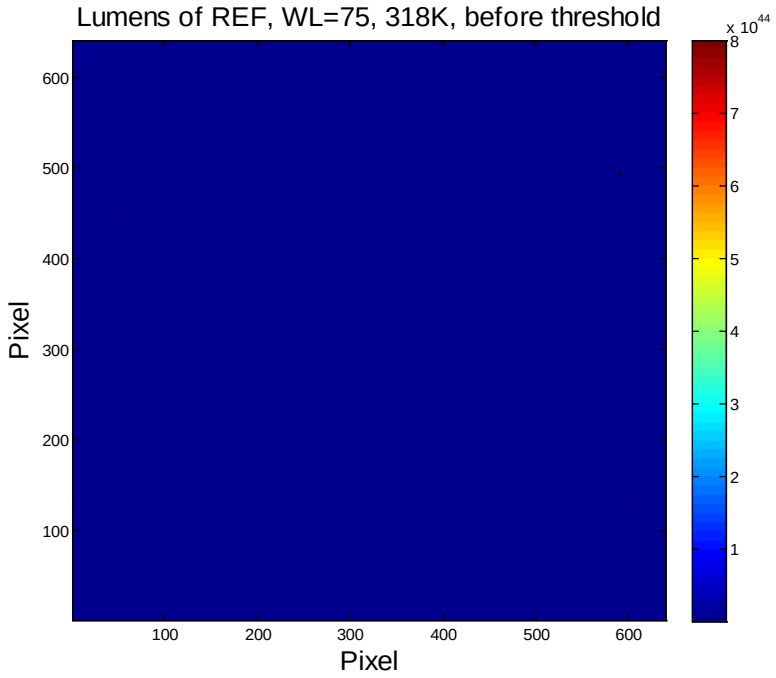

Figure 45 Lumens of Jet Flow before Threshold, WL=75, 45℃, REF

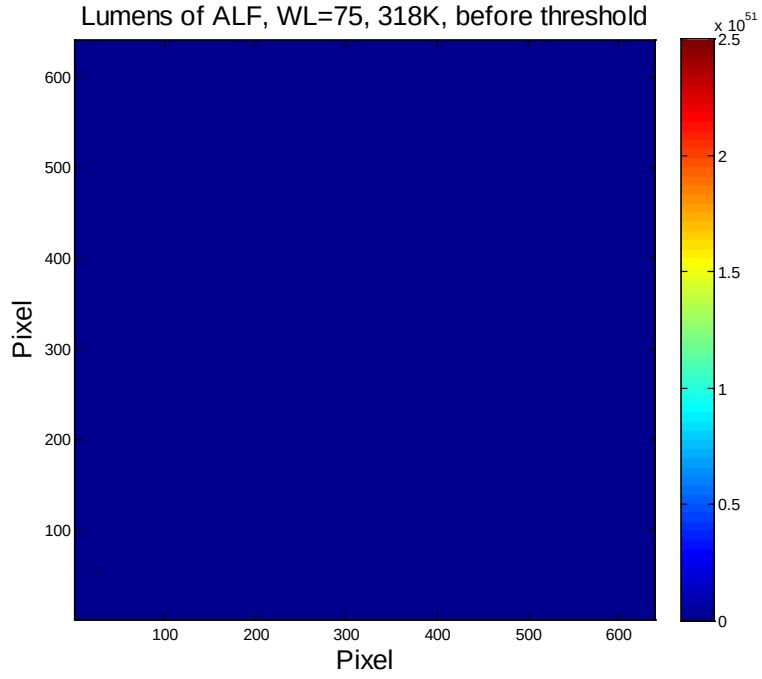

Figure 46 Lumens of Jet Flow before Threshold, WL=75, 45℃, ALF

Given the fact that the highest lumens value during the intensity calibration is obtained when the Neutral Density Filter ND003 alone is applied, therefore the threshold is set as $10^{-0.3}$=0.5012. For ALF image, any pixel carrying lumens value higher than 0.5012× Tr(WL=75, T=45℃) is reset to be 0. However, considering the fact that the key parameter calculated is the transmission ratio of each pair of matching pixel ($Tr = \frac{\text{lumens of ALF}}{\text{lumens of REF}}$), those pixels carrying lumens values over 0.5012 in REF are reset to be 1.0. In this way, those pixels carrying noise information are eliminated in the transmission ratio distribution after the threshold. Lumens contours for the jet flow after threshold are shown in Figure 47 and Figure 48. As indicated, after the threshold, the shape of the jet flow in REF and ALF images can be obviously observed, while before threshold, basically nothing is distinguishable from the lumens contour with noise information, and the lumens values' for both REF and ALF images are absolutely beyond their reasonable ranges. After the threshold, the lumens value of REF image ranges in 0 to 1.0, lumens value of ALF image ranges in 0 to 0.25.

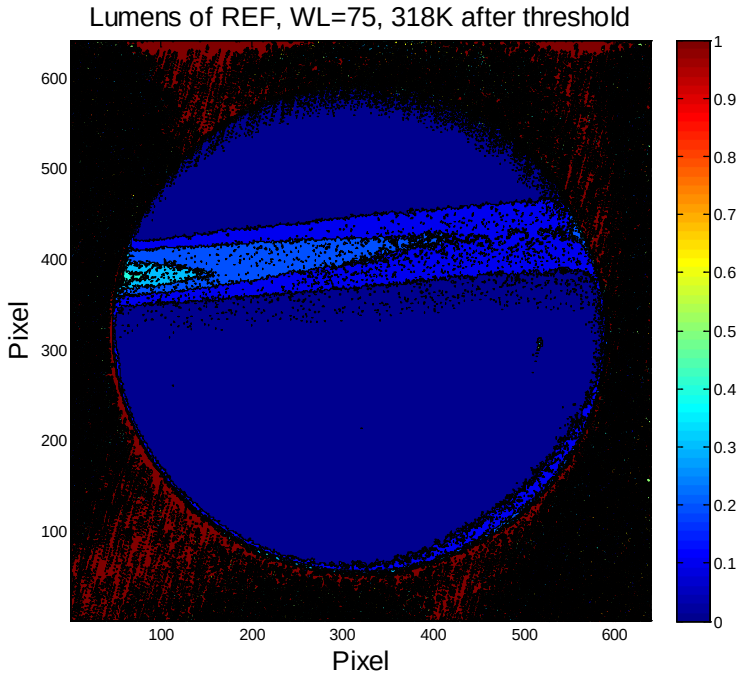

Figure 47 Lumens of Jet Flow after Threshold, 45℃, REF

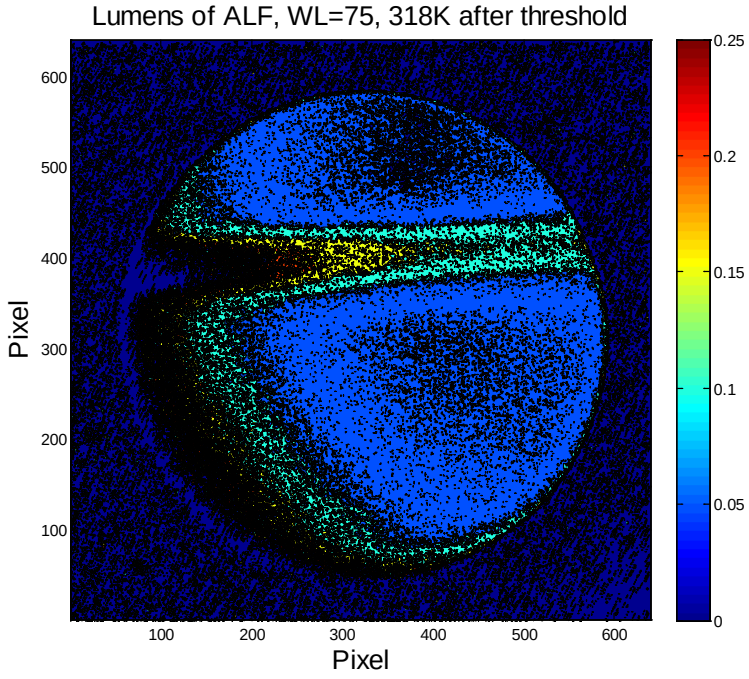

Figure 48 Lumens of Jet Flow after Threshold, 45℃, ALF

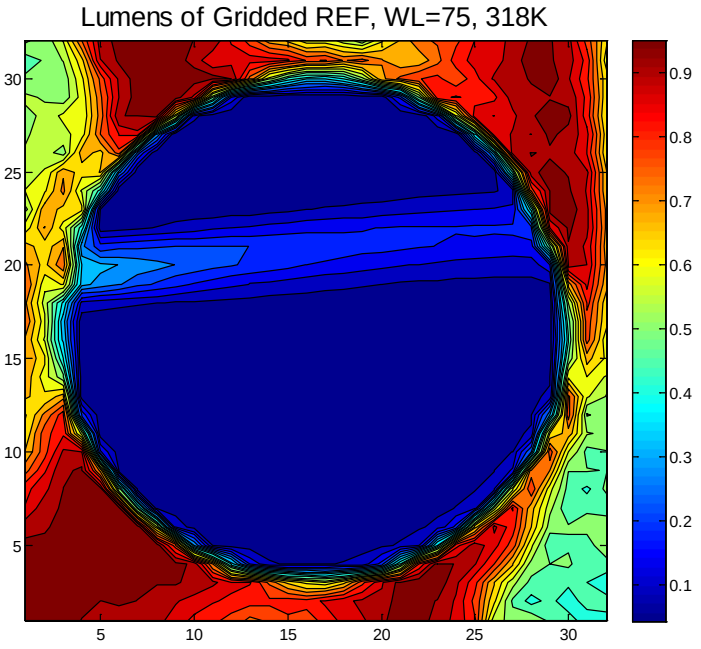

Figure 49 Lumens of Gridded Jet Flow, 20×20, 45℃, REF

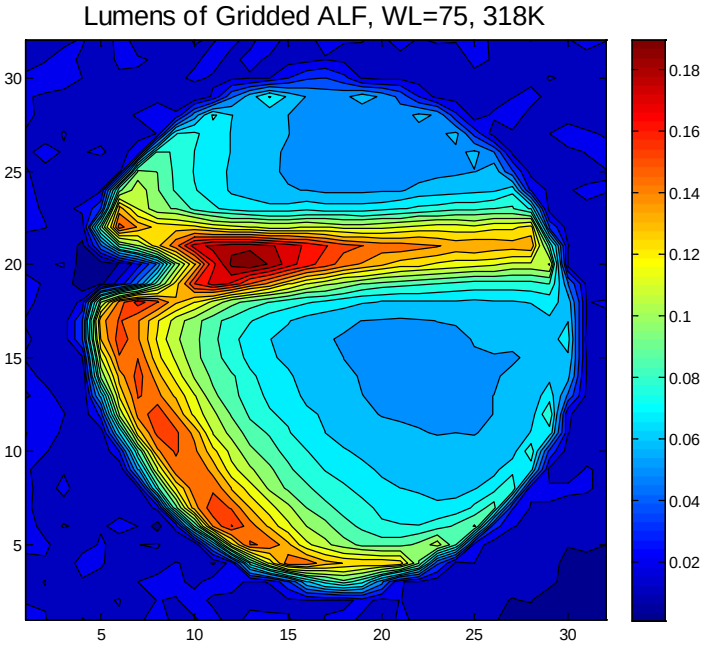

Figure 50 Lumens of Gridded Jet Flow, 20×20, 45℃, ALF

Although spatial calibration has been performed, error in matching pixels between images still exists. To further eliminate this matching error, image gridding is applied in this study to obtain more accurate transmission ratio distribution. In detail, the REF and ALF images are gridded by 20×20 in pixels. The lumens values of the 20×20 pixel area are summed up and then divided by the number of pixels in that area. Lumens distribution after gridding for jet flow under 45℃ at WL=75 for REF and ALF are presented in Figure 49 and Figure 50.

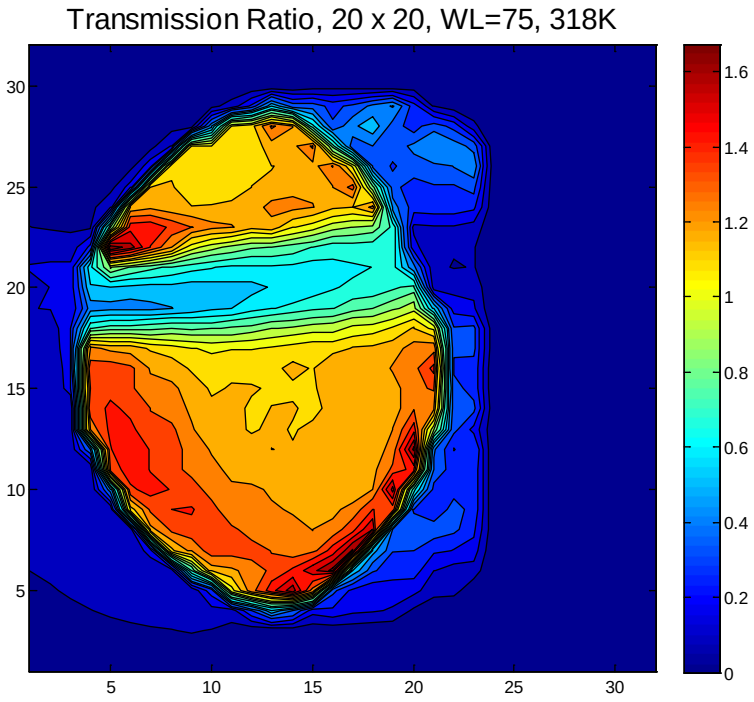

Figure 51 Transmission Ratio, WL=75, 45℃

Figure 51 presents the transmission ratio distribution. Figure 52 shows the original transmission ratio calibration curve for the laser source under 45℃ and the curve fit for the section of the curve selected for velocity measurement, indicated in blue and red, respectively. The selected section for velocity measurement is curve fitted using 9-order polynomial, with R^2=0.9982. The curve fit result for this section of transmission ratio curve is: $\Delta\upsilon = a_i \times tr^{10-i}$, i=1~10, coefficients of each order is shown in Table 3. Using this curve fit equation, the corresponding frequency shift is obtained as shown in Figure 53.

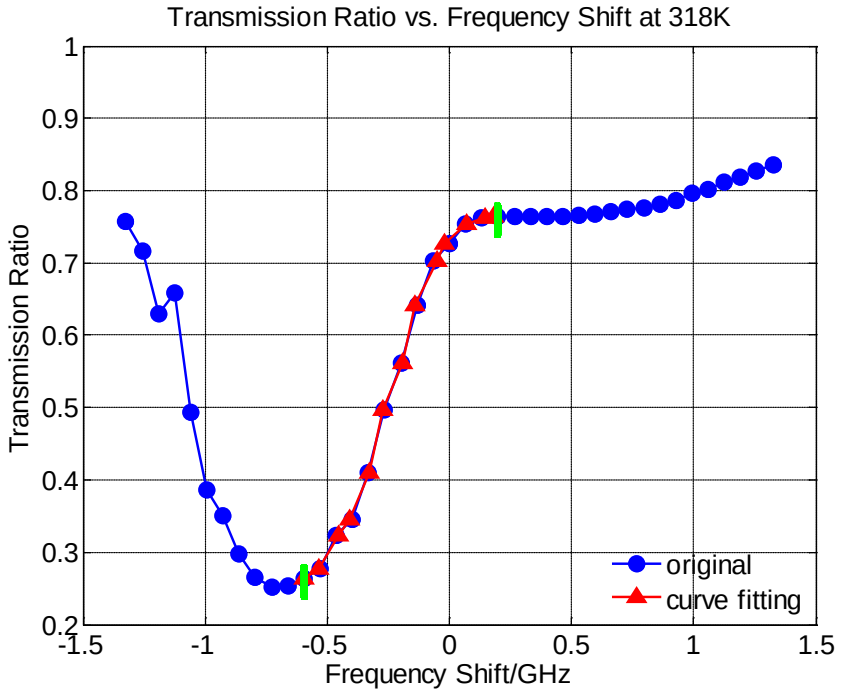

Figure 52 Transmission Ratio Curve Section for Velocity Measurement, 45℃

Table 3 Curve Fit Coefficients for Transmission Ratio Curve, 45℃

Term	*Coefficient*	*Term*	*Coefficient*
tr^9	8.8743e+05	tr^8	-4.0810e+06
tr^7	8.2200e+06	tr^6	-9.5113e+06
tr^5	6.9622e+0.6	tr^4	-3.3413e+06
tr^3	1.0508e+06	tr^2	-2.0873e+05
tr	2.3763e+04	*1*	-1.1822e+03

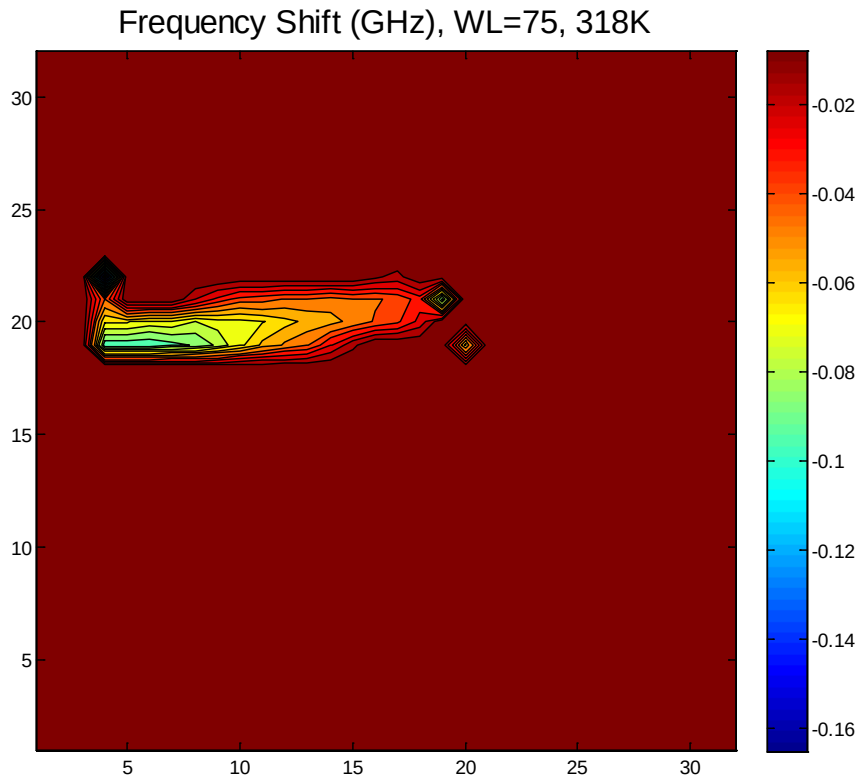

Figure 53 Frequency Shift of Jet Flow (GHz), 45℃,

As shown in Figure 53, the frequency shift ranges from -0.16GHz to -0.02GHz, and corresponding measured velocity of jet is shown in Figure 54. The actual flow speed measured by the manometer is 110mph, which is 48.89m/s, the measured velocity ranges

from 0 to 48m/s. As indicated by both the frequency shift distribution and the measured velocity distribution, the region of jet flow is composed of several different sub-layers. The center region of the jet flow has the highest velocity. In both vertical direction and horizontal direction, as the velocity of the jet flow reduces as the location of interest moves farther from the center of the jet flow.

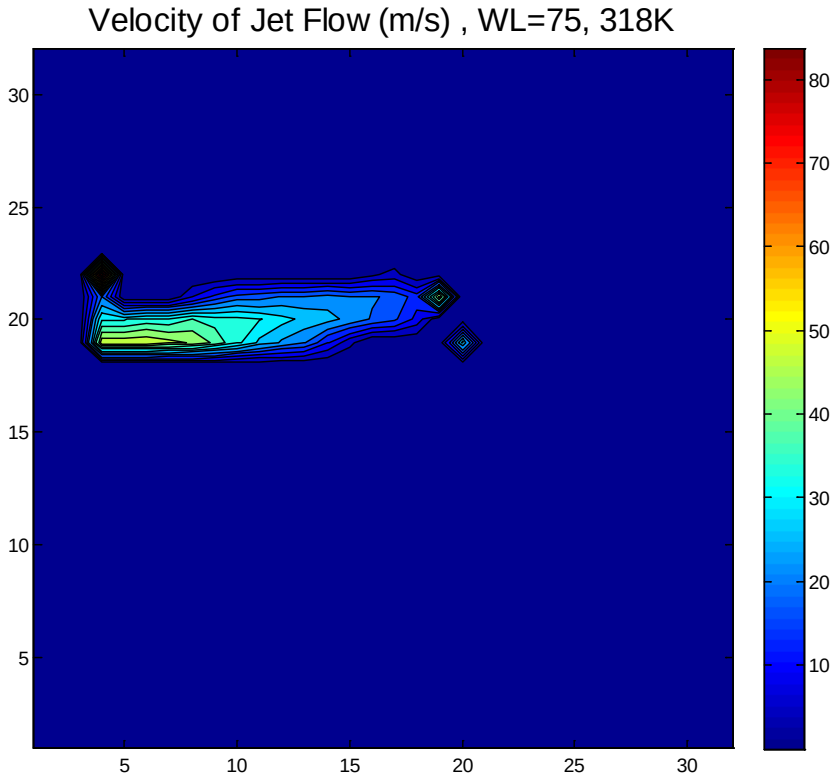

Figure 54 Measured Velocity of Jet Flow (m/s), 45℃,

7.4.2. Subsonic Jet Flow Measurement under 40℃, 105mph

With both ALF cell heated to and stabilized at 40℃ and laser source set to be WL=75, the grayscale contours of the jet flow for REF and ALF are shown in Figure 55 and Figure 56.

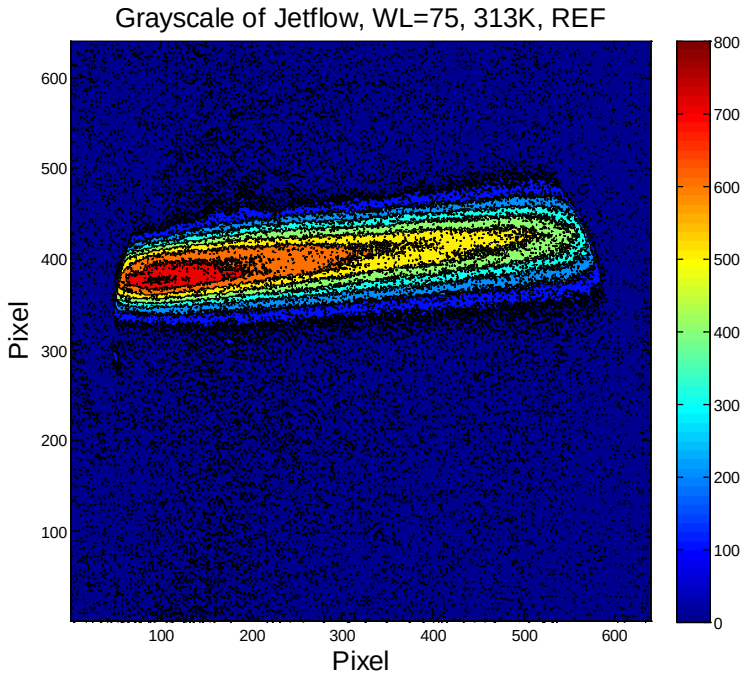

Figure 55 Grayscale of Subsonic Jet Flow, WL=75, 40℃, REF

According to intensity calibration results for each pixel obtained in Section 6.2, the grayscale information is transferred into 'lumens', the virtual parameter indicating the power of the scattered light collected by Phantom camera.

Like the situation for flow jet under 45℃**,** at this stage, the raw lumens contour still contains significant noise in the signal, including noise from singular points in

intensity calibration results, as well as noise coming from the test environment. Therefore, thresholds are applied to the raw lumens to obtain more accurate lumens distribution for the jet flow. Figure 57 and Figure 58 present the lumens distribution in REF and ALF images for jet flow before thresholding.

Given the fact that the highest lumens value during the intensity calibration is obtained when the Neutral Density Filter ND003 alone is applied, therefore the threshold is set as $10^{-0.3}$=0.5012. For ALF image, any pixel carrying lumens value higher than 0.5012× Tr(WL=75, T=40℃) is reset to be 0. However, considering the fact that the key parameter calculated is the transmission ratio of each pair of matching pixel ($Tr = \frac{\text{lumens of ALF}}{\text{lumens of REF}}$), those pixels carrying lumens values over 0.5012 in REF are reset to be 1.0.

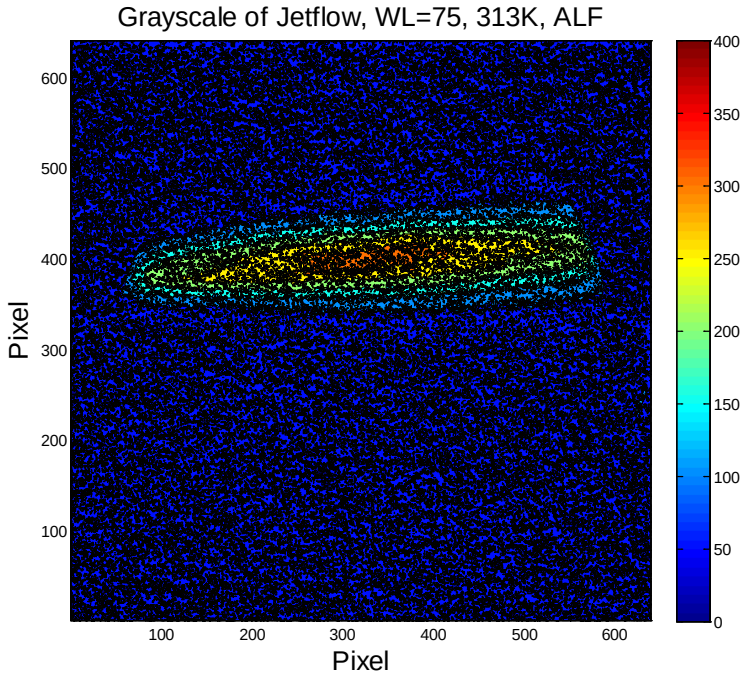

Figure 56 Grayscale of Subsonic Jet Flow, WL=75, 40℃ , ALF

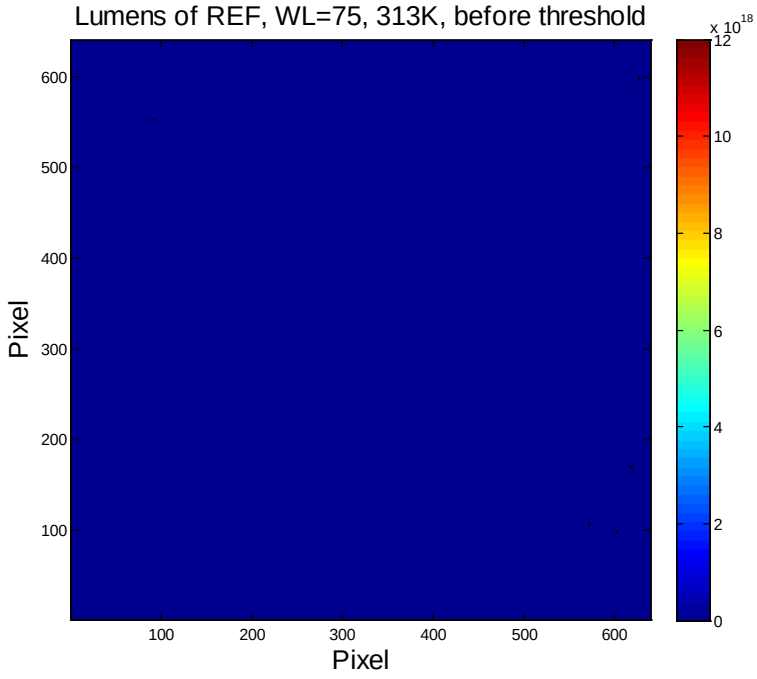

Figure 57 Lumens of Jet Flow before Threshold, WL=75, 40℃ , REF

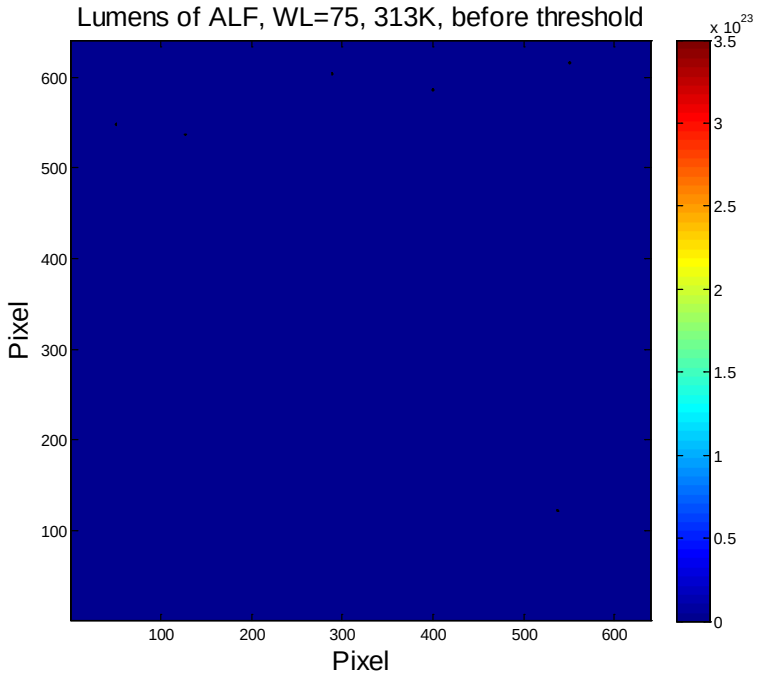

Figure 58 Lumens of Jet Flow before Threshold, WL=75, 40℃ , ALF

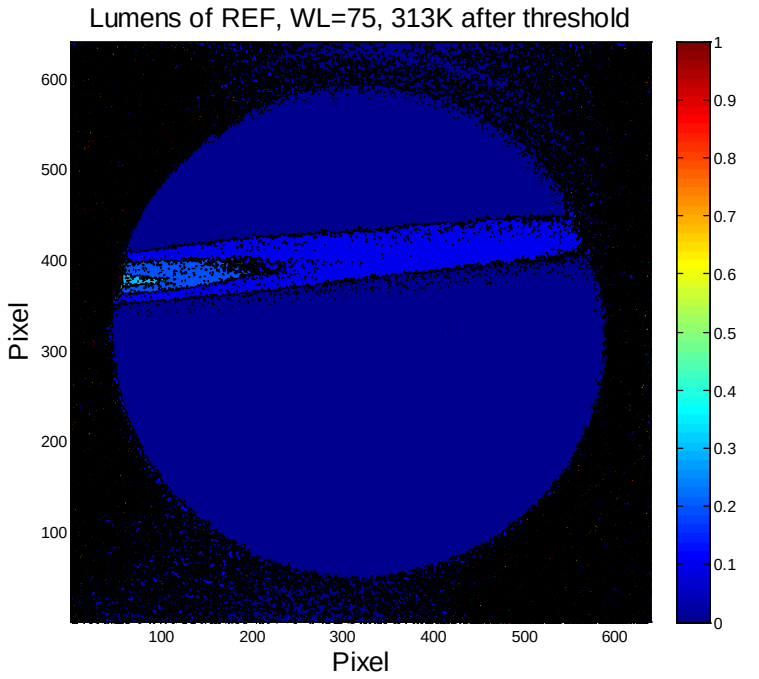

Figure 59 Lumens of Jet Flow after Threshold, 40℃ , REF

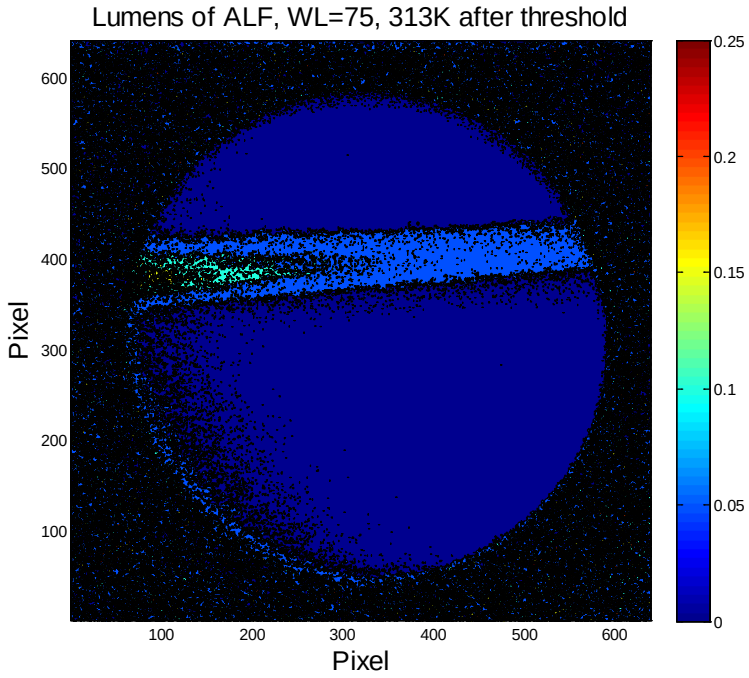

Figure 60 Lumens of Jet Flow after Threshold, 40℃ , ALF

In this way, those pixels carrying noise information are eliminated in the transmission ratio distribution after the threshold.

Lumens contours for the jet flow after threshold are shown in Figure 59 and Figure 60. As indicated, after the first threshold, the shape of the jet flow in REF and ALF images can be obviously observed, while before threshold, basically nothing is distinguishable from the lumens contour with noise information, and the lumens values' for both REF and ALF images are absolutely beyond their reasonable ranges.

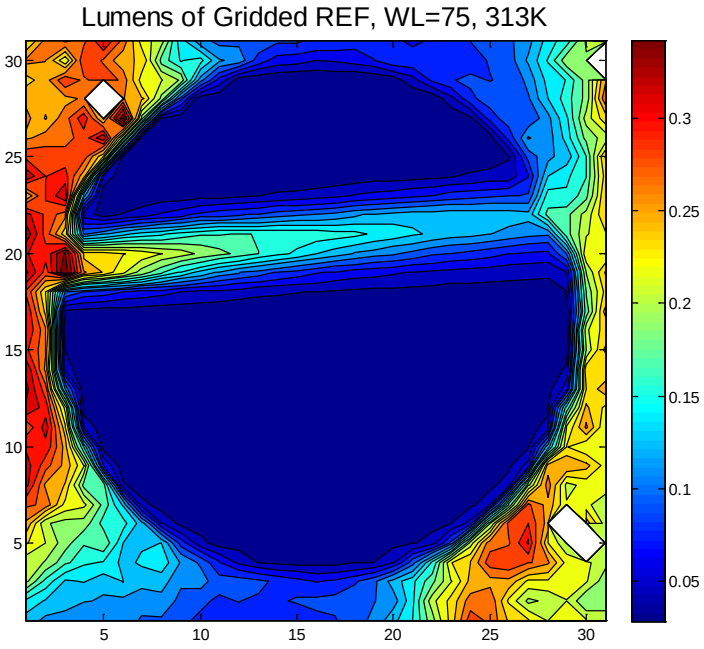

Figure 61 Lumens of Gridded Jet Flow, 20×20, 40℃, REF

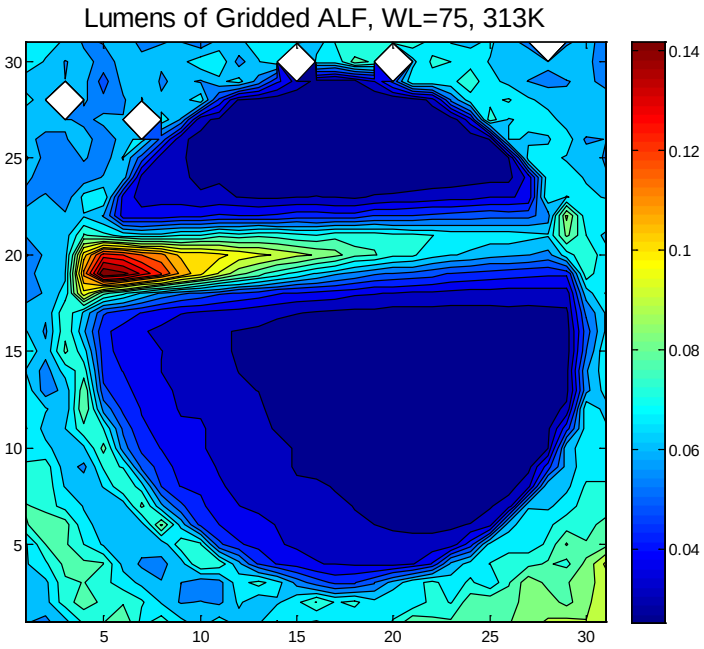

Figure 62 Lumens of Gridded Jet Flow, 20×20, 40℃, ALF

Although spatial calibration has been performed, error in matching pixels between images still exists. To further eliminate this matching error, image gridding is applied in this study to obtain more accurate transmission ratio distribution. In detail, the REF and ALF images are gridded by 20×20 in pixels. The lumens values of the 20×20 pixel area are summed up and then divided by the number of pixels in that area. Lumens distribution after gridding for jet flow under 40℃ at WL=75 for REF and ALF are presented in Figure 61 and Figure 62.

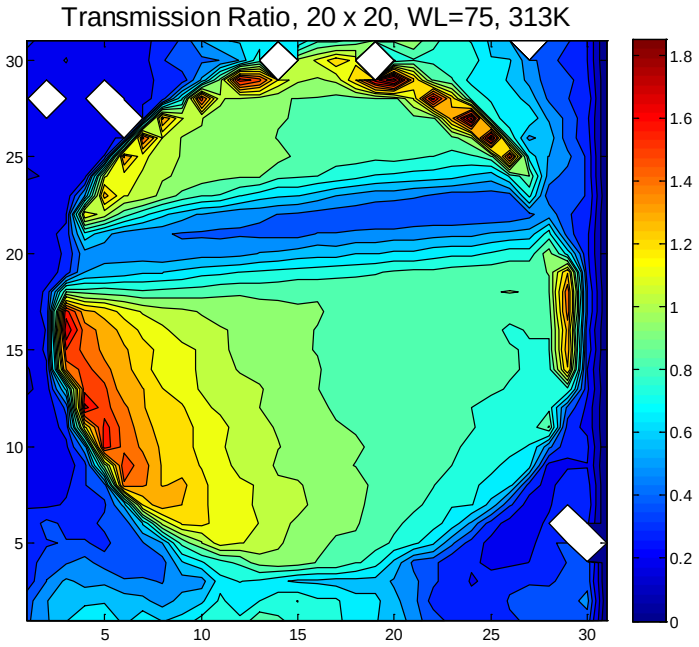

Figure 63 Transmission Ratio, WL=75, 40℃

Figure 63 presents the transmission ratio distribution. Figure 64 shows the original transmission ratio calibration curve for the laser source under 40℃ and the curve

fit for the section of the curve selected for velocity measurement, indicated in blue and red, respectively. The selected section for velocity measurement is curve fitted using 9-order polynomial, with R^2=0.9998. The curve fit result for this section of transmission ratio curve is: $\Delta\upsilon = a_i \times tr^{10-i}$, i=1~10, coefficients of each order is shown in Table 4. The corresponding frequency shift is obtained using this curve fit equation, as shown in Figure 65.

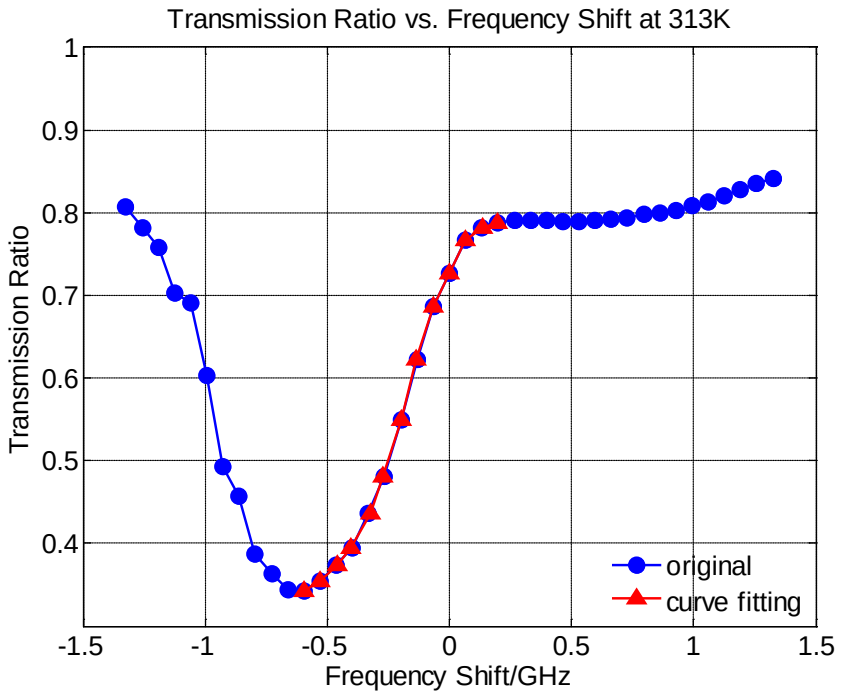

Figure 64 Transmission Ratio Curve Section for Velocity Measurement, 40℃

Table 4 Curve Fit Coefficients for Transmission Ratio Curve, 40℃

Term	*Coefficient*	*Term*	*Coefficient*
tr^9	8.2758e+05	tr^8	-4.0878e+06
tr^7	8.8916e+06	tr^6	-1.1177e+07
tr^5	8.9487e+06	tr^4	-4.7323e+06
tr^3	1.6533e+06	tr^2	-3.6805e+05
tr	4.7402e+04	*1*	-2.6933e+03

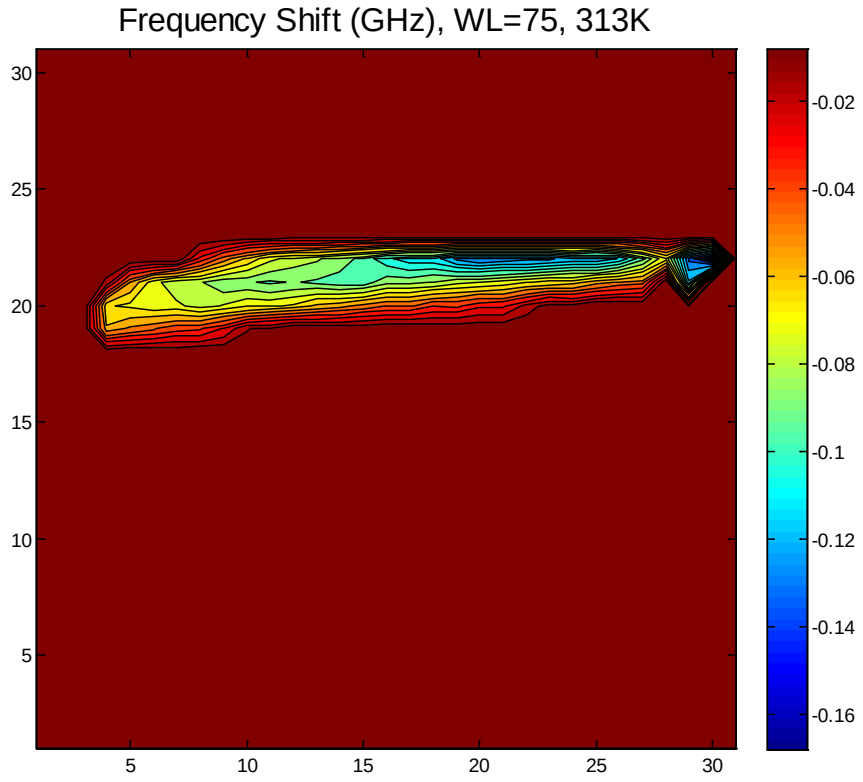

Figure 65 Frequency Shift of Jet Flow, 40℃

As shown in Figure 65, the frequency shift ranges from -0.18 GHz to -0.01 GHz, and corresponding measured velocity of jet is shown in Figure 66. The actual flow speed measured by the manometer is 105mph, which is 46.67m/s. The measured velocity

ranges from 0 to 46m/s. As indicated by both the frequency shift distribution and the measured velocity distribution, the region of jet flow is composed of several different sub-layers. The center region of the jet flow has the highest velocity. In both vertical direction and horizontal direction, as the velocity of the jet flow reduces as the location of interest moves farther from the center of the jet flow.

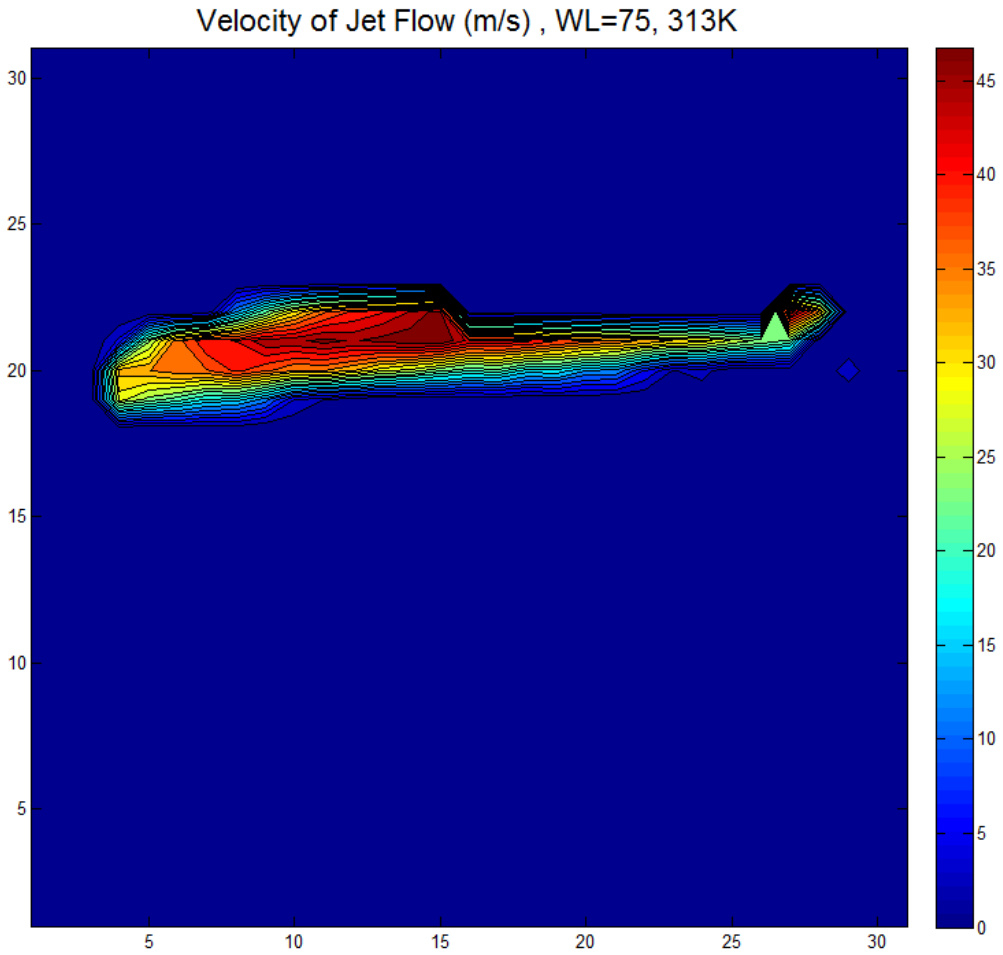

Figure 66 Measured Velocity of Jet Flow, 40℃

7.4.3. Subsonic Jet Flow Measurement under 35℃, 120mph

With both ALF cell heated to and stabilized at 35℃ and laser source set to be WL=75, the grayscale contours of the jet flow for REF and ALF are shown in Figure 67 and Figure 68.

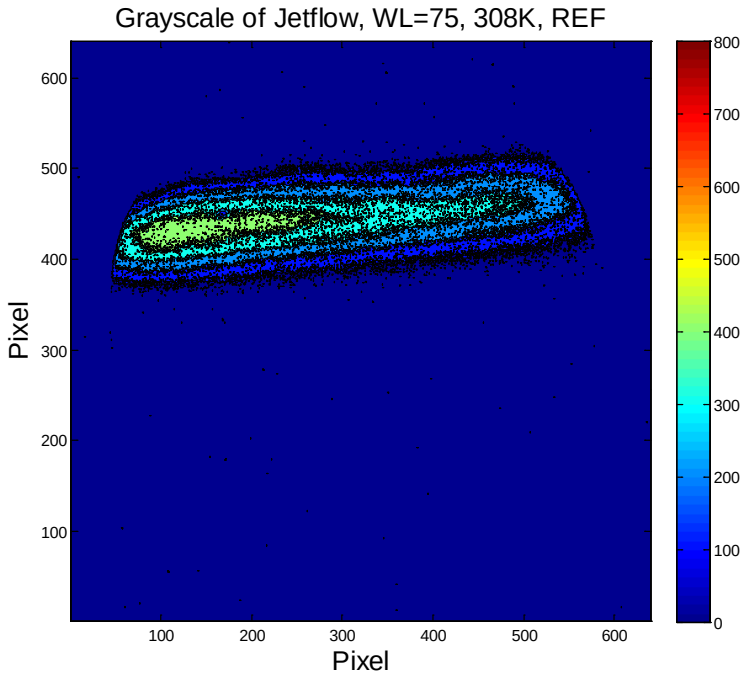

Figure 67 Grayscale of Subsonic Jet Flow, WL=75, 35℃ , REF

According to intensity calibration results for each pixel obtained in Section 6.2, the grayscale information is transferred into 'lumens', the virtual parameter indicating the power of the scattered light collected by Phantom camera.

Like the situation for flow jet under 40℃**,** at this stage, the raw lumens contour still contains significant noise in the signal, including noise from singular points in

intensity calibration results, as well as noise coming from the test environment. Therefore, thresholds are applied to the raw lumens to obtain more accurate lumens distribution for the jet flow. Figure 69 and Figure 70 present the lumens distribution in REF and ALF images for jet flow before thresholding.

Given the fact that the highest lumens value during the intensity calibration is obtained when the Neutral Density Filter ND003 alone is applied, therefore the threshold is set as $10^{-0.3}$=0.5012. For the ALF image, any pixel carrying a lumens value higher than 0.5012× Tr(WL=75, T=35℃) is reset to be 0. However, considering the fact that the key parameter calculated is the transmission ratio of each pair of matching pixel ($Tr = \frac{\text{lumens of ALF}}{\text{lumens of REF}}$), those pixels carrying lumens values over 0.5012 in REF are reset to be 1.0.

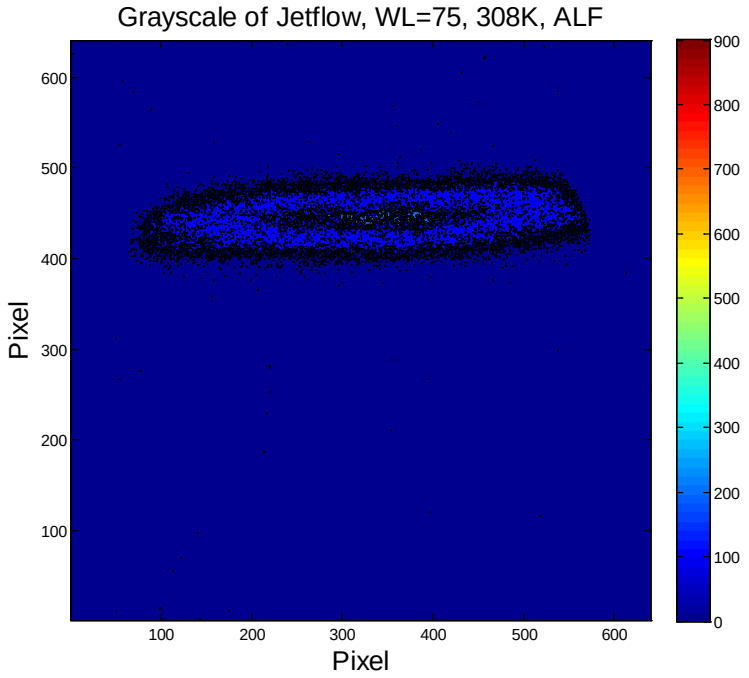

Figure 68 Grayscale of Subsonic Jet Flow, WL=75, 35℃, ALF

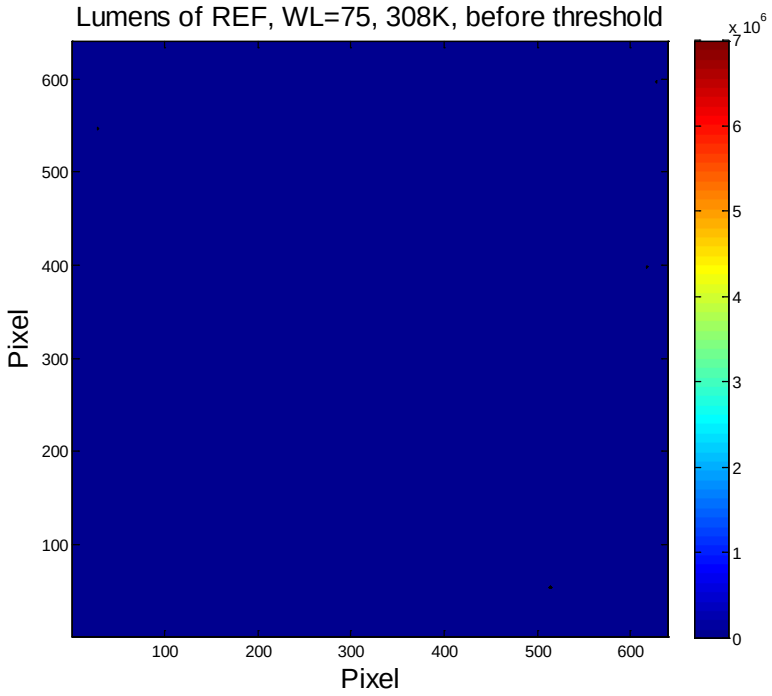

Figure 69 Lumens of Jet Flow before Threshold, WL=75, 35℃ , REF

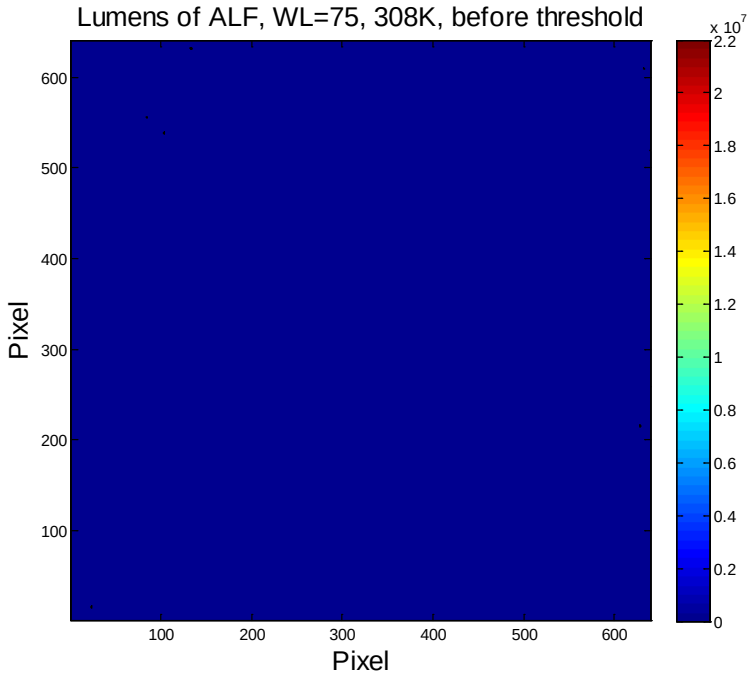

Figure 70 Lumens of Jet Flow before Threshold, WL=75, 35℃ , ALF

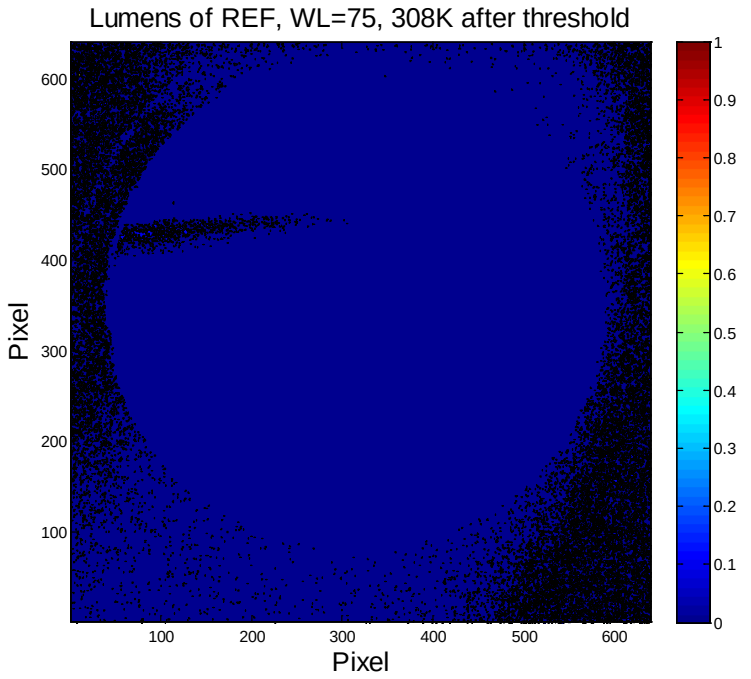

Figure 71 Lumens of Jet Flow after Threshold, 35℃ , REF

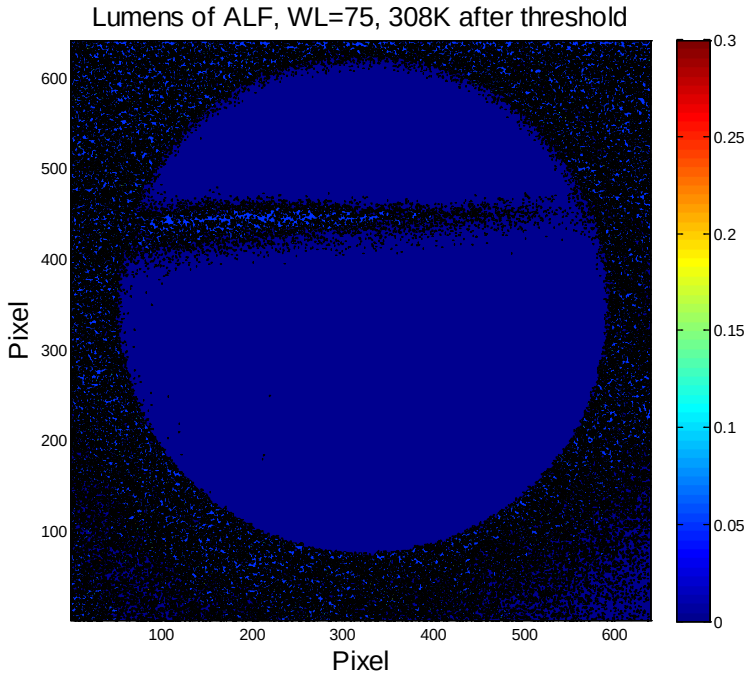

Figure 72 Lumens of Jet Flow after Threshold, 35℃ , ALF

In this way, those pixels carrying noise information are eliminated in the transmission ratio distribution after the threshold.

Lumens contours for the jet flow after the threshold are shown in Figure 71 and Figure 72. As indicated, after the threshold, the shape of the jet flow in REF and ALF images can be obviously observed, while before threshold, basically nothing is distinguishable from the lumens contour with noise information, and the lumens values' for both REF and ALF images are absolutely beyond their reasonable ranges.

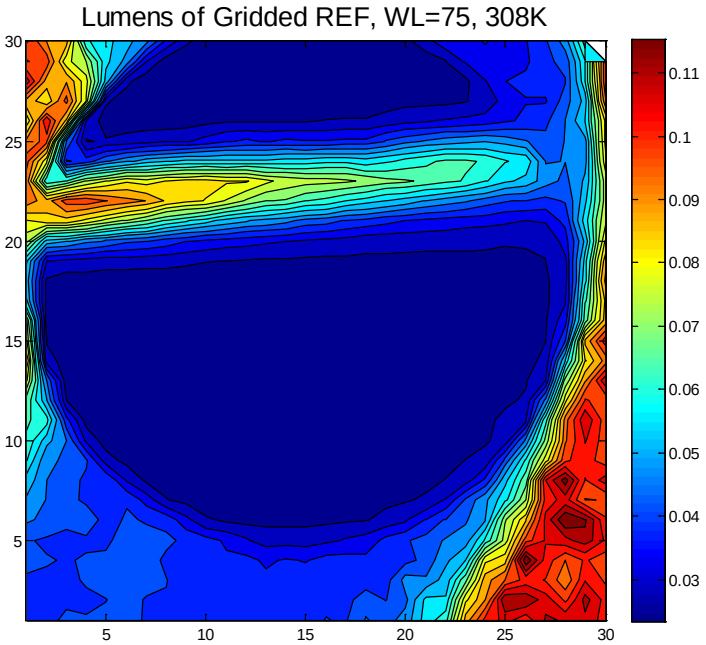

Figure 73 Lumens of Gridded Jet Flow, 20×20, 35℃, REF

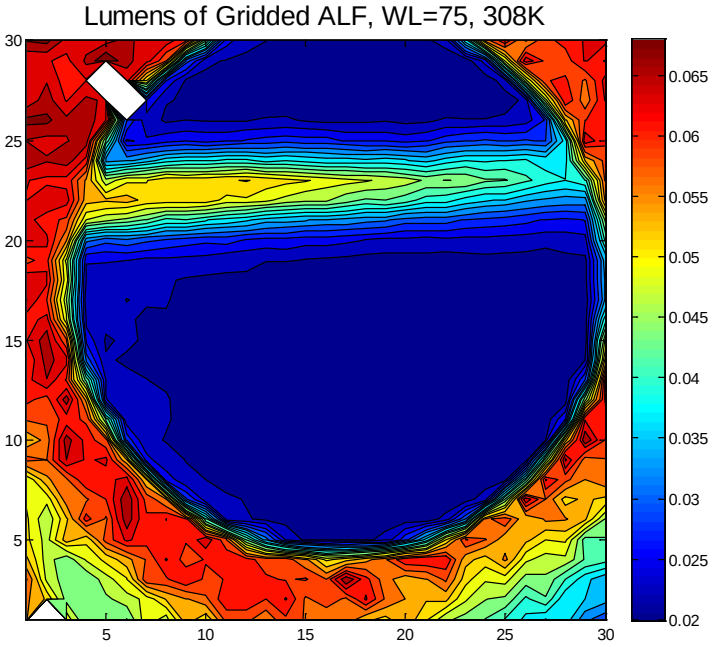

Figure 74 Lumens of Gridded Jet Flow, 20×20, 35℃ , ALF

Although spatial calibration has been performed, error in matching pixels between images still exists. To further eliminate this matching error, image gridding is applied in this study to obtain more accurate transmission ratio distribution. In detail, the REF and ALF images are gridded by 20×20 in pixels. The lumens values of the 20×20 pixel area are summed up and then divided by the number of pixels in that area. Lumens distribution after gridding for jet flow under 35℃ at WL=75 for REF and ALF are presented in Figure 73 and Figure 74.

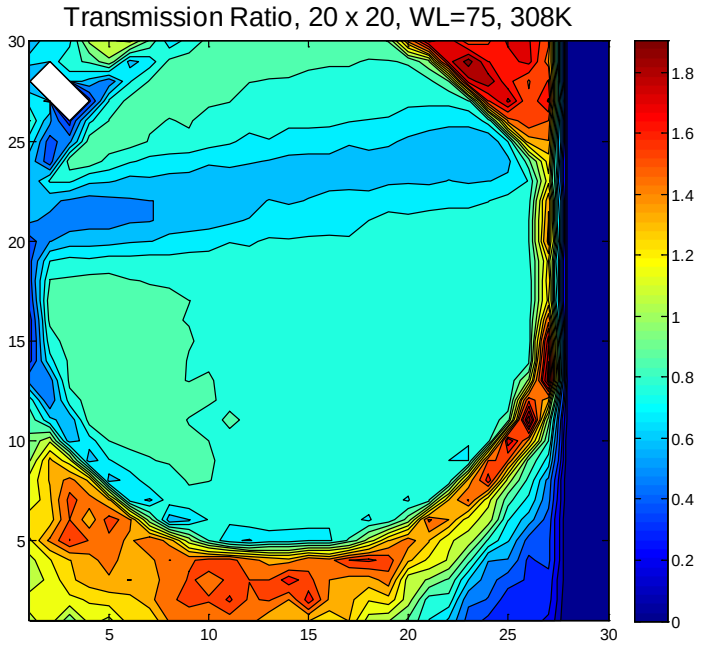

Figure 75 Transmission Ratio, WL=75, 35℃

Figure 75 presents the transmission ratio distribution. Figure 76 shows the original transmission ratio calibration curve for the laser source under 40℃ and the curve

fit for the section of the curve selected for velocity measurement, indicated in blue and red, respectively. The selected section for velocity measurement is curve fitted using 9-order polynomial, with R^2=0.9958. The curve fit result for this section of transmission ratio curve is: $\Delta\upsilon = a_i \times tr^{10-i}$, i=1~10, coefficients of each order is shown in Table 5. The corresponding frequency shift is obtained using this curve fit equation, as shown in Figure 77.

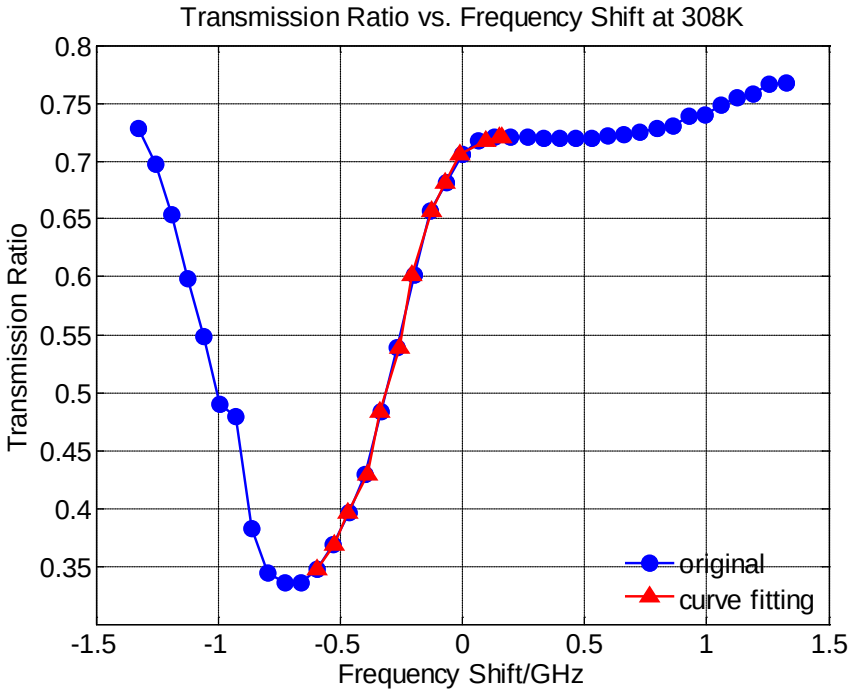

Figure 76 Transmission Ratio Curve Section for Velocity Measurement, 35℃

Table 5 Curve Fit Coefficients for Transmission Ratio Curve, 35℃

Term	*Coefficient*	*Term*	*Coefficient*
tr^9	1.4153e+07	tr^8	-6.7479e+07
tr^7	1.4190e+8	tr^6	-1.7272e+08
tr^5	1.3408e+08	tr^4	-6.8827e+07
tr^3	2.3362e+07	tr^2	-5.0557e+06
tr	6.3293e+05	*1*	-3.4926e+04

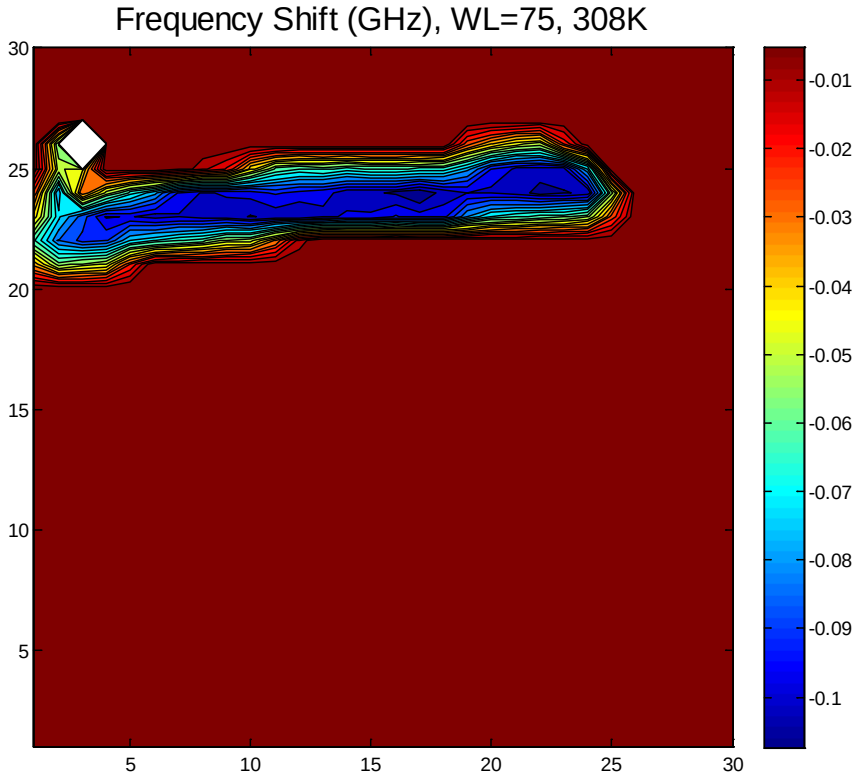

Figure 77 Frequency Shift of Jet Flow, 35℃

As shown in Figure 81, the frequency shift ranges from -0.1 GHz to -0.01 GHz, and corresponding measured velocity of jet is shown in Figure 78. The actual flow speed measured by the manometer is 120mph, which is 53.33/s. The measured velocity ranges

from 0 to 56m/s. As indicated by both the frequency shift distribution and the measured velocity distribution, the region of jet flow is composed of several different sub-layers. The center region of the jet flow has the highest velocity. In both vertical direction and horizontal direction, as the velocity of the jet flow reduces as the location of interest moves farther from the center of the jet flow.

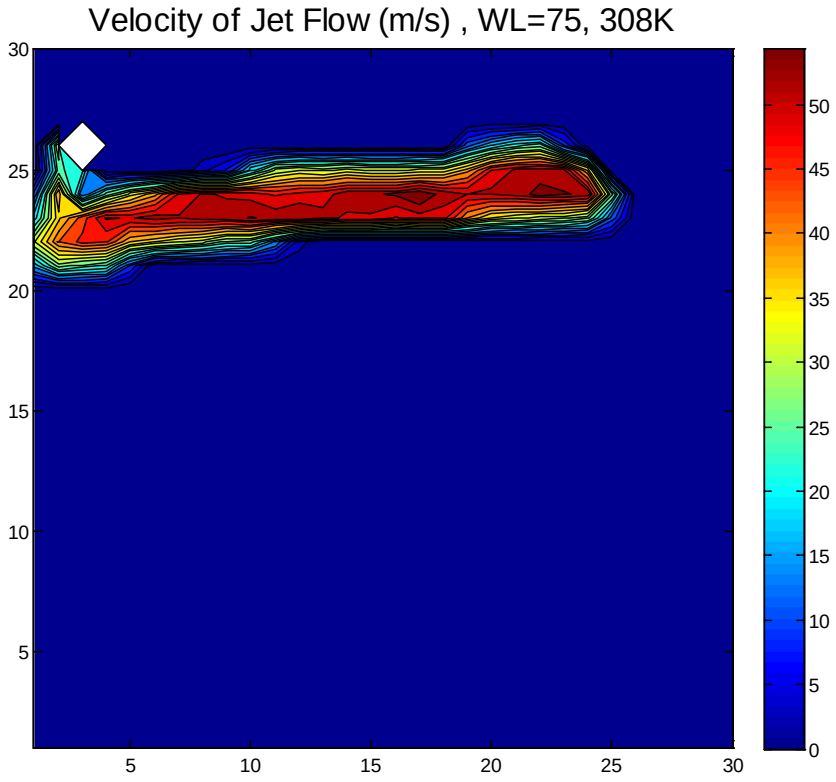

Figure 78 Measured Velocity of Jet Flow, 35℃

7.4.4. Subsonic Jet Flow Measurement under 30℃, 125mph

With both ALF cell heated to and stabilized at 30℃, the laser source is set to be WL=75, the grayscale contours of the jet flow for REF and ALF are shown in Figure 79 and Figure 80.

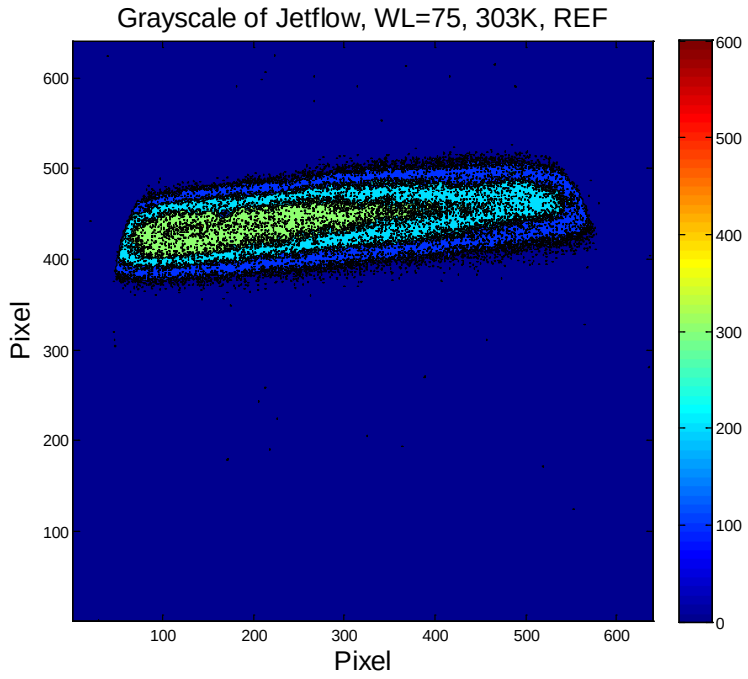

Figure 79 Grayscale of Subsonic Jet Flow, WL=75, 30℃, REF

According to intensity calibration results for each pixel obtained in Section 6.2, the grayscale information is transferred into 'lumens', the virtual parameter indicating the power of the scattered light collected by Phantom camera.

Like the situation for flow jet under 40℃**,** at this stage, the raw lumens contour still contains significant noise in the signal, including noise from singular points in

intensity calibration results, as well as noise coming from the test environment. Therefore, thresholds are applied to the raw lumens to obtain more accurate lumens distribution for the jet flow. Figure 81 and Figure 82 present the lumens distribution in REF and ALF images for jet flow before thresholding.

Given the fact that the highest lumens value during the intensity calibration is obtained when the Neutral Density Filter ND003 alone is applied, therefore the threshold is set as $10^{-0.3}$=0.5012. For ALF image, any pixel carrying lumens value higher than 0.5012× Tr(WL=75, T=30℃) is reset to be 0. However, considering the fact that the key parameter calculated is the transmission ratio of each pair of matching pixel ($Tr = \frac{\text{lumens of ALF}}{\text{lumens of REF}}$), those pixels in REF carrying lumens values over 0.5012 are reset to be 1.0.

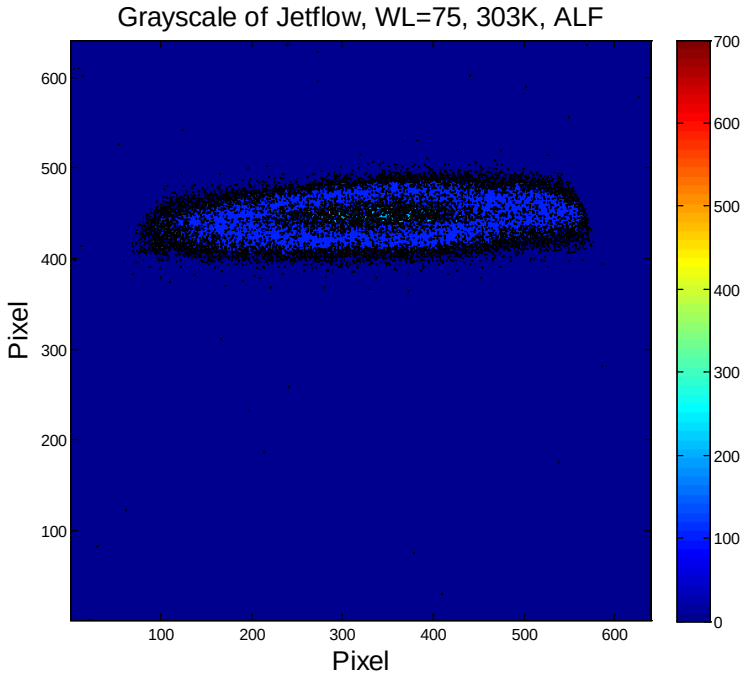

Figure 80 Grayscale of Subsonic Jet Flow, WL=75, 30℃, ALF

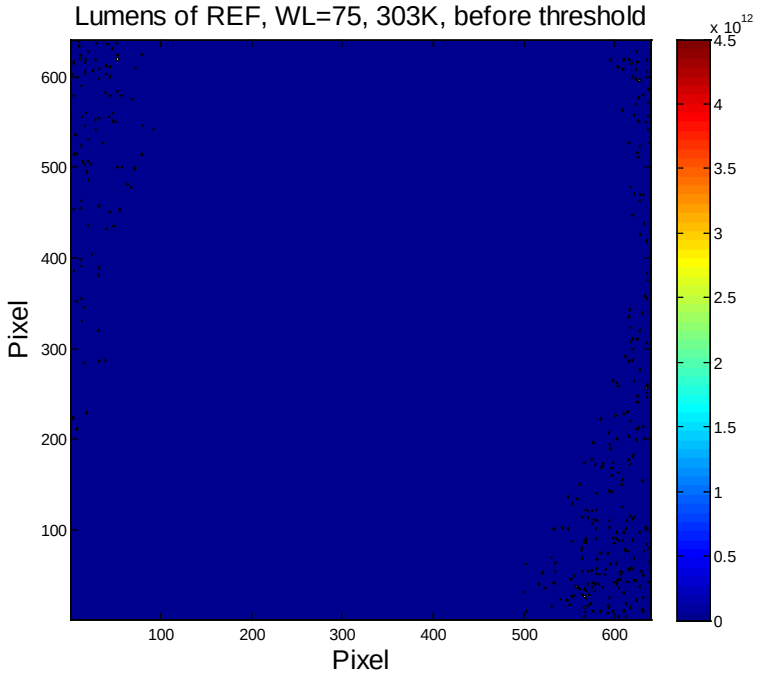

Figure 81 Lumens of Jet Flow before Threshold, WL=75, 30℃ , REF

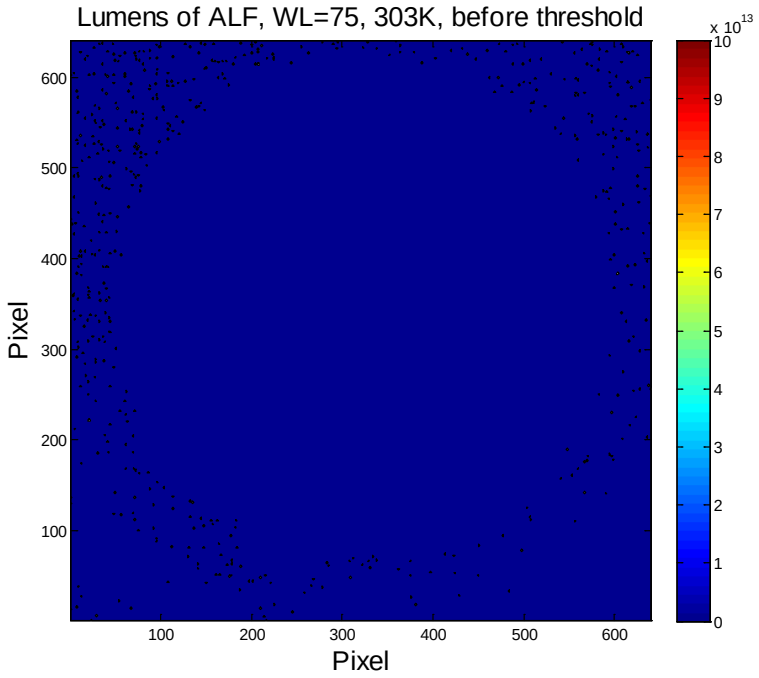

Figure 82 Lumens of Jet Flow before Threshold, WL=75, 30℃ , ALF

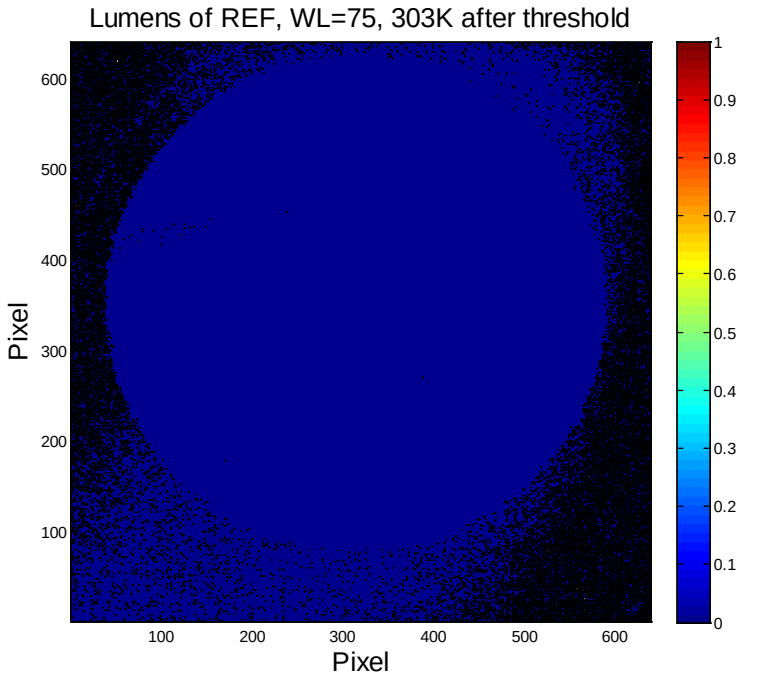

Figure 83 Lumens of Jet Flow after Threshold, 30℃ , REF

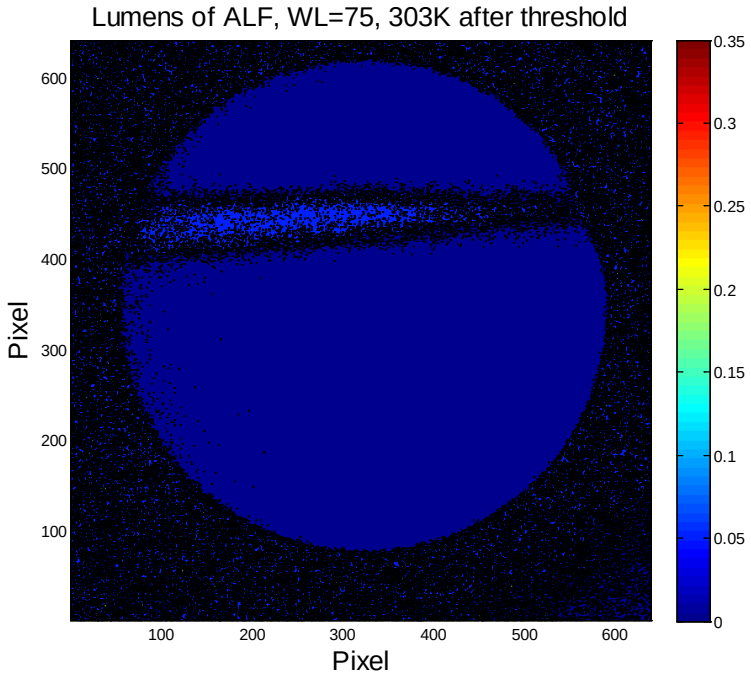

Figure 84 Lumens of Jet Flow after Threshold, 30℃ , ALF

In this way, those pixels carrying noise information are eliminated in the transmission ratio distribution after the threshold.

Lumens contours for the jet flow after the threshold are shown in Figure 83 and Figure 84. As indicated, after the threshold, the shape of the jet flow in REF and ALF images can be obviously observed, while before threshold, basically nothing is distinguishable from the lumens contour with noise information, and the lumens values' for both REF and ALF images are absolutely beyond their reasonable ranges.

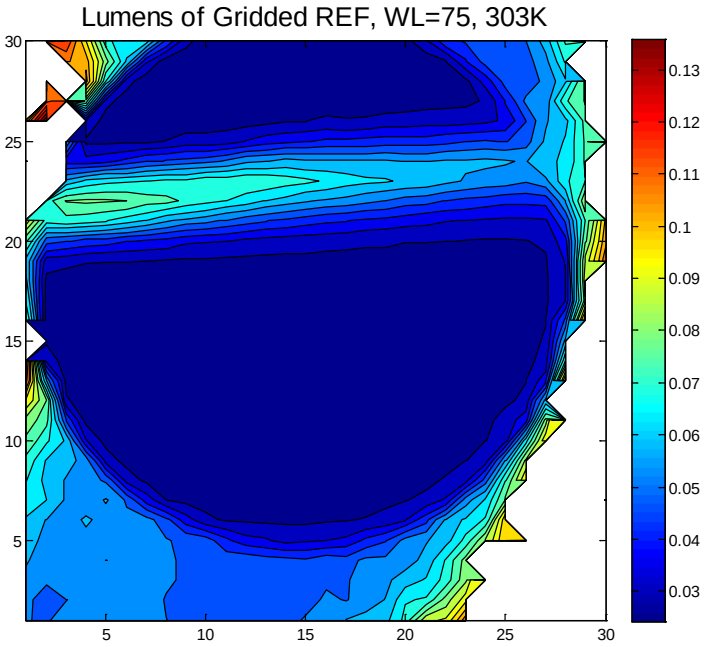

Figure 85 Lumens of Gridded Jet Flow, 20×20, 30℃, REF

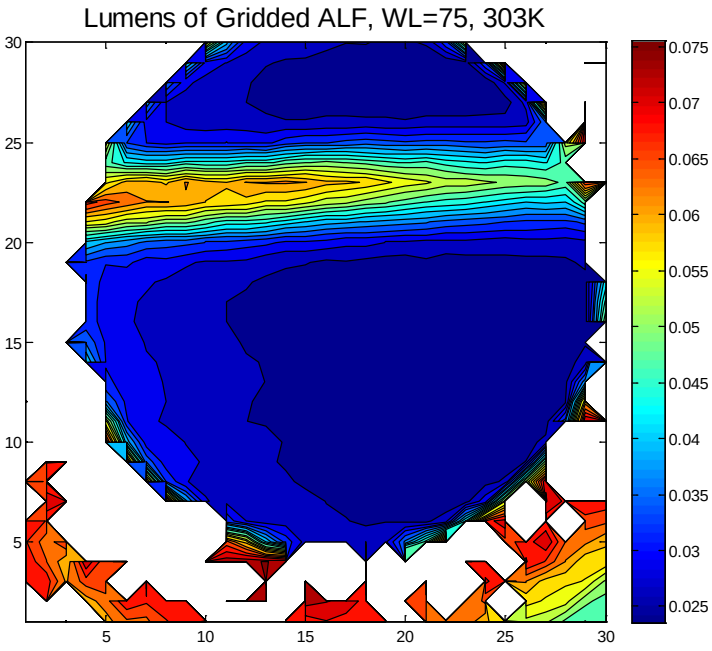

Figure 86 Lumens of Gridded Jet Flow, 20×20, 30℃, ALF

Although spatial calibration has been performed, error in matching pixels between images still exists. To further eliminate this matching error, image gridding is applied in this study to obtain more accurate transmission ratio distribution. In detail, the REF and ALF images are gridded by 20×20 in pixels. The lumens values of the 20×20 pixel area are summed up and then divided by the number of pixels in that area. Lumens distribution after gridding for jet flow under 30℃ at WL=75 for REF and ALF are presented in Figure 85 and Figure 86.

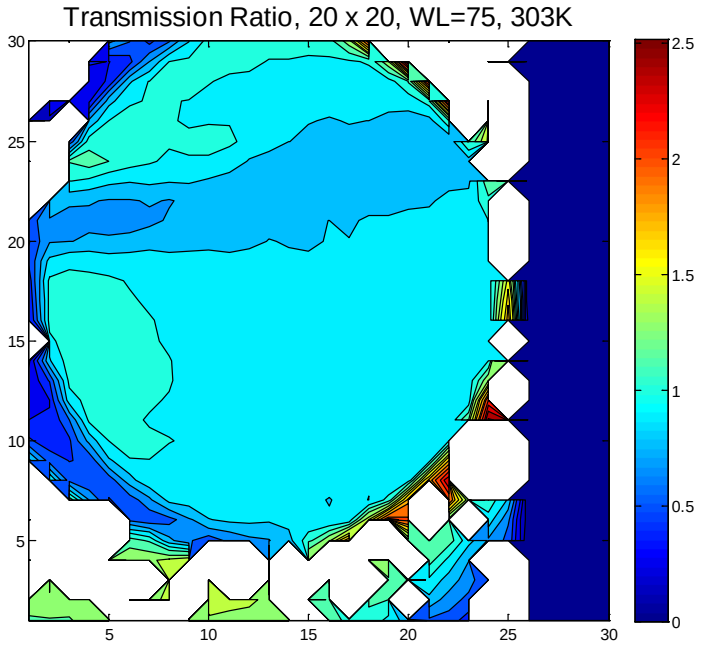

Figure 87 Transmission Ratio, WL=75, 30℃

Figure 87 presents the transmission ratio distribution. Figure 88 shows the original transmission ratio calibration curve for the laser source under 30℃ and the curve

fit for the section of the curve selected for velocity measurement, indicated in blue and red, respectively. The selected section for velocity measurement is curve fitted using 9-order polynomial, with R^2=0.9215. The curve fit result for this section of transmission ratio curve is: $\Delta\upsilon = a_i \times tr^{10-i}$, i=1~10, coefficients of each order is shown in Table 6. The corresponding frequency shift is obtained using this curve fit equation, as shown in Figure 89.

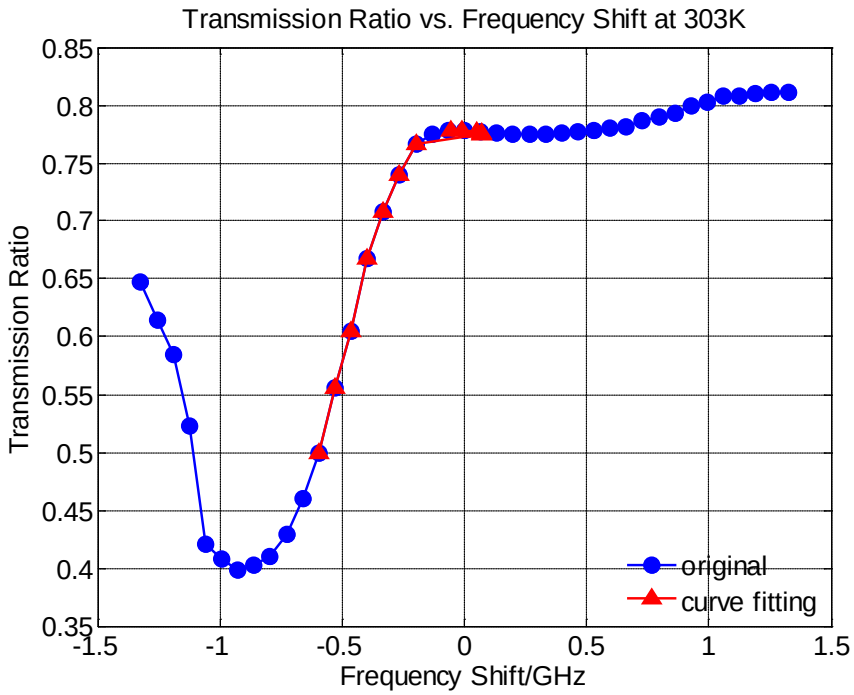

Figure 88 Transmission Ratio Curve Section for Velocity Measurement, 30℃

Table 6 Curve Fit Coefficients for Transmission Ratio Curve, 30℃

Term	*Coefficient*	*Term*	*Coefficient*
tr^9	-1.1574e+11	tr^8	7.0316e+07
tr^7	-1.8940e+12	tr^6	2.9684e+12
tr^5	-2.9829e+12	tr^4	1.9928e+12
tr^3	-8.8512e+11	tr^2	2.5199e+11
tr	-4.1725e+10	*1*	3.0611e+09

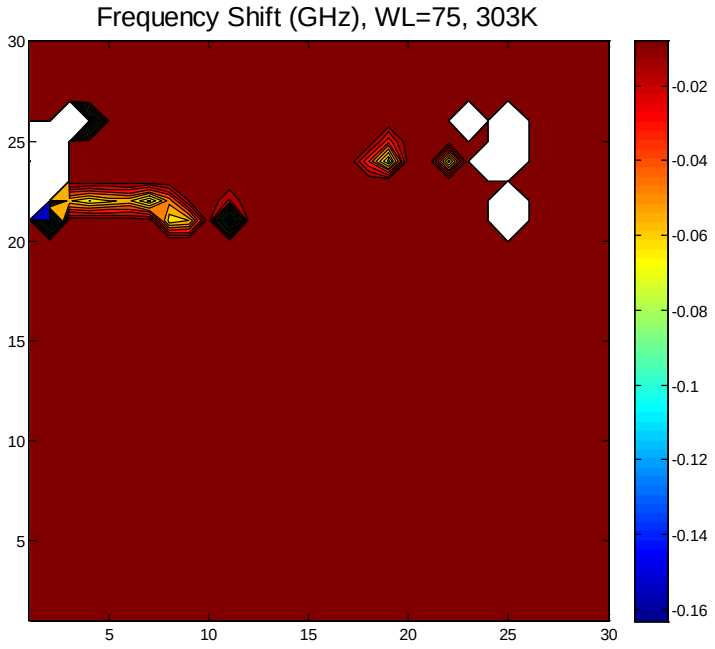

Figure 89 Frequency Shift of Jet Flow, 30℃

As shown in Figure 89, the frequency shift ranges from -0.16 GHz to -0.02 GHz, corresponding measured velocity of jet flow is shown in Figure 90. The actual flow speed measured by the manometer is 125mph, which is 55.56/s. The measured velocity ranges from 0 to 250m/s, indicating much bigger error than measurements under temperatures from 45℃ to 35℃. As indicated by the frequency shift distribution and the

measured velocity distribution, the sub-layers that compose the whole jet flow is difficult to recognize and distinguish at 30℃, the resolution is very low.

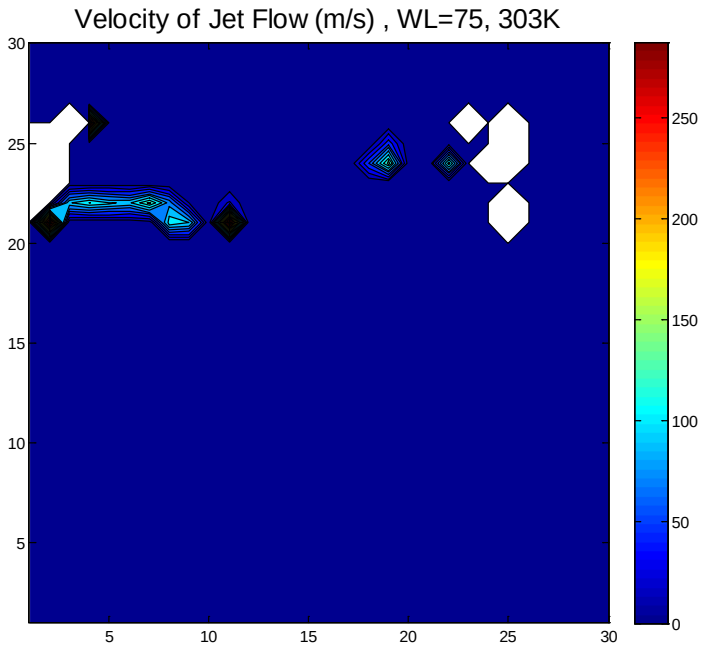

Figure 90 Measured Velocity of Jet Flow, 30℃

7.4.5. Subsonic Jet Flow Measurement under 25℃, 132mph

With both ALF cell are heated to and stabilized at 25℃, the laser source is set to be WL=75, the grayscale contours of the jet flow for REF and ALF are shown in Figure 91 and Figure 92.

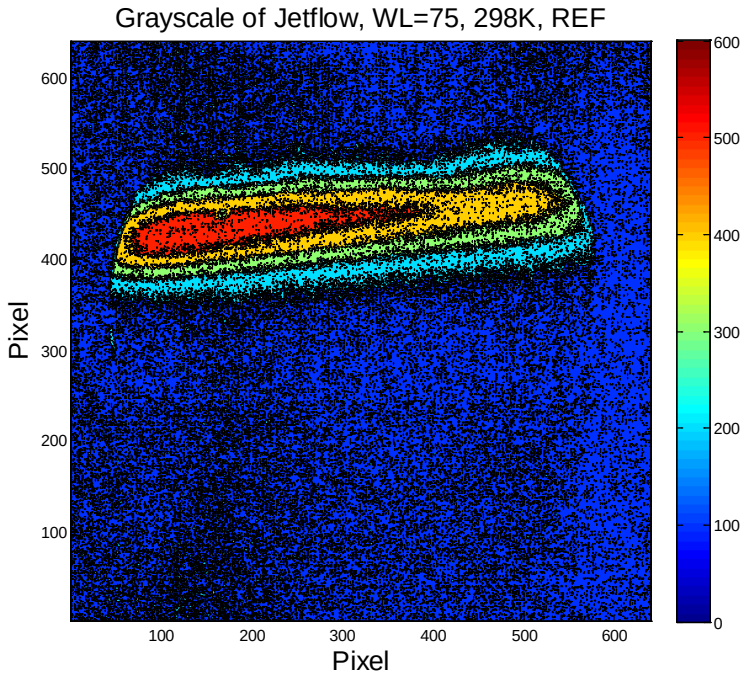

Figure 91 Grayscale of Subsonic Jet Flow, WL=75, 25℃, REF

According to intensity calibration results for each pixel obtained in Section 6.2, the grayscale information is transferred into 'lumens', the virtual parameter indicating the power of the scattered light collected by Phantom camera.

Like the situation for flow jet under 40℃**,** at this stage, the raw lumens contour still contains significant noise in the signal, including noise from singular points in

intensity calibration results, as well as noise coming from the test environment. Therefore, thresholds are applied to the raw lumens to obtain more accurate lumens distribution for the jet flow. Figure 93 and Figure 94 present the lumens distribution in REF and ALF images for jet flow before thresholding.

Given the fact that the highest lumens value during the intensity calibration is obtained when the Neutral Density Filter ND003 alone is applied, therefore the threshold is set as $10^{-0.3}$=0.5012. For ALF image, any pixel carrying lumens value higher than 0.5012× Tr(WL=75, T=25℃) is reset to be 0. However, considering the fact that the key parameter calculated is the transmission ratio of each pair of matching pixel ($Tr = \frac{\text{lumens of ALF}}{\text{lumens of REF}}$), those pixels carrying lumens values over 0.5012 in REF are reset to be 1.0.

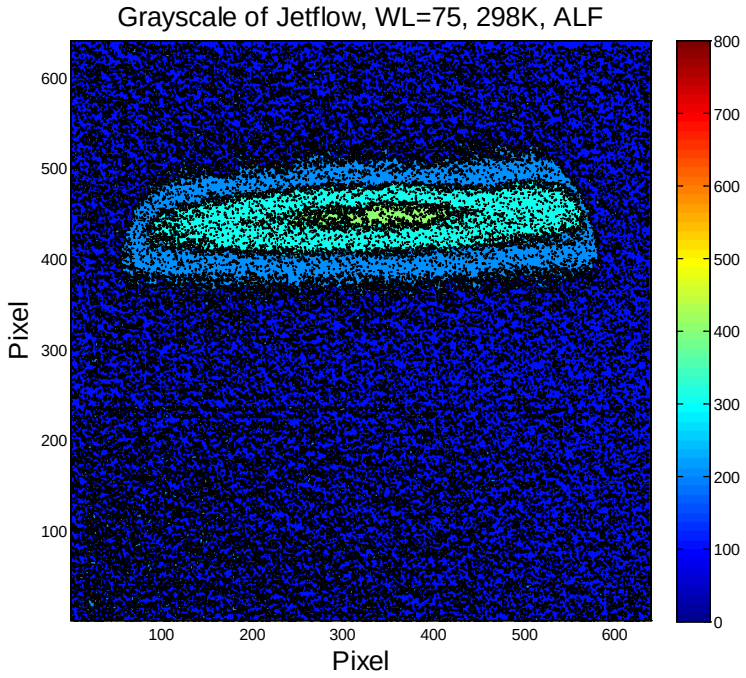

Figure 92 Grayscale of Subsonic Jet Flow, WL=75, 25℃, ALF

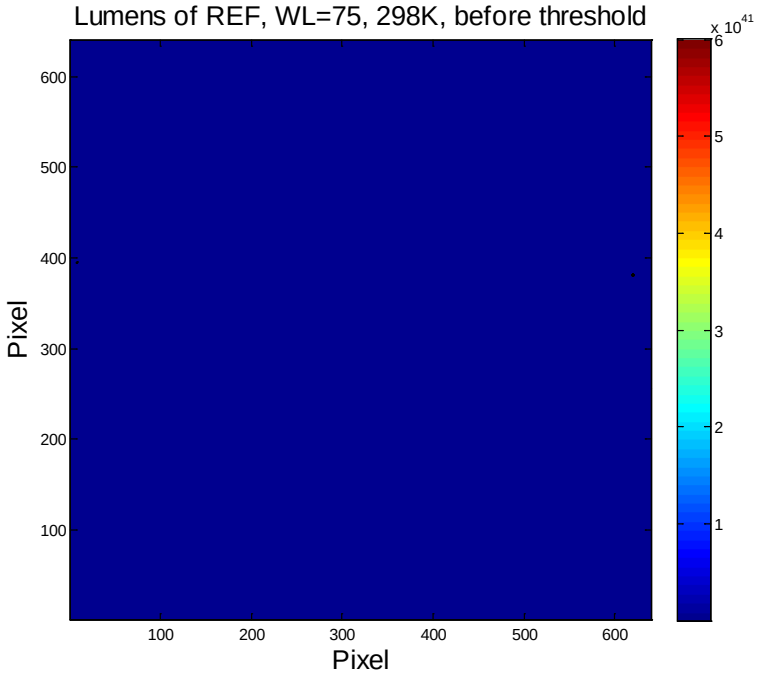

Figure 93 Lumens of Jet Flow before Threshold, WL=75, 25℃ , REF

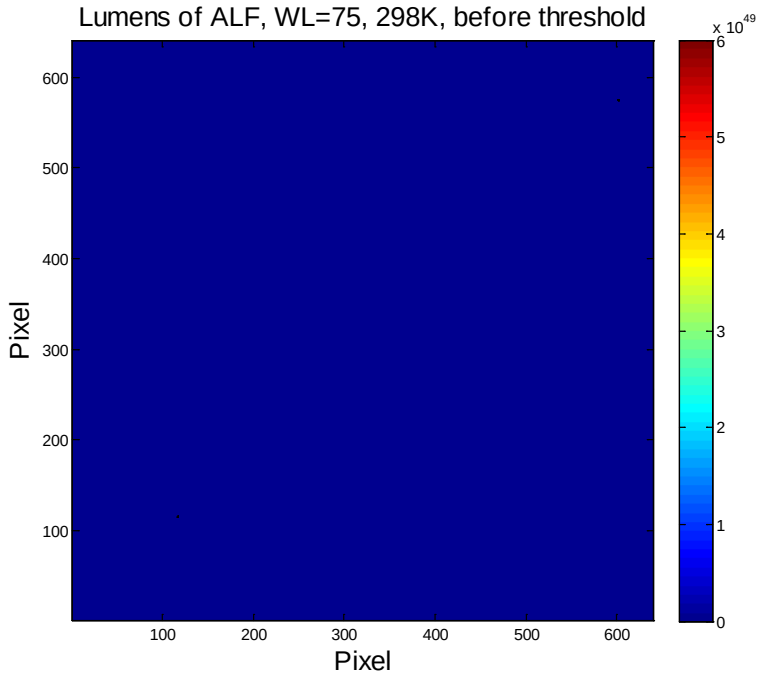

Figure 94 Lumens of Jet Flow before Threshold, WL=75, 25℃ , ALF

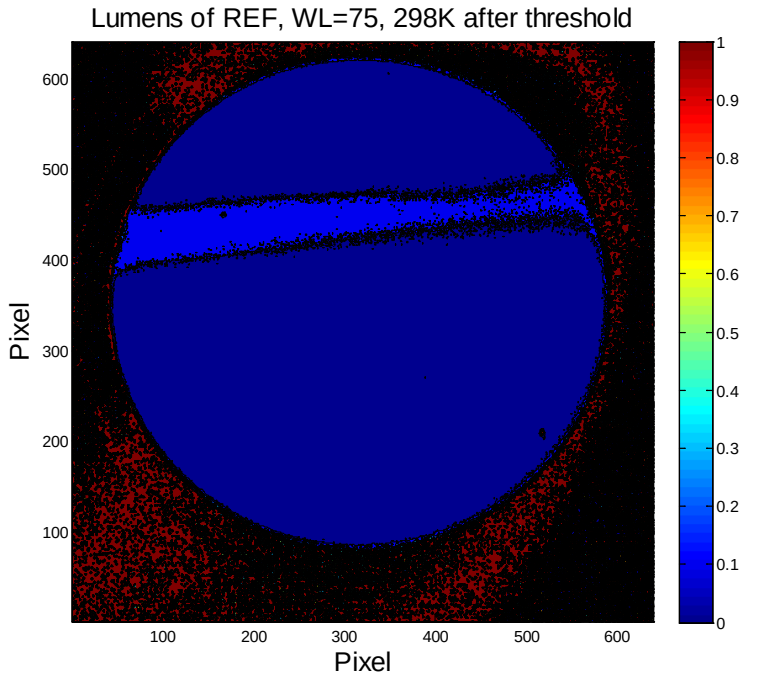

Figure 95 Lumens of Jet Flow after Threshold, 25℃ , REF

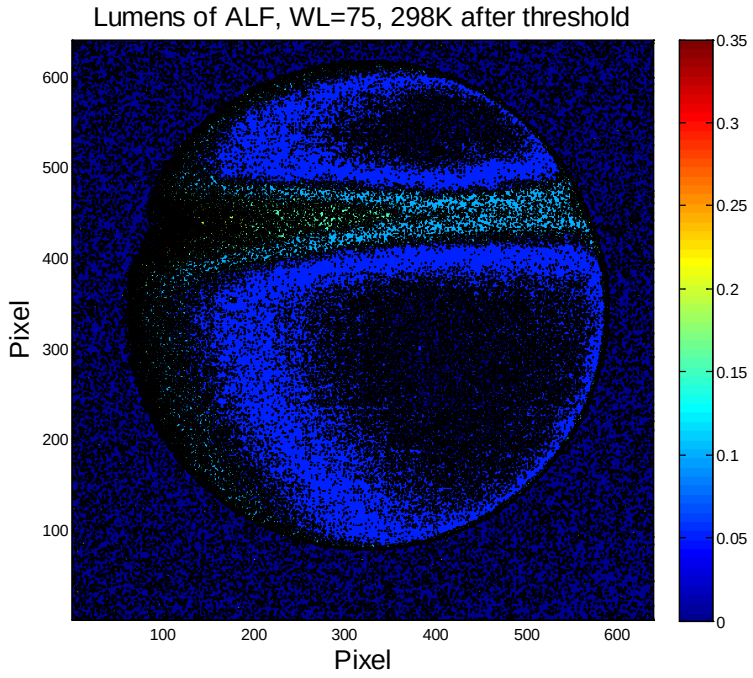

Figure 96 Lumens of Jet Flow after Threshold, 25℃ , ALF

In this way, those pixels carrying noise information are eliminated in the transmission ratio distribution after the threshold.

Lumens contours for the jet flow after threshold are shown in Figure 95 and Figure 96. As indicated, after the threshold, the shape of the jet flow in REF and ALF images can be obviously observed, while before threshold, basically nothing is distinguishable from the lumens contour with noise information, and the lumens values' for both REF and ALF images are absolutely beyond their reasonable ranges.

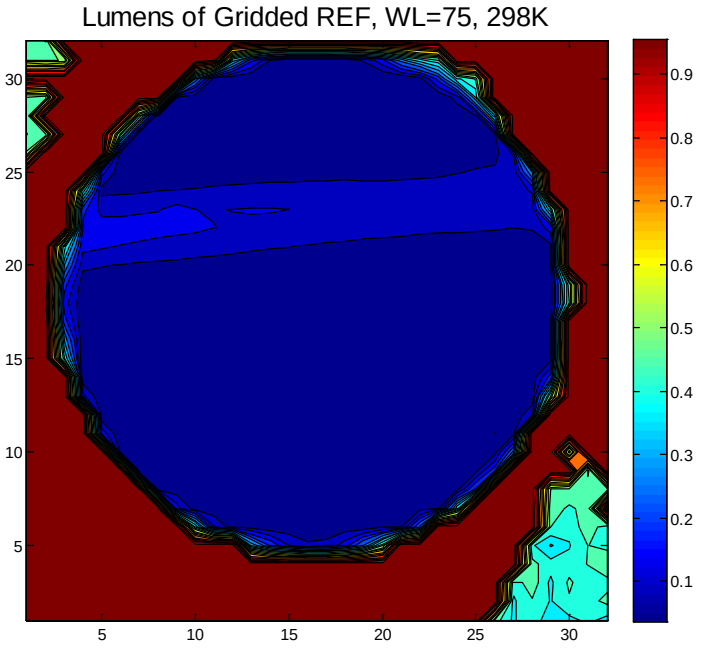

Figure 97 Lumens of Gridded Jet Flow, 20×20, 25℃, REF

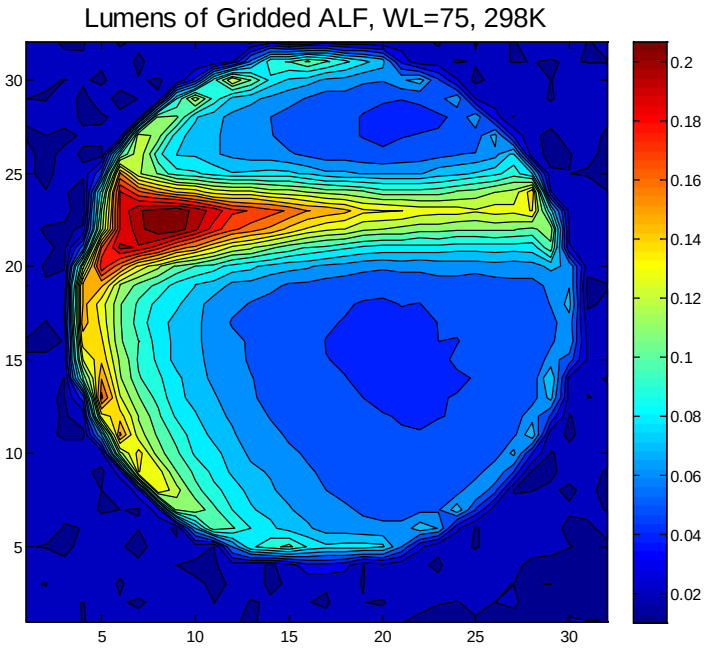

Figure 98 Lumens of Gridded Jet Flow, 20×20, 25℃, ALF

Although spatial calibration has been performed, error in matching pixels between images still exists. To further eliminate this matching error, image gridding is applied in this study to obtain more accurate transmission ratio distribution. In detail, the REF and ALF images are gridded by 20×20 in pixels. The lumens values of the 20×20 pixel area are summed up and then divided by the number of pixels in that area. Lumens distribution after gridding for jet flow under 25℃ at WL=75 for REF and ALF are presented in Figure 97 and Figure 98.

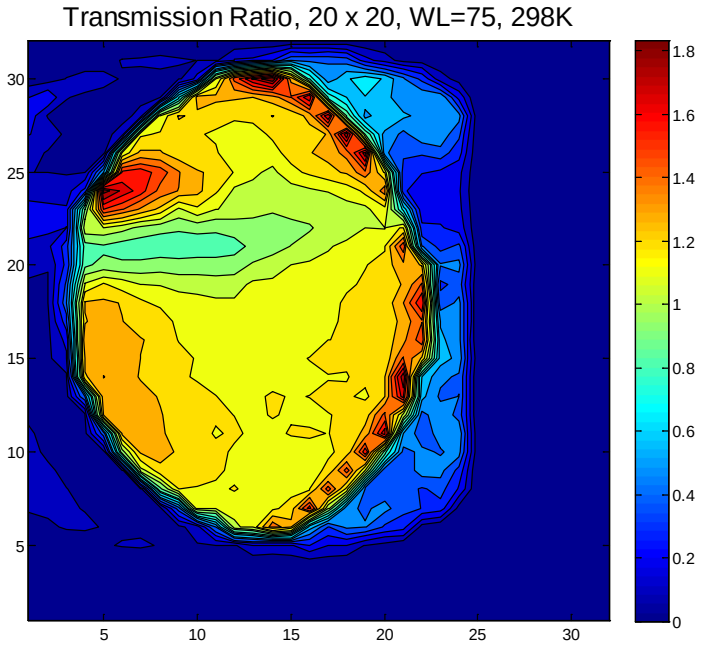

Figure 99 Transmission Ratio, WL=75, 25℃

Figure 99 presents the transmission ratio distribution. Figure 100 shows the original transmission ratio calibration curve for the laser source under 25℃ and the curve

fit for the section of the curve selected for velocity measurement, indicated in blue and red, respectively. The selected section for velocity measurement is curve fitted using 9-order polynomial, with R^2=0.9610. The curve fit result for this section of transmission ratio curve is: $\Delta\upsilon = a_i \times tr^{10-i}$, i=1~10, coefficients of each order is shown in Table 7. The corresponding frequency shift is obtained using this curve fit equation, as shown in Figure 101.

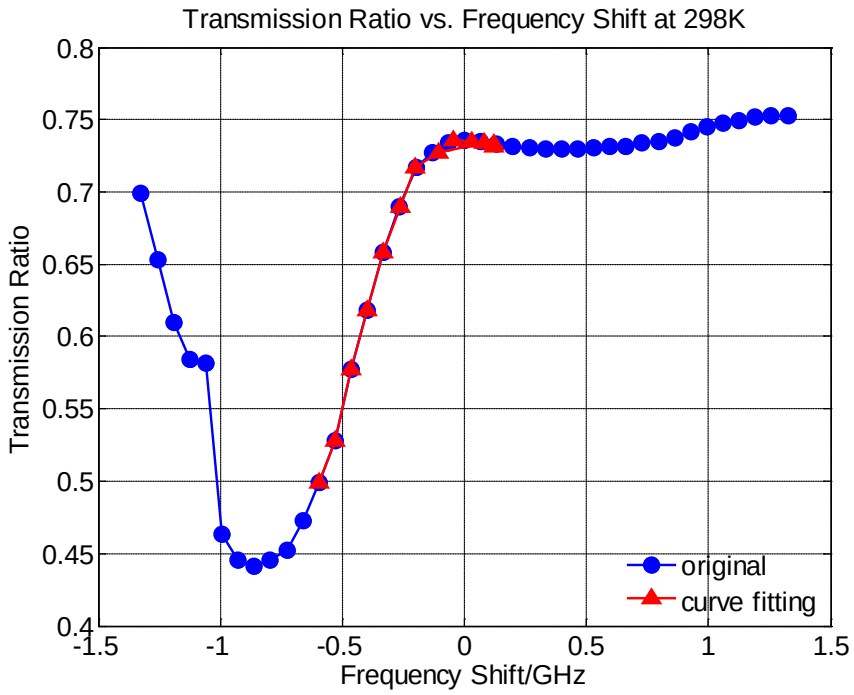

Figure 100 Transmission Ratio Curve Section for Velocity Measurement, 25℃

Table 7 Curve Fit Coefficients for Transmission Ratio Curve, 25℃

Term	*Coefficient*	*Term*	*Coefficient*
tr^9	-2.7741e+11	tr^8	1.5954e+12
tr^7	-4.0692e+12	tr^6	6.0414e+12
tr^5	-5.7533e+12	tr^4	3.6444e+12
tr^3	-1.5355e+12	tr^2	4.1492e+11
tr	-6.5247e+10	*1*	4.5490e+09

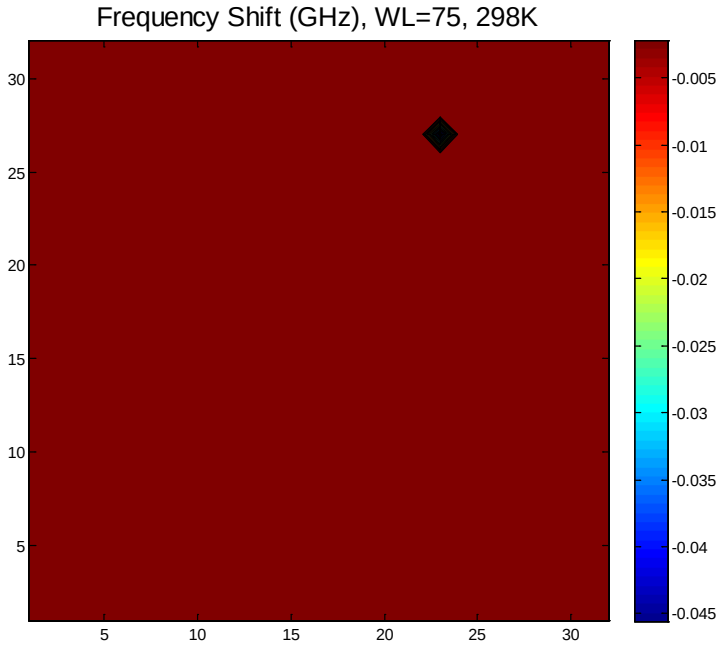

Figure 101 Frequency Shift of Jet Flow, 25℃

The actual flow speed measured by the manometer is 132mph, namely 58.67m/s. However, as shown in Figure 101 and Figure 102, the measured frequency shift and corresponding velocity of the jet flow under 25℃ basically do not contain much useful information.

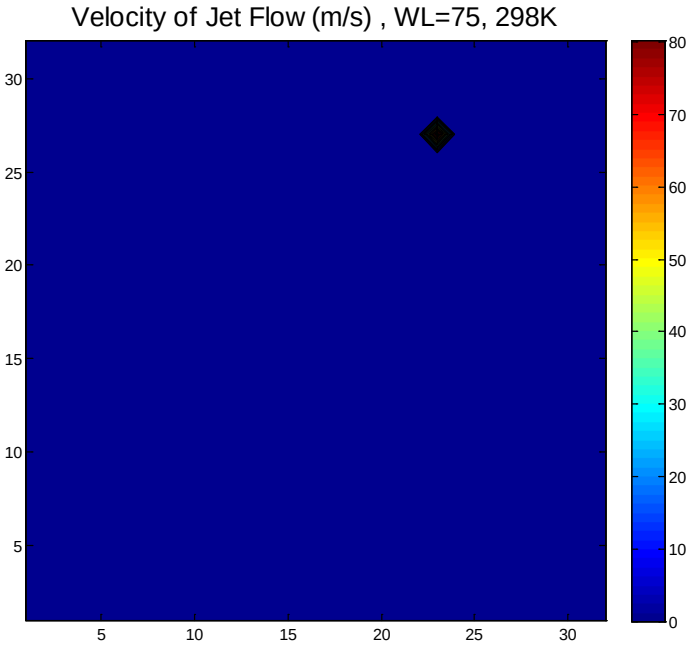

Figure 102 Velocity Measurement of Jet Flow, 25℃

8. CONCLUSIONS AND RECOMMENDATIONS

8.1. Conclusions

Based upon above results and discussions, the feasibility of the simplified DGV system in this study is proved.

The simplification from two cameras for traditional DGV to single camera of the simplified DGV brings great cost reduction, as well as conveniences for data processing and analysis, especially for spatial calibration, intensity calibration, data reduction.

The filtering characteristics of the ALF cell are highly dependent on its thermal status, actually on its temperature as observed in this study. The transmission ratio curve has higher slope under higher temperature, which means higher resolution and accuracy for velocity measurement of the DGV the temperature range from 25℃ to 45℃.

8.2. Recommendations

It has been noticed during this study that interference exists between the two observing windows for REF and ALF images in the form of light rings accompanying each window, and this interference has inevitably brought error into the data analysis and final results. Elimination of these interferences will help improve the accuracy of the simplified DGV system.

Given that the transmission ratio curve is sensitive to the temperature, which the ALF cells are heated to, as well as that the curve on the laser side is used as the reference curve for calculation of frequency shift and final velocity, applying temperature

controllers of higher accuracy and stability would further improve the consistency in temperature of the two ALF cells and ensure the reliability of the reference transmission ratio curve, finally resulting in improvement on the velocity measurement.

REFERENCES

[1] Gaharan, C. A., 1996, "The Development of a Doppler Global Velocimeter and its Image Processing Schemes for Whole-Field Measurements of Velocity," PhD Dissertation, Texas A&M University, College Station, Texas.

[2] Yeh, Y., and H. Z. Cummins, 1964, "Localized Fluid Flow Measurements with a He-Ne Laser Spectrometer," Applied Physics Letters, 4 (10), 176-178.

[3] Komine, H., 1990, "System for Measuring Velocity Field of Fluid Flow Utilizing a Laser-Doppler Spectral Image Converter," United States Patent No. 4,919,536, Northrop Corp., Hawthorne, CA.

[4] Meyers, J. F. and Komine, H., 1991, "Doppler Global Velocimetry A New Way to Look at Velocity," Proceedings of the ASME 4th International Conference on Laser Anemometry, Cleveland, OH.

[5] Meyers, J. F., Lee, J. W. and Cavone, A. A., 1991, "Signal Processing Schemes for Doppler Global Velocimetry," IEEE – 14th International Congress on Instrumentation in Aerospace Simulation Facilities, Rockville, MD.

[6] Meyers, J. F., 1992, "Doppler Global Velocimetry-The Next Generation?" AIAA Paper 92-3897.

[7] Meyers, J. F., 1994, "Development of Doppler Global Velocimetry for Wind Tunnel Testing," AIAA Paper 94-2582.

[8] Ford, H. D. and R. P. Tatam, 1995, "Imaging System Considerations in Doppler Global Velocimetry," *Proceedings of SPIE 2546, Optical Techniques in Fluid, Thermal, and Combustion Flow,* **2546** pp. 454- 464.

[9] Smith, M. W., Northam, G. B. and Drummond, J. P., 1996, "Application of Absorption Filter Planar Doppler Velocimetry to Sonic and Supersonic Jets," AIAA Journal, 34 (3), pp.434-441.

[10] Smith, M. W., 1998, "The Reduction of Laser Speckle Noise in Planar Doppler Velocimetry Systems," AIAA Paper 98-2607.

[11] McKenzie, R. L., 1996, "Measurement Capabilities of Planar Doppler Velocimetry Using Pulsed Lasers," Applied Optics, 35 (6), pp. 948-964.

[12] McKenzie, R. L., 1997, "Planar Doppler Velocimetry Performance in Low-Speed Flows," AIAA Paper 97-0498.

[13] Morrison, G. L., Gaharan C. A., and DeOtte Jr, R. E, 1995, "Doppler Global Velocimetry: Problems and Pitfalls," Flow Measurement and Instrumentation, 6 (2), pp. 83-91.

[14] Roehle, I., 1996, "Three-dimensional Doppler Global Velocimetry in the Flow of a Fuel Spray Nozzle and in the Wake Region of a Car," Flow Measurement and Instrumentation 7 (3-4), pp. 287-294.

[15] Muller, H., Lemacher, T., Pape, N., Strunck, V., and Dophenide, D., 2008, "3D-DGV for Flow Field Investigation in Pipes," Technical paper, Physikalisch-Technische Bundesanstalt, Branschweig, Germany.

[16] Nobes, D. S., Ford, H. D., and Tatam, R. P., 2004, "Instantaneous, Three-Component Planar Doppler Velocimetry Using Imaging Fibre Bundles," Experiments in Fluids 36 (1), pp. 3-10.

[17] Willert, C., Stockhausen, G., Klinner, J., Lempereur, C., Barricau, P., Loiret, P., and Raynal, J. C., 2007, "Performance and Accuracy Investigations of Two Doppler Global Velocimetry Systems Applied in Parallel," Measurement Science and Technology, 18 (8), pp. 2504-2512.

[18] Arnette, S. A., Elliott, G. S., and Mosedale, A. D. and Carter, C. D., 2000, "Two-Color Planar Doppler Velocimetry," AIAA Journal 38 (11), pp. 2001-2006.

[19] Willert, C., Hassa, C., Stockhausen, G., Jarius, M., Voges, M., and Klinner, J., 2006, "Combined PIV and DGV Applied to a Pressurized Gas Turbine Combustion Facility," Measurement Science and Technology, 17 (7), pp. 1670-1679.

[20] Chan, V. S. S., Heyes, A. L., Robinson, D. I., and Turner, J. T., 1995, "Iodine Absorption Filters for Doppler Global Velocimetry," Measurement Science and Technology, 6 (6), pp. 784-794.

[21] Miles, R. B., Lempert, W. R., and Forkey, J., 1991, "Instantaneous Velocity Fields and Background Suppression by Filtered Rayleigh Scattering," AIAA Paper 91-0357.

[22] Naylor S., and Kuhlman J., 1997, "Accuracy Studies of a Two-Component Doppler Global Velocimeter (DGV)," AIAA Paper 97-0508.

[23] Nelson, B., 2008, “The Development of a Frequency Control System of a Seeded Laser for DGV Application”, MSc Thesis, Texas A&M University, College Station, Texas.

APPENDIX A. MATLAB PROGRAM

```
%% lvm_import.m


function data = lvm_import(filename,verbose)
%LVM_IMPORT Imports data from a LabView LVM file
% DATA = LVM_IMPORT(FILENAME,VERBOSE) returns the data from a LVM
(.lvm)
%  ASCII text file created by LabView.
%
% FILENAME    The name of the .lvm file, with or without ".lvm" extension
%
% VERBOSE     How many messages to display. Default is 1 (few messages),
%             0 = silent, 2 = display file information and all messages
%
% DATA        The data found in the LVM file. DATA is a structure with
%             fields corresponding to the Segments in the file (see below)
%             and LVM file header information.
%
%
% This function imports data from a text-formatted LabView Measurement File
%  (LVM, extension ".lvm") into MATLAB. A LVM file can have multiple
%  Segments, so that multiple measurements can be combined in a single
%  file. The output variable DATA is a structure with fields named
%  'Segment1', 'Segment2', etc. Each Segment field is a structure with
%  details about the data in the Segment and the actual data in the field
%  named 'data'. The column labels and units are stored as cell arrays that
%  correspond to the columns in the array of data.
% The size of the data array depends on the type of x-axis data that is
%  stored in the LVM file and the number of channels (num_channels).
%  There are three cases:
%  1) No x-data is included in the file ('No')
%   The data array will have num_channels columns (one column per channel
%   of data).
%  2) One column of x-data is included in the file ('One')
%   The first column of the data array will be the x-values, and the data
%   array will have num_channels+1 columns.
%  3) Each channel has its own x-data ('Multi')
%   Each channel has two columns, one for x-values, and one for data. The
%   data array will have num_channels*2 columns, with the x-values and
%   corresponding data in alternating columns. For example, in a Segment
```

```
%   with 4 channels, columns 1,3,5,7 will be the x-values for the data in
%   columns 2,4,6,8.
%
% Note: because MATLAB only works with a "." decimal separator, importing
%  large LVM files that use a "," (or other character) will be noticeably
%  slower. Use a "." decimal separator to avoid this issue.
%
% The LVM file specification is available at:
%   http://zone.ni.com/devzone/cda/tut/p/id/4139
%
%
% Example:
%
%  Use the following command to read in the data from a file containing two
%   Segments:
%
% >> d=lvm_import('testfile.lvm',2);
%
% Importing testfile.lvm:
%
% Import complete. 2 Segments found.
%
% >> d
% d =
%       X_Columns: 'One'
%            user: 'YZ'
%     Description: 'Pressure, Flowrate, Heat, Power, Analog Voltage, Pump on, Temp'
%            date: '2014/06/13'
%            time: '12:18:02.156616'
%           clock: [2008 3 26 12 18 2.156616]
%        Segment1: [1x1 struct]
%        Segment2: [1x1 struct]
%
% >> d.Segment1
% ans =
%            Notes: 'Some notes regarding this data set'
%     num_channels: 8
%          y_units: {8x1 cell}
%          x_units: {8x1 cell}
%               X0: [8x1 double]
%          Delta_X: [8x1 double]
%    column_labels: {9x1 cell}
%             data: [211x9 double]
%          Comment: 'This data rulz'
```

```
%
% >> d.Segment1.column_labels{2}
% ans =
% Thermocouple1
%
% >> plot(d.Segment1.data(:,1),d.Segment1.data(:,2));
% >> xlabel(d.Segment1.column_labels{1});
% >> ylabel(d.Segment1.column_labels{2});
%
%
%
% M.A. Hopcroft
%      < mhopeng at gmail.com >
%

% MH Sep2013
% v2.2  fixes for case of comma separator in multi-segment files
%       use cell2mat for performance improvement
%       (thanks to <die-kenny@t-online.de> for bug report and testing)
% MH May2012
% v2.1  handle "no separator" bug
%       (thanks to <adnan.cheema@gmail.com> for bug report and testing)
%       code & comments cleanup
%       remove extraneous column labels (X_Value for "No X" files; Comment)
%       clean up verbose output
%       change some field names to NI names ("Delta_X","X_Columns","Date")
% MH Mar2012
% v2.0  fix "string bug" related to comma-separated decimals
%       handle multiple Special Headers correctly
%       fix help comments
%       increment version number to match LabView LVM writer
% MH Sep2011
% v1.3  handles LVM Writer version 2.0 (files with decimal separator)
%       Note: if you want to work with older files with a non-"." decimal
%       separator character, change the value of "data.Decimal_Separator"
% MH Sep2010
% v1.2  bugfixes for "Special" header in LVM files.
%       (Thanks to <bobbyjoe23928@gmail.com> for suggestions)
% MH Apr2010
% v1.1  use case-insensitive comparisons to maintain compatibility with
%       NI LVM Writer version 1.00
%
% MH MAY2009
% v1.02 Add filename input
```

```
% MH SEP2008
% v1.01 Fix comments, add Cells
% v1.00 Handle all three possibilities for X-columns (No,One,Multi)
%       Handle LVM files with no header
% MH AUG2008
% v0.92 extracts Comment for each Segment
% MH APR2008
% v0.9  initial version
%

%#ok<*ASGLU>

% message level
if nargin < 2, verbose = 1; end
if verbose >= 1, fprintf(1,'\nlvm_import v2.2\n'); end

% ask for filename if not provided already
if nargin < 1
   filename=input(' Enter the name of the .lvm file: ','s');
   fprintf(1,'\n');
end


%% Open the data file
% open and verify the file
fid=fopen(filename);
if fid ~= -1, % then file exists
   fclose(fid);
else
   filename=strcat(filename,'.lvm');
   fid=fopen(filename);
   if fid ~= -1, % then file exists
      fclose(fid);
   else
      error(['File not found in current directory! (' pwd ')']);
   end
end

% open the validated file
fid=fopen(filename);

if verbose >= 1, fprintf(1,' Importing %s:\n\n',filename); end
if verbose >= 2, fprintf(1,' File Header:\n'); end
```

```
% is it really a LVM file?
linein=fgetl(fid);
if verbose >= 2, fprintf(1,'%s\n',linein); end
if ~strcmp(sscanf(linein,'%s'),'LabVIEWMeasurement')
   try
      data.Segment1.data = dlmread(filename,'\t');
      if verbose >= 1, fprintf(1,'This file appears to be an LVM file with no header.\n');
end
      if verbose >= 1, fprintf(1,'Data was copied, but no other information is
available.\n'); end
      return
   catch fileEx
      error('This does not appear to be a text-format LVM file (no header).');
   end
end


%% Process file header
% The file header contains several fields with useful information

% default values
data.Decimal_Separator = '.';
text_delimiter='\t';
data.X_Columns='One';

% File header contains date, time, etc.
% Also the file delimiter and decimal separator (LVM v2.0)
while 1

   % get a line from the file
   linein=fgetl(fid);
   % handle spurious carriage returns
   if isempty(linein), linein=fgetl(fid); end
   if verbose >= 2, fprintf(1,'%s\n',linein); end
   % what is the tag for this line?
   t_in = textscan(linein,'%s');
   if isempty(t_in{1})
      tag='notag';
   else
      tag = t_in{1}{1};
   end
   % exit when we reach the end of the header
   if strcmpi(tag,'***End_of_Header***')
      if verbose >= 2, fprintf(1,'\n'); end
```

```
        break
    end

    % get the value corresponding to the tag
    if ~strcmp(tag,'notag')
        v_in = textscan(linein,'%*s %s','delimiter','\t','whitespace','','MultipleDelimsAsOne',
1);
        if ~isempty(v_in{1})
            val = v_in{1}{1};

            switch tag
                case 'Date'
                    data.Date = val;
                case 'Time'
                    data.Time = val;
                case 'Operator'
                    data.user = val;
                case 'Description'
                    data.Description = val;
                case 'Project'
                    data.Project = val;
                case 'Separator'
                    if strcmp(val,'Tab')
                        text_delimiter='\t';
                    elseif strcmp(val,'Comma')
                        text_delimiter=',';
                    end
                case 'X_Columns'
                    data.X_Columns = val;
                case 'Decimal_Separator'
                    data.Decimal_Separator = val;
            end

        end
    end

end

% create matlab-formatted date vector
if isfield(data,'time') && isfield(data,'date')
    dt = textscan(data.Date,'%d','delimiter','/');
    tm = textscan(data.Time,'%d','delimiter',':');
    if length(tm{1})==3
        data.clock=[dt{1}(1) dt{1}(2) dt{1}(3) tm{1}(1) tm{1}(2) tm{1}(3)];
```

```
    elseif length(tm{1})==2
        data.clock=[dt{1}(1) dt{1}(2) dt{1}(3) tm{1}(1) tm{1}(2) 0];
    else
        data.clock=[dt{1}(1) dt{1}(2) dt{1}(3) 0 0 0];
    end
end



%% Process segments
% process data segments in a loop until finished
segnum = 1;

while 1
    %segnum = segnum +1;
    fieldnm = ['Segment' num2str(segnum)];

    %% - Segment header
    if verbose >= 1, fprintf(1,' Segment %d:\n\n',segnum); end
    % loop to read segment header
    while 1
        % get a line from the file
        linein=fgetl(fid);
        % handle spurious carriage returns/blank lines/end of file
        while isempty(linein), linein=fgetl(fid); end
        if feof(fid), break; end
        if verbose >= 2, fprintf(1,'%s\n',linein); end

        % Ignore "special segments"
        % "special segments" can hold other types of data. The type tag is
        % the first line after the Start tag. As of version 2.0,
        % LabView defines three types:
        %  Binary_Data
        %  Packet_Notes
        %  Wfm_Sclr_Meas
        % In theory, users can define their own types as well. LVM_IMPORT
        %  ignores any "special segments" it finds.
        % If special segments are handled in future versions, recommend
        %  moving the handler outside the segment read loop.
        if strfind(linein,'***Start_Special***')
            special_seg = 1;
            while special_seg

                while 1 % process lines until we find the end of the special segment
```

```
            % get a line from the file
            linein=fgetl(fid);
            % handle spurious carriage returns
            if isempty(linein), linein=fgetl(fid); end
            % test for end of file
            if linein==-1, break; end
            if verbose >= 2, fprintf(1,'%s\n',linein); end
            if strfind(linein,'***End_Special***')
               if verbose >= 2, fprintf(1,'\n'); end
               break
            end
         end

         % get the next line and proceed with file
         %  (there may be additional Special Segments)
         linein=fgetl(fid);
         % handle spurious carriage returns/blank lines/end of file
         while isempty(linein), linein=fgetl(fid); end
         if feof(fid), break; end
         if isempty(strfind(linein,'***Start_Special***'))
            special_seg = 0;
            if verbose >= 1, fprintf(1,' [Special Segment ignored]\n\n'); end
         end
      end
   end % end special segment handler


   % what is the tag for this line?
   t_in = textscan(linein,'%s');
   if isempty(t_in{1})
      tag='notag';
   else
      tag = t_in{1}{1};
   end
   % exit when we reach the end of the header
   if strcmpi(tag,'***End_of_Header***')
      if verbose >= 2, fprintf(1,'\n'); end
      break
   end


   switch tag
      case 'Notes'
         %d_in = textscan(linein,'%*s %s','delimiter','\t','whitespace','');
```

```
            d_in = linein;
            data.(fieldnm).Notes=d_in;
        case 'Test_Name'
            %d_in = textscan(linein,'%*s %s','delimiter','\t','whitespace','');
            d_in = linein;
            data.(fieldnm).Test_Name = d_in;  %d_in{1}{1};
        case 'Channels'
            numchan = textscan(linein,'%*s %d',1);
            data.(fieldnm).num_channels = numchan{1};
        case 'Samples'
            numsamp = textscan(linein,'%s','delimiter',text_delimiter);
            numsamp1 = numsamp{1};
            numsamp1(1)=[]; % remove tag "Samples"
            numsamp2=str2num(cell2mat(numsamp1));
%#ok<ST2NM>
            data.(fieldnm).num_samples = numsamp2(:)';
        case 'Y_Unit_Label'
            Y_units = textscan(linein,'%s','delimiter',text_delimiter);
            data.(fieldnm).y_units=Y_units{1}';
            data.(fieldnm).y_units(1)=[]; % remove tag
        case 'Y_Dimension'
            Y_Dim = textscan(linein,'%s','delimiter',text_delimiter);
            data.(fieldnm).y_type=Y_Dim{1}';
            data.(fieldnm).y_type(1)=[]; % remove tag
        case 'X_Unit_Label'
            X_units = textscan(linein,'%s','delimiter',text_delimiter);
            data.(fieldnm).x_units=X_units{1}';
            data.(fieldnm).x_units(1)=[];
        case 'X_Dimension'
            X_Dim = textscan(linein,'%s','delimiter',text_delimiter);
            data.(fieldnm).x_type=X_Dim{1}';
            data.(fieldnm).x_type(1)=[]; % remove tag
        case 'X0'
            [Xnought, val]=strtok(linein);
            if ~strcmp(data.Decimal_Separator,'.')
                val = strrep(val,data.Decimal_Separator,'.');
            end
            data.(fieldnm).X0 = sscanf(val,'%e');
        case 'Delta_X' %,
            [Delta_X, val]=strtok(linein);
            if ~strcmp(data.Decimal_Separator,'.')
                val = strrep(val,data.Decimal_Separator,'.');
            end
            data.(fieldnm).Delta_X = sscanf(val,'%e');
```

```
    end

  end % end reading segment header loop


  % after each segment header is the row of column labels
  linein=fgetl(fid);
  Y_labels = textscan(linein,'%s','delimiter',text_delimiter);
  data.(fieldnm).column_labels=Y_labels{1}';
  % The X-column always exists, even if it is empty. Remove if not used.
  if strcmpi(data.X_Columns,'No')
    data.(fieldnm).column_labels(1)=[];
  end
  % remove empty entries and "Comment" label
  if any(strcmpi(data.(fieldnm).column_labels,'Comment'))

data.(fieldnm).column_labels=data.(fieldnm).column_labels(1:find(strcmpi(data.(fieldn
m).column_labels,'Comment'))-1);
  end
  % display column labels
  if verbose >= 1
    fprintf(1,' Data Columns:\n | ');
    for i=1:length(data.(fieldnm).column_labels)
      fprintf(1,'%s | ',data.(fieldnm).column_labels{i});
    end
    fprintf(1,'\n\n');
  end



  %% - Segment Data
  % Create a format string for textscan depending on the number/type of
  %  channels. If there are additional segments, texscan will quit when
  %  it comes to a text line which does not fit the format, and the loop
  %  will repeat.
  if verbose >= 1, fprintf(1,' Importing data from Segment %d...',segnum); end

  % How many data columns do we have? (including X data)
  switch data.X_Columns
    case 'No'
      % an empty X column exists in the file
      numdatacols = data.(fieldnm).num_channels+1;
      xColPlural='no X-Columns';
    case 'One'
```

```
            numdatacols = data.(fieldnm).num_channels+1;
            xColPlural='one X-Column';
        case 'Multi'
            numdatacols = data.(fieldnm).num_channels*2;
            xColPlural='multiple X-Columns';
    end

    % handle case of not using periods (aka "dot" or ".") for decimal point separators
    %  (LVM version 2.0+)
    if ~strcmp(data.Decimal_Separator,'.')
        if verbose >= 2, fprintf(1,'\n  (using decimal separator
"%s")\n',data.Decimal_Separator); end

        % create a format string for reading data as numbers
        fs = '%f'; for i=2:numdatacols, fs = [fs ' %f']; end              %#ok<AGROW>
        % add one more column for the comment field
        fs = [fs ' %s'];                                          %#ok<AGROW>
        rawdata=[];
        while 1
            cline=fgetl(fid);
            if isempty(cline) || (isnumeric(cline) && cline==-1), break; end
            cline=strrep(cline,',','.');
            cread = textscan(cline,fs,'delimiter',text_delimiter);
            if isempty(rawdata) && all(size(cread{size(cread,2)})) > 0
                % save first row comment as The Comment for this segment
                data.(fieldnm).Comment = cread{size(cread,2)}{1};
            end
            rawdata=[rawdata; cread(1:numdatacols)];                %#ok<AGROW>
        end

    else
        % create a format string for reading data as numbers
        fs = '%f'; for i=2:numdatacols, fs = [fs ' %f']; end                %#ok<AGROW>
        % add one more column for the comment field
        fs = [fs ' %s'];                                          %#ok<AGROW>
        % read the data from file
        rawdata = textscan(fid,fs,'delimiter',text_delimiter);
        % save first row comment as The Comment for this segment
        data.(fieldnm).Comment = rawdata{size(rawdata,2)}{1};
    end

    % v2.2 use cell2mat here instead of a loop for better performance
    % consolidate data into a simple array, ignore comments
    data.(fieldnm).data=cell2mat(rawdata(:,1:numdatacols));
```

```
    % If we have a "No X data" file, remove the first column (it is empty/NaN)
    if strcmpi(data.X_Columns,'No')
        data.(fieldnm).data=data.(fieldnm).data(:,2:end);
    end

    if verbose >= 1, fprintf(1,' complete (%g data
points).\n\n',length(data.(fieldnm).data)); end

    % test for end of file
    if feof(fid)
        if verbose >= 2, fprintf(1,' [End of File]\n\n'); end
        break;
    else
        segnum = segnum+1;
    end


end % end process segment


if verbose >= 1, fprintf(1,'\n Import complete. File has %s and %d Data
Segments.\n\n',xColPlural,segnum); end


% close the file
fclose(fid);
return
```

```
%% lvm_simplified_batch.m

clear all
close all
clc
mean = zeros(41,2);
c=299792458;
for n=25:5:45
for i = 1:1:41
    k=25*i-525;
    filename = ['C:\Users\ZY\Desktop\YZ Test Data\setpid\' num2str(n) ' Celsius\'
num2str(n) '_' num2str(k) '_.lvm']

    %['C:\Users\ZY\Desktop\YZ Test Data\setpid\25 Celsius\25_' num2str(k) '_.lvm']
    d=lvm_import(filename,2);
    trarray_i=d.Segment1.data(:,4);
    mean(i,2)=nanmean(trarray_i);
    mean(i,1)=c./532-c./(532+(1.25e-3)/500*k);
    %filename='transmission_ratio.xlsx';
    m=mean;


end
 t=n/5-4; %t=n/5-4; %specify the sheet name in order of the temperatures
 sheet= ['Sheet' num2str(t)];
 writefile = ['C:\Users\ZY\Desktop\YZ Test Data\setpid\TR_20140623'];
 xlswrite(writefile,mean,sheet);

end
f=xlsread('C:\Users\ZY\Desktop\YZ Test Data\setpid\TR_20140623','Sheet3','A:A');
tr=xlsread('C:\Users\ZY\Desktop\YZ Test Data\setpid\TR_20140623','Sheet3','B:B');
plot(f,tr,'-bo','LineWidth',2,'MarkerFaceColor','b', 'MarkerSize',10)
title('Transmission Ratio vs. Frequency Shift', 'FontSize',24)
xlabel('Frequency Shift/GHz','FontSize',24);
ylabel('Transmission Ratio', 'FontSize',24);
set(gca,'FontSize',24); %set the fontsize of values of both axes in the plot
grid;
p=polyfit(f,tr,6); %get expression of tr in terms of f
%q=polyfit(tr,f,6); %get expression of f in terms of tr
hold on
curvefittr=p(1)*f.^6+p(2)*f.^5+p(3)*f.^4+p(4)*f.^3+p(5)*f.^2+p(6)*f+p(7);
%curvefitf=q(1)*tr.^6+q(2)*tr.^5+q(3)*tr.^4+q(4)*tr.^3+q(5)*tr.^2+q(6)*tr+q(7);
trfit=curvefittr;
%ffit=curvefitf;
```

```
plot(f, curvefittr, '-r^','LineWidth',2,'MarkerFaceColor', 'r','MarkerSize',10);
%plot(curvefitf,tr , '-cv','LineWidth',2,'MarkerFaceColor', 'c','MarkerSize',10);
hleg=legend('original','curve fitting tr(f)','curve fitting f(tr)');
legend('boxoff'); %get rid of the box of the legends
%set(hleg,'Location','SouthEast'); %designate the location of the legend
meantr=sum(tr)/i;
SST=0;
SSE=0;
for r=1:1:41
   %SST=0;
   SST=SST+(tr(r)-meantr)^2;
   %SSE=0;
   SSE=SSE+(tr(r)-trfit(r))^2;
end
R_squared=1-SSE/SST;
```

```
%% centroid_calculation.m

clear all
close all
clc
%% get the background image and the signal image files for processing
[fname,pathname]=uigetfile('C:\Users\ZY\Desktop\YZ Test Data\*.tif','Select image file for processing')
%ask to select the video file for processing, fname = 'C:\Users\ZY\Desktop\122.tif';
%[fname_bg,pathname_bg]=uigetfile('C:\Users\ZY\Desktop\YZ Test Data\*.tif','Select backgournd image file for processing')

filename = strcat(pathname,fname);
%assign directory of the chosen image to 'pathname', assign filename of the chosen image to 'filename'

[pathstr, fnameM, ext] = fileparts(filename);
%function 'fileparts'returns the path, file name and file name extension for the specified 'filename'

%mkdir('C:\Users\ZY\Desktop\YZ Test Data','Data Analysis')
%make the 'C:\Users\ZY\Desktop\DGV Image Processing\Image processing' further and create a folder named 'Data Analysis'

mkdir('C:\Users\ZY\Desktop\YZ Test Data',fnameM)
%create a new folder named the same as the string value of 'fnameM' under the folder 'YZ Test Data'

cd=fullfile('C:\Users\ZY\Desktop\YZ Test Data', fnameM);
%builds a full file name (including its full directory) for the file named as fnameM

%% read in image data
info = imfinfo(fname);
num_images = numel(info);

%B=0;
%for k = 1:num_images
%    B=B+double(imread(fname, k));
%end
B=double(imread(fname));
%BG=double(imread(fname_bg));
%C=B/num_images;
refarray=B((1:640),(1:640));
alfarray=B((1:640),(641:1280));
```

```
ratio=alfarray./refarray;

%% REF image processing,get rid of noise
[rrow, rcol]=size(refarray);
rmean=sum(sum(refarray))/(rrow*rcol);
for i=1:rrow
   for j=1:rcol
      if refarray(i,j)<rmean
        refarray(i,j)=0;
      else
        refarray(i,j)=255;
      end
   end
end

fig(3)=figure;
imshow(refarray,[0,255]);%title('modified refarray')

%% ALF image,get rid of noise
[row, col]=size(B);mean=sum(sum(B))/(row*col);
[arow, acol]=size(alfarray);
amean=sum(sum(alfarray))/(arow*acol);
for i=1:arow
   for j=1:acol
      if alfarray(i,j)<mean
        alfarray(i,j)=0;
      else
        alfarray(i,j)=255;
      end
   end
end

fig(4)=figure;
imshow(alfarray,[0,255]); %title('modified alfarray')


%% Centroid calculation for REF image and ALF image
%REF image
figure; imshow(refarray);
rw=refarray==0;%By thresholding, value for pixels composing dots have been set to be
0;
figure; imshow(rw);
sr=regionprops(rw, 'Centroid');
figure;imshow(refarray);
```

```
hold on
rpixel=zeros(numel(sr),2);
for k=1:numel(sr)
   %centroid_k=sr(k).Centroid; %centroid location read by code
    centroid_k=round(sr(k).Centroid); % centroid location after rounding off
    rpixel(k,1)=sr(k).Centroid(1);rpixel(k,2)=sr(k).Centroid(2);%pixel is the array
containing the pixel coordinates of dots
    rrpixel=round(rpixel);
    plot(centroid_k(1), centroid_k(2),'b.','MarkerSize',5);
end
hold off
%writefile = ['C:\Users\ZY\Desktop\YZ Test Data\setpid\TR' num2str(n) 'Celsius'];
%xlswrite(writefile,mean)%,sheet);

%ALF image
figure; imshow(alfarray);
aw=alfarray==0;%By thresholding, value for pixels composing dots have been set to be
0;
figure; imshow(aw);
sa=regionprops(aw, 'Centroid');
figure;imshow(alfarray);
hold on
apixel=zeros(numel(sa),2);
for k=1:numel(sa)
   %centroid_k=sa(k).Centroid;
    centroid_k=round(sa(k).Centroid); % centroid location after rounding off
    apixel(k,1)=sa(k).Centroid(1);apixel(k,2)=sa(k).Centroid(2);%pixel is the array
containing the pixel coordinates of dots
    aapixel=round(apixel);
    plot(centroid_k(1), centroid_k(2),'b.','MarkerSize',5);
end
hold off
save(fullfile(cd,fnameM));
```

```
%% pixel_to_spatial_calculation_and_matching.m

%% based on centroid information obtained from code 'centroid_estimation', calculate
the corresponding (x,y) for each set of (i,j)

spacing=0.206; %cm, spatial spacing in dot array printed out
center=320; % pixel location of both i and j for the center
[rrpixelrow, rrpixelcol]=size(rrpixel);%get the values of row and column for REF pixel
matrix
[aapixelrow, aapixelcol]=size(aapixel);%get the values of row and column for ALF pixel
matrix
%% calculate the corresponding (x,y) for each set of (i,j) for REF image
rp2s=zeros(max([rrpixelrow,aapixelrow]),rrpixelcol+2);
%generate new matrix rp2s containing pixel coordinate and correponding
%spatial coordinate for REF image

rp2s(:,1)=rrpixel(:,1);%assign pixel coordinate i to 1st column of matrix rp2s, REF
image
rp2s(:,2)=rrpixel(:,2);%assign pixel coordinate j to 2nd column of matrix rp2s, REF
image
for i=1:rrpixelrow %calculate corresponding x,y to i,j for REF image
   for j=1:rrpixelcol
      rp2s(i,j+2)=spacing*(round((center-rrpixel(i,j))/20));
   end
   rp2s(i,3)=-rp2s(i,3);
end

%% calculate the corresponding (x,y) for each set of (i,j) for ALF image
ap2s=zeros(max([rrpixelrow,aapixelrow]),aapixelcol+2);
aapixel(aapixelrow+1:max([rrpixelrow,aapixelrow]),1)=0;
aapixel(aapixelrow+1:max([rrpixelrow,aapixelrow]),2)=0;

ap2s(:,1)=aapixel(:,1);%assign pixel coordinate i to 1st column of matrix ap2s, ALF
image
ap2s(:,2)=aapixel(:,2);%assign pixel coordinate i to 2nd column of matrix ap2s, ALF
image
for i=1:aapixelrow %calculate corresponding x,y to i,j for ALF image
   for j=1:aapixelcol
      ap2s(i,j+2)=spacing*(round((center-aapixel(i,j))/20));
   end
   ap2s(i,3)=-ap2s(i,3);
end
```

```
%% find pixel locations in REF and ALF which corresponds to the same spatial
locations and form the spatial calibration result
scal=zeros(max([rrpixelrow,aapixelrow]),aapixelcol+4);% matrix for spatial calibration
result
% in the matrix of scal: 1st~2nd col--x,y; 3rd~4th col--ri,rj; 5th~6th col--ai,aj

for i=1:max([rrpixelrow,aapixelrow])
%form a new matrix 'scal(spatial calibration results)' containg x,y; i,j for REF and
corresponding i,j for ALF
   for j=1:max([rrpixelrow,aapixelrow])
      if rp2s(i,3)==ap2s(j,3) && rp2s(i,4)==ap2s(j,4)
        scal(i,1) =rp2s(i,3); scal(i,2)=rp2s(i,4);scal(i,3)=rp2s(i,1);scal(i,4)=rp2s(i,2);
scal(i,5)=ap2s(j,1);scal(i,6)=ap2s(j,2);
      else
      end

   end

end


%% removing 0 rows in scal
scali=1;
while scali<=size(scal,1)
      if scal(scali,:)==0
        scal(scali,:)=[];
        size(scal,1);
        scali;

      else
        scali=scali+1;
      end
end
save(fullfile(cd,'spatial calibration'));
```

pixel_to_space_transform.m

```
%% extract data from scal, form rxscal and ryscal, each cell value is spatial location,
row and column are i and j
[scalrow,scalcol]=size(scal);
rxscal=zeros(640,640);
ryscal=zeros(640,640);
for i=1:scalrow
   %for j=1:640
   %for j=3:4
      rxscal(scal(i,3),scal(i,4))=scal(i,1);
      ryscal(scal(i,3),scal(i,4))=scal(i,2);
   %end
   %end
end
%% extract data from scal, form axscal and ayscal, each cell value is spatial location,
row and column are i and j
[scalrow,scalcol]=size(scal);
axscal=zeros(640,640);
ayscal=zeros(640,640);
for i=1:scalrow
   %for j=1:640
   %for j=3:4
      axscal(scal(i,5),scal(i,6))=scal(i,1);
      ayscal(scal(i,5),scal(i,6))=scal(i,2);
   %end
   %end
end
%% calculate coeffcients for ri, rj and ai,aj to transform to x,y
ri=scal(:,3);
rj=scal(:,4);
ai=scal(:,5);
aj=scal(:,6);
x=scal(:,1);
y=scal(:,2);
rM=[ones(size(ri)),ri,rj];
aM=[ones(size(ai)),ai,aj];
recox=rM\x;
recoy=rM\y;
alcox=aM\x;
alcoy=aM\y;
x=recox(1)+recox(2)*ri+recox(3)*rj;
y=recoy(1)+recoy(2)*ri+recoy(3)*rj;
x=alcox(1)+alcox(2)*ri+alcox(3)*rj;
```

```
y=alcoy(1)+alcoy(2)*ri+alcoy(3)*rj;

%% (i,j) to x transform, REF
i=1:20:640;j=1:20:640;
figure;[I,J]=meshgrid(i,j);
X=recox(1)+recox(2)*I+recox(3)*J;
colormap(jet); surf(I,J,X);
axis([1 640 1 640 -4 4])
xlabel('i','FontSize',16);
ylabel('j', 'FontSize',16);
zlabel('x','FontSize',16);
set(gca,'FontSize',16);
title('Transform from (i, j) to x, REF');
hold on;
for i=1:640
   for j=1:640
     if rxscal(i,j)~=0
      plot3(i,j,rxscal(i,j),'o','MarkerFaceColor','b','MarkerEdgeColor','w','MarkerSize',6);
     else
     end
   end
end
hold off;
hxlabel = get(gca,'xlabel');
set(get(gca,'xlabel'),'position',[300 -100 -4],'Rotation',0);
hylabel = get(gca,'ylabel');
set(get(gca,'ylabel'),'position',[-100 300 -4],'Rotation',0);

%% (i,j) to y transform, REF
i=1:20:640;j=1:20:640;
figure;[I,J]=meshgrid(i,j);
Y=recoy(1)+recoy(2)*I+recoy(3)*J;
colormap(jet); surf(I,J,Y);
axis([1 640 1 640 -4 4])
xlabel('i','FontSize',16);
ylabel('j', 'FontSize',16);
zlabel('y','FontSize',16);
set(gca,'FontSize',16);
title('Transform from (i, j) to y, REF');
hold on;
for i=1:640
   for j=1:640
     if ryscal(i,j)~=0
      plot3(i,j,ryscal(i,j),'o','MarkerFaceColor','b','MarkerEdgeColor','w','MarkerSize',6);
```

```
      else
      end
    end
end
hold off;
view([125 30]);
hxlabel = get(gca,'xlabel');
set(get(gca,'xlabel'),'position',[300 700 -4],'Rotation',0);
hylabel = get(gca,'ylabel');
set(get(gca,'ylabel'),'position',[800 300 -4],'Rotation',0);
%% (i,j) to x transform, ALF
i=1:20:640;j=1:20:640;
figure;[I,J]=meshgrid(i,j);
X=alcox(1)+alcox(2)*I+alcox(3)*J;
colormap(jet); surf(I,J,X);
axis([1 640 1 640 -4 4])
xlabel('i','FontSize',16);
ylabel('j', 'FontSize',16);
zlabel('x','FontSize',16);
set(gca,'FontSize',16);
title('Transform from (i, j) to x, ALF');
hold on;
for i=1:640
    for j=1:640
      if axscal(i,j)~=0
       plot3(i,j,axscal(i,j),'o','MarkerFaceColor','b','MarkerEdgeColor','w','MarkerSize',6);
      else
      end
    end
end
hold off;
hxlabel = get(gca,'xlabel');
set(get(gca,'xlabel'),'position',[300 -100 -4],'Rotation',0);
hylabel = get(gca,'ylabel');
set(get(gca,'ylabel'),'position',[-100 300 -4],'Rotation',0);
%% (i,j) to y transform, ALF
i=1:20:640;j=1:20:640;
figure;[I,J]=meshgrid(i,j);
Y=alcoy(1)+alcoy(2)*I+alcoy(3)*J;
colormap(jet); surf(I,J,Y);
axis([1 640 1 640 -4 4])
xlabel('i','FontSize',16);
ylabel('j', 'FontSize',16);
zlabel('y','FontSize',16);
```

```
set(gca,'FontSize',16);
title('Transform from (i, j) to y, ALF');
hold on;
for i=1:640
    for j=1:640
      if ayscal(i,j)~=0
       plot3(i,j,ayscal(i,j),'o','MarkerFaceColor','b','MarkerEdgeColor','w','MarkerSize',6);
      else
      end
    end
end
hold off;
view([125 30]);
hxlabel = get(gca,'xlabel');
set(get(gca,'xlabel'),'position',[300 700 -4],'Rotation',0);
hylabel = get(gca,'ylabel');
set(get(gca,'ylabel'),'position',[800 300 -4],'Rotation',0);
```

space _to_ pixel _transform.m

```
%% calculate coeffcients for x, y to transform to ri,rj and ai,aj
ri=scal(:,3);
rj=scal(:,4);
ai=scal(:,5);
aj=scal(:,6);
x=scal(:,1);
y=scal(:,2);
rsM=[ones(size(x)),x,y];
asM=[ones(size(x)),x,y];
recoi=rsM\ri;
recoj=rsM\rj;
alcoi=asM\ri;
alcoj=asM\rj;
i=recoi(1)+recoi(2)*x+recox(3)*y;
j=recoj(1)+recoj(2)*x+recoj(3)*y;
i=alcoi(1)+alcoi(2)*x+alcoi(3)*y;
j=alcoj(1)+alcoj(2)*x+alcoj(3)*y;

%% (x,y) to i transform, REF
x=-4:0.1:4;y=-4:0.1:4;
figure;[X,Y]=meshgrid(x,y);
I=recoi(1)+recoi(2)*X+recoi(3)*Y;
colormap(jet); surf(X,Y,I);
axis([-4 4 -4 4 -100 800])
xlabel('x','FontSize',16);
ylabel('y', 'FontSize',16);
zlabel('i','FontSize',16);
set(gca,'FontSize',16);
title('Transform from (x, y) to i, REF');
hold on;
for i=1:640
   for j=1:640
     if rxscal(i,j)~=0

plot3(rxscal(i,j),ryscal(i,j),i,'o','MarkerFaceColor','b','MarkerEdgeColor','w','MarkerSize',
6);
     elseif ryscal(i,j)~=0

plot3(rxscal(i,j),ryscal(i,j),i,'o','MarkerFaceColor','b','MarkerEdgeColor','w','MarkerSize',
6);
     else
     end
```

```
    end
end
hold off;
hxlabel = get(gca,'xlabel');
set(get(gca,'xlabel'),'position',[-1 -7 -10],'Rotation',0);
hylabel = get(gca,'ylabel');
set(get(gca,'ylabel'),'position',[-6 -1 -10],'Rotation',0);

%% (x,y) to j transform, REF
x=-4:0.1:4;y=-4:0.1:4;
figure;[X,Y]=meshgrid(x,y);
J=recoj(1)+recoj(2)*X+recoj(3)*Y;
colormap(jet); surf(X,Y,J);
axis([-4 4 -4 4 -100 800])
xlabel('x','FontSize',16);
ylabel('y', 'FontSize',16);
zlabel('j','FontSize',16);
set(gca,'FontSize',16);
title('Transform from (x, y) to j, REF');
hold on;
for i=1:640
    for j=1:640
      if ryscal(i,j)~=0

plot3(rxscal(i,j),ryscal(i,j),j,'o','MarkerFaceColor','b','MarkerEdgeColor','w','MarkerSize',
6);
      elseif rxscal(i,j)~=0

plot3(rxscal(i,j),ryscal(i,j),j,'o','MarkerFaceColor','b','MarkerEdgeColor','w','MarkerSize',
6);
      else
      end
    end
end
hold off;
view([125 30]);
hxlabel = get(gca,'xlabel');
set(get(gca,'xlabel'),'position',[1 6 -10],'Rotation',0);
hylabel = get(gca,'ylabel');
set(get(gca,'ylabel'),'position',[7 1 -10],'Rotation',0);
%% (x,y) to i transform, ALF
x=-4:0.1:4;y=-4:0.1:4;
figure;[X,Y]=meshgrid(x,y);
I=recoi(1)+recoi(2)*X+recoi(3)*Y;
```

```
colormap(jet); surf(X,Y,I);
axis([-4 4 -4 4 -100 800])
xlabel('x','FontSize',16);
ylabel('y', 'FontSize',16);
zlabel('i','FontSize',16);
set(gca,'FontSize',16);
title('Transform from (x, y) to i, ALF');
hold on;
for i=1:640
   for j=1:640
      if axscal(i,j)~=0

plot3(axscal(i,j),ayscal(i,j),i,'o','MarkerFaceColor','b','MarkerEdgeColor','w','MarkerSize'
,6);
      elseif ayscal(i,j)~=0

plot3(axscal(i,j),ayscal(i,j),i,'o','MarkerFaceColor','b','MarkerEdgeColor','w','MarkerSize'
,6);
      else
      end
   end
end
hold off;
hxlabel = get(gca,'xlabel');
set(get(gca,'xlabel'),'position',[-1 -7 -10],'Rotation',0);
hylabel = get(gca,'ylabel');
set(get(gca,'ylabel'),'position',[-6 -1 -10],'Rotation',0);
%% (x,y) to j transform, ALF
x=-4:0.1:4;y=-4:0.1:4;
figure;[X,Y]=meshgrid(x,y);
J=alcoj(1)+alcoj(2)*X+alcoj(3)*Y;
colormap(jet); surf(X,Y,J);
axis([-4 4 -4 4 -100 800])
xlabel('x','FontSize',16);
ylabel('y', 'FontSize',16);
zlabel('j','FontSize',16);
set(gca,'FontSize',16);
title('Transform from (x, y) to j, ALF');
hold on;
for i=1:640
   for j=1:640
      if ayscal(i,j)~=0
```

```
plot3(axscal(i,j),ayscal(i,j),j,'o','MarkerFaceColor','b','MarkerEdgeColor','w','MarkerSize'
,6);
      elseif axscal(i,j)~=0

plot3(axscal(i,j),ayscal(i,j),j,'o','MarkerFaceColor','b','MarkerEdgeColor','w','MarkerSize'
,6);
      else
      end
   end
end
hold off;
view([125 30]);
hxlabel = get(gca,'xlabel');
set(get(gca,'xlabel'),'position',[1 6 -10],'Rotation',0);
hylabel = get(gca,'ylabel');
set(get(gca,'ylabel'),'position',[7 1 -10],'Rotation',0);
```

intensity_calibration.m

```
%**************************************************************************
*****
%  intensity_calibration.m
%
%  PROGRAM DESCRIPTION
%  The following program is designed to load in the TIFF pictures for an intensity
calibration.
%  Prove the logarithmic response to light intensity of the CMOS sensor pixels
%  Perform a 4-order polynomial curve fit on the data for each pixel.
%  Output coefficients for 4-order polynomial and save them for both ALF and REF in
the form of '.mat'.
%  Input:   12-bit TIFF pictures, pixel resolution: 1280 x 800
%  Output:  alogalf: 4th order coefficient for ALF camera pixels
%           blogalf: 3rd order coefficient for ALF camera pixels
%           clogalf: 2nd order coefficient for ALF camera pixels
%           dlogalf: 1st order coefficient for ALF camera pixels
%           elogalf: Constant Intercept for ALF camera pixels
%
%           alogref: 4th order coefficient for REF camera pixels
%           blogref: 3rd order coefficient for REF camera pixels
%           clogref: 2nd order coefficient for REF camera pixels
%           dlogref: 1st order coefficient for REF camera pixels
%           elogref: Constant Intercept for REF camera pixels
%
%  Written by: Yong Zheng
%           06-24-14
%**************************************************************************
*****
clear all
close all
clc
for i =1:6
   [fname(i,:),pathname(i,:)]=uigetfile('C:\Users\ZY\Desktop\*.tif','Select image file for
processing in order of applied OD');
   %select the image files taken under 5 different ODs

   filename(i,:) = strcat(pathname(i,:),fname(i,:));
   %assign directory of the chosen image to 'pathname', assign filename of the chosen
image to 'filename'
   [pathstr(i,:), fnameM(i,:), ext(i,:)] = fileparts(filename(i,:)); %function
'fileparts'returns the path, file name and extension for the specified 'filename'
```

```
    %mkdir(pathstr(i,:),fnameM(i,:)); %create a new folder named the same as the string value of 'fnameM' under the folder fnameM_i
    cd(i,:)=fullfile(pathstr(i,:), fnameM(i,:)); %builds a full file name (including its full directory) for the file named as fnameM
    Iref(:,:,i)=uint16(double(imread (cd(i,:), 'tif', 'PixelRegion', {[1 640], [1 640]})));%+3841;
    Ialf(:,:,i)=uint16(double(imread (cd(i,:), 'tif', 'PixelRegion', {[1 640], [641 1280]})));%+3841;

end

   Iref1=Iref(:,:,1); Iref1=double(Iref1);
   Iref2=Iref(:,:,2); Iref2=double(Iref2);
   Iref3=Iref(:,:,3); Iref3=double(Iref3);
   Iref4=Iref(:,:,4); Iref4=double(Iref4);
   Iref5=Iref(:,:,5); Iref5=double(Iref5);
   Iref6=Iref(:,:,6); Iref6=double(Iref6);
   Ialf1=Ialf(:,:,1); Ialf1=double(Ialf1);
   Ialf2=Ialf(:,:,2); Ialf2=double(Ialf2);
   Ialf3=Ialf(:,:,3); Ialf3=double(Ialf3);
   Ialf4=Ialf(:,:,4); Ialf4=double(Ialf4);
   Ialf5=Ialf(:,:,5); Ialf5=double(Ialf5);
   Ialf6=Ialf(:,:,6); Ialf6=double(Ialf6);


% 'Lumens', T=10^(-OD)
T1=10^(-.3);
T2=10^(-.6);
T3=10^(-.9);
T4=10^(-.3)*10^(-.9);
T5=10^(-.6)*10^(-.9);
T6=10^(-.3)*10^(-.6)*10^(-.9);
L=[T6, T5, T4, T3, T2, T1];

% Reserve space in memory for the variables aalf, balf, aref, and bref
alogalf=zeros(640,640); blogalf=zeros(640,640); clogalf=zeros(640,640);
dlogalf=zeros(640,640); elogalf=zeros(640,640);
alogref=zeros(640,640); blogref=zeros(640,640); clogref=zeros(640,640);
dlogref=zeros(640,640); elogref=zeros(640,640);

alogalfI2L=zeros(640,640); blogalfI2L=zeros(640,640); clogalfI2L=zeros(640,640);
dlogalfI2L=zeros(640,640); elogalfI2L=zeros(640,640);
alogrefI2L=zeros(640,640); blogrefI2L=zeros(640,640); clogrefI2L=zeros(640,640);
dlogrefI2L=zeros(640,640); elogrefI2L=zeros(640,640);
```

```
% Perfrom a logarithmic fit for each of the pixels and store the variables 'a'
% and 'b' in to their respective matrix;
for i=1:640
       m=i
   for j=1:640
       Ia=[Ialf6(i,j), Ialf5(i,j), Ialf4(i,j), Ialf3(i,j), Ialf2(i,j), Ialf1(i,j)];
       palf=polyfit(L,Ia,4);
       alogalf(i,j)=palf(1,1); blogalf(i,j)=palf(1,2); clogalf(i,j)=palf(1,3);
dlogalf(i,j)=palf(1,4); elogalf(i,j)=palf(1,5);

       palfI2L=polyfit(Ia,L,4);
       alogalfI2L(i,j)=palfI2L(1,1); blogalfI2L(i,j)=palfI2L(1,2);
clogalfI2L(i,j)=palfI2L(1,3); dlogalfI2L(i,j)=palfI2L(1,4); elogalfI2L(i,j)=palfI2L(1,5);


       Ir=[Iref6(i,j), Iref5(i,j), Iref4(i,j), Iref3(i,j), Iref2(i,j), Iref1(i,j)];
       pref=polyfit(L,Ir,4);
       alogref(i,j)=pref(1,1); blogref(i,j)=pref(1,2); clogref(i,j)=pref(1,3);
dlogref(i,j)=pref(1,4); elogref(i,j)=pref(1,5);

       prefI2L=polyfit(Ir,L,4);
       alogrefI2L(i,j)=prefI2L(1,1); blogrefI2L(i,j)=prefI2L(1,2);
clogrefI2L(i,j)=prefI2L(1,3); dlogrefI2L(i,j)=prefI2L(1,4); elogrefI2L(i,j)=prefI2L(1,5);

   end
end


%% plot contour of scope and intercept distribution for REF and ALF
figure (1);
contour(alogalf);
axis square;
xlabel('Pixel in Column','FontSize',16);
ylabel('Pixel in Row', 'FontSize',16);
set(gca,'FontSize',16); colorbar;set(gcf,'color','white');
title('4th Order Coefficient Distribution of ALF Image');

figure (2);
contour(blogalf);
axis square;
xlabel('Pixel in Column','FontSize',16);
ylabel('Pixel in Row', 'FontSize',16);
set(gca,'FontSize',16); colorbar;set(gcf,'color','white');
title('3rd Order Coefficient Distribution of ALF Image');
```

```
figure (3);
contour(clogalf);
axis square;
xlabel('Pixel in Column','FontSize',16);
ylabel('Pixel in Row', 'FontSize',16);
set(gca,'FontSize',16); colorbar;set(gcf,'color','white');
title('2nd Order Coefficient Distribution of ALF Image');

figure (4);
contour(dlogalf);
axis square;
xlabel('Pixel in Column','FontSize',16);
ylabel('Pixel in Row', 'FontSize',16);
set(gca,'FontSize',16); colorbar;set(gcf,'color','white');
title('1st Order Coefficient Distribution of ALF Image');

figure (5);
contour(elogalf);
axis square;
xlabel('Pixel in Column','FontSize',16);
ylabel('Pixel in Row', 'FontSize',16);
set(gca,'FontSize',16); colorbar;set(gcf,'color','white');
title('Constant Intercept Distribution of ALF Image');

figure (6);
contour(alogref);
axis square;
xlabel('Pixel in Column','FontSize',16);
ylabel('Pixel in Row', 'FontSize',16);
set(gca,'FontSize',16); colorbar;set(gcf,'color','white');
title('4th Order Coefficient Distribution of REF Image');

figure (7);
contour(blogref);
axis square;
xlabel('Pixel in Column','FontSize',16);
ylabel('Pixel in Row', 'FontSize',16);
set(gca,'FontSize',16); colorbar;set(gcf,'color','white');
title('3rd Order Coefficient Distribution of REF Image');

figure (8);
contour(clogref);
axis square;
```

```
xlabel('Pixel in Column','FontSize',16);
ylabel('Pixel in Row', 'FontSize',16);
set(gca,'FontSize',16); colorbar;set(gcf,'color','white');
title('2nd Order Coefficient Distribution of REF Image');

figure (9);
contour(dlogref);
axis square;
xlabel('Pixel in Column','FontSize',16);
ylabel('Pixel in Row', 'FontSize',16);
set(gca,'FontSize',16); colorbar;set(gcf,'color','white');
title('1st Order Coefficient Distribution of REF Image');

figure (10);
contour(elogref);
axis square;
xlabel('Pixel in Column','FontSize',16);
ylabel('Pixel in Row', 'FontSize',16);
set(gca,'FontSize',16); colorbar;set(gcf,'color','white');
title('Constant Intercept Distribution of REF Image');

save(fullfile(pathstr(1,:),'20140728 intensity calibration 4th order polynomial'));

%% plot logarithmic response of a single pixel in REF and ALF corresponding to spatial
location(x=-2.060cm,y=0.412cm)
figure(11);
i=119; j=274;
      L = [T6, T5, T4, T3, T2, T1];
      Ir =
alogref(i,j)*(L.^4)+blogref(i,j)*(L.^3)+clogref(i,j).*(L.^2)+dlogref(i,j).*L+elogref(i,j);
      plot(L,Ir,'-rv','LineWidth',2,'MarkerFaceColor', 'r','MarkerSize',10);hold on;
      Ireforg=[Iref6(i,j), Iref5(i,j), Iref4(i,j), Iref3(i,j), Iref2(i,j), Iref1(i,j)];
      plot(L,Ireforg,'-ro','MarkerFaceColor','r','MarkerSize',10);
      hold off;
meanIr=sum(Ireforg)/6;
SSTr=0; SSEr=0;
for r=1:6
   SSTr=SSTr+(Ireforg(r)-meanIr)^2;
   SSEr=SSEr+(Ireforg(r)-
(alogref(i,j)*(L(r).^4)+blogref(i,j)*(L(r).^3)+clogref(i,j).*(L(r).^2)+dlogref(i,j).*L(r)+el
ogref(i,j)))^2;
end
R_squaredr=1-SSEr/SSTr;
```

```
figure; ii=124;jj=282;
      L=[T6, T5, T4, T3, T2, T1];

Ia=alogalf(ii,jj)*(L.^4)+blogalf(ii,jj).*(L.^3)+clogalf(ii,jj).*(L.^2)+dlogalf(ii,jj).*L+elog
alf(ii,jj);
      plot(L,Ia,'-k<','LineWidth',2,'MarkerFaceColor', 'k','MarkerSize',10); hold on;
      Ialforg=[Ialf6(ii,jj),Ialf5(ii,j),Ialf4(ii,jj),Ialf3(ii,jj),Ialf2(ii,jj),Ialf1(ii,jj)];
      plot(L,Ialforg,'-ko','MarkerFaceColor','k','MarkerSize',10);
meanIa=sum(Ialforg)/6;
SSTa=0; SSEa=0;
for r=1:6
   SSTa=SSTa+(Ialforg(r)-meanIa)^2;
   SSEa=SSEa+(Ialforg(r)-
(alogalf(ii,jj)*(L(r).^4)+blogalf(ii,jj).*(L(r).^3)+clogalf(ii,jj).*(L(r).^2)+dlogalf(ii,jj).*L(
r)+elogalf(ii,jj)))^2;
end
R_squareda=1-SSEa/SSTa;
      title('Logarithmic Response to Intensity (x=-2.060cm, y=0.412cm)','FontSize', 14);
      hleg=legend('REF, Curvefit, R^2=0.9999','REF, Original','ALF, Curvefit,
R^2=0.9997','ALF, Original');
      legend('boxoff'); %get rid of the box of the legends
      set(hleg,'Location','NorthWest'); %designate the location of the legend
      xlabel('Lumens','FontSize',16);ylabel('Grayscale Level','FontSize',
16);set(gca,'FontSize',16); hold off;


%% plot logarithmic response of a single pixel in REF and ALF corresponding to spatial
location(x=-2.060cm, y=-1.236m)
figure (12);
i=117;j=433;
      L=[T6, T5, T4, T3, T2, T1];

Ir=alogref(i,j)*(L.^4)+blogref(i,j)*(L.^3)+clogref(i,j).*(L.^2)+dlogref(i,j).*L+elogref(i,j
);
      plot(L,Ir,'-rv','LineWidth',2,'MarkerFaceColor', 'r','MarkerSize',10);hold on;
      Ireforg=[Iref6(i,j),Iref5(i,j),Iref4(i,j),Iref3(i,j),Iref2(i,j),Iref1(i,j)];
      plot(L,Ireforg,'-ro','MarkerFaceColor','r','MarkerSize',10);
      hold off;
meanIr=sum(Ireforg)/6;
SSTr=0; SSEr=0;
for r=1:6
   SSTr=SSTr+(Ireforg(r)-meanIr)^2;
```

```
   SSEr=SSEr+(Ireforg(r)-
(alogref(i,j)*(L(r).^4)+blogref(i,j)*(L(r).^3)+clogref(i,j).*(L(r).^2)+dlogref(i,j).*L(r)+el
ogref(i,j)))^2;
end
R_squaredr=1-SSEr/SSTr;

figure; ii=123;jj=439;
      L=[T6, T5, T4, T3, T2, T1];

Ia=alogalf(ii,jj)*(L.^4)+blogalf(ii,jj).*(L.^3)+clogalf(ii,jj).*(L.^2)+dlogalf(ii,jj).*L+elog
alf(ii,jj);
      plot(L, Ia,'-k<','LineWidth',2,'MarkerFaceColor', 'k','MarkerSize',10); hold on;
      Ialforg=[Ialf6(ii,jj), Ialf5(ii,j), Ialf4(ii,jj), Ialf3(ii,jj), Ialf2(ii,jj), Ialf1(ii,jj)];
      plot(L, Ialforg, '-ko', 'MarkerFaceColor', 'k', 'MarkerSize', 10);
meanIa=sum(Ialforg)/6;
SSTa=0; SSEa=0;
for r=1:6
   SSTa=SSTa+(Ialforg(r)-meanIa)^2;
   SSEa=SSEa+(Ialforg(r)-
(alogalf(ii,jj)*(L(r).^4)+blogalf(ii,jj).*(L(r).^3)+clogalf(ii,jj).*(L(r).^2)+dlogalf(ii,jj).*L(
r)+elogalf(ii,jj)))^2;
end
R_squareda=1-SSEa/SSTa;
      title('Logarithmic Response to Intensity (x=-2.060cm, y=-1.236cm)','FontSize', 14);
      hleg=legend('REF, Curvefit, R^2=0.9997','REF, Original', 'ALF, Curvefit,
R^2=0.9924','ALF, Original');
      legend('boxoff'); %get rid of the box of the legends
      set(hleg, 'Location', 'NorthWest'); %designate the location of the legend
      xlabel('Lumens','FontSize',16);ylabel('Grayscale Level', 'FontSize',
16);set(gca,'FontSize',16);
hold off;
```